

185-35199

CR-168037
R82AEB2A3

NASA-CR-168037
19850026886



National Aeronautics and
Space Administration

ENERGY EFFICIENT ENGINE

HIGH PRESSURE TURBINE THERMAL BARRIER COATING SUPPORT TECHNOLOGY REPORT

by

E.C. Duderstadt and P. Agarwal

GENERAL ELECTRIC COMPANY

LIBRARY

JUN 22 1983

LANGLEY RESEARCH
LIBRARY, NASA
HAMPTON, VIRGINIA

Prepared for

National Aeronautics and Space Administration

NASA LEWIS RESEARCH CENTER
Contract NAS3-20643



NF01883

This Page Intentionally Left Blank

FOREWORD

This report presents the results of the high pressure turbine thermal barrier coating technology design performed by the General Electric Company for the National Aeronautics and Space Administration, Lewis Research Center, under Contract NAS3-20643. This work was performed as part of the Aircraft Energy Efficiency (ACEE) Program, Energy Efficient Engine (E³ Project). Mr. C.C. Ciepluch is the NASA Project Manager. The NASA Project Engineers responsible for this effort are Mr. T. Strom and Mr. R. Dengler. The General Electric Project Manager is Mr. R.W. Bucy and the report was prepared by Mr. E.C. Duderstadt and Dr. P. Agarwal of the General Electric Company, Aircraft Engine Business Group, Evendale, Ohio.

This Page Intentionally Left Blank

TABLE OF CONTENTS

<u>Section</u>		<u>Page</u>
1.0	SUMMARY	1
2.0	INTRODUCTION	4
3.0	SELECTION OF A THERMAL BARRIER COATING SYSTEM	6
3.1	Candidate Coating System Selection	6
3.2	Establishment of Plasma Spray Parameters	8
3.3	Comparison of Candidate Coating Systems	8
3.3.1	Metallography	8
3.3.2	X-ray Diffraction Phase Analyses	10
3.3.3	Tensile Bond Testing	10
3.3.4	Bend Testing	14
3.3.5	Erosion Testing	14
3.3.6	Thermal Cycle Testing	16
3.3.7	Furnace Exposure Testing	16
3.3.8	High Velocity Dynamic Oxidation Testing	20
3.3.9	Selection of Three Coating Systems	28
3.4	Additional Evaluation of Three Coating Systems	28
3.4.1	Thermal Cycle Testing	28
3.4.2	High Cycle Fatigue Testing	31
3.4.3	Furnace Exposure Testing	34
3.4.4	Tensile Bond Testing	34
3.4.5	Impact Testing	36
3.4.6	Summary of Additional Evaluation	39
3.5	Comparison of $ZrO_2-20\%Y_2O_3$ TBC With NASA TBC	43
3.5.1	Thermal Cycle Testing	43
3.5.2	Thermal Exposure Testing	47
3.5.3	Tensile Bond Testing	47
3.5.4	Impact Testing	47
3.5.5	Metallography	47
3.5.6	Summary	47
4.0	EVALUATION OF TBC EFFECT ON MECHANICAL PROPERTIES OF SUBSTRATE ALLOYS	50
5.0	APPLICATION OF TBC TO TURBINE COMPONENTS	55
5.1	Development of Procedure for Coating Blades	55
5.2	Masking Procedures	60
5.3	Procedure for Coating Vanes	62

TABLE OF CONTENTS (Concluded)

<u>Section</u>		<u>Page</u>
6.0	TESTING OF THERMAL-BARRIER-COATED COMPONENTS	67
6.1	Cascade Rig Test	67
6.2	Component High Cycle Fatigue Tests	78
6.3	Engine Tests	79
6.3.1	First Engine Test	79
6.3.2	Second Engine Test	83
6.3.3	Posttest Analyses	86
7.0	CONCLUSIONS	112
8.0	RECOMMENDATIONS	113
	REFERENCES	114

LIST OF ILLUSTRATIONS

<u>Figure</u>		<u>Page</u>
1.	Typical Microstructures of Candidate Coating Systems.	9
2.	Tensile Bond Strengths in the As-Coated Condition and After 1255 K (1800° F)/200-Hour and 1366 K (2000° F)/200-Hour Exposures (Average of Three Specimens).	13
3.	Bend Test Results Showing Extent of Coating Spallation in the As-Coated Condition and After 1255 K (1800° F)/200-Hour and 1366 K (2000° F)/200-Hour Exposures (Three-Specimen Average).	15
4.	Erosion Test Results (Average of Two Specimens).	17
5.	Thermal Shock Test Rig.	18
6.	Thermal Cycle for Thermal Shock Testing.	18
7.	Thermal Cycle Test Results.	19
8.	Bend Test Results on Thermal-Barrier-Coated Specimens With ZrO ₂ -20%Y ₂ O ₃ Top Coat.	22
9.	First High Velocity Dynamic Oxidation Test Schedule.	25
10.	Second High Velocity Dynamic Oxidation Test Schedule.	26
11.	Thermal Cycle Test Results.	30
12.	Thermal Expansion of Substrate Alloys and ZrO ₂ -Y ₂ O ₃ .	32
13.	DS René 150, High Cycle Fatigue Specimens Coated With Candidate TBC Systems.	33
14.	High Cycle Fatigue Test Results on Uncoated 1255 K (1800° F) and Thermal-Barrier-Coated 1280 K (1850° F) Specimens.	35
15.	Typical Features of TBC Specimens After Impact at 90° and 20° Incidence Angles.	38
16.	Results of Thermal Cycle Testing of HfO ₂ TBC With Ballistic Impact Damage (20° Impact Angle).	40
17.	Results of Thermal Cycle Testing of ZrO ₂ -24%MgO TBC With Ballistic Impact Damage (20° Impact Angle).	41
18.	Results of Thermal Cycle Testing of ZrO ₂ -20%Y ₂ O ₃ TBC With Ballistic Impact Damage (20° Impact Angle).	42

LIST OF ILLUSTRATIONS (Continued)

<u>Figure</u>		<u>Page</u>
19.	Comparison of Test Results on ZrO_2 -8% Y_2O_3 and ZrO_2 -20% Y_2O_3 TBC's.	44
20.	Thermal Cycle Test Results for ZrO_2 -8% Y_2O_3 and ZrO_2 -20% Y_2O_3 Coatings on EA Ni-Cr-Al-Hf-Coated DS René 150 Specimens.	45
21.	Thermal Cycle Test Results for ZrO_2 -8% Y_2O_3 and ZrO_2 -20% Y_2O_3 Coatings on DS René 150 Specimens After 90° Incidence Impact.	46
22.	Microstructure of ZrO_2 -8% Y_2O_3 TBC.	48
23.	Scanning Electron Micrograph and EDAX Results on ZrO_2 -8% Y_2O_3 TBC.	49
24.	Results of 1255 K (1800° F), High Cycle Fatigue Testing Comparing Specimens With and Without Thermal Barrier Coating.	52
25.	Results of 1255 K (1800° F), Low Cycle Fatigue Testing Comparing Specimens With and Without Thermal Barrier Coating.	53
26.	Results of 1255 K (1800° F), Stress Rupture Testing Comparing Specimens With and Without Thermal Barrier Coating.	54
27.	CF6-50, Stage 1 Blades With Increasing Number of Coating Passes of ZrO_2 -20% Y_2O_3 Ceramic Layers.	57
28.	Sketch of Metal Masks Used in Coating of CF6-50, Stage 1, HPT Blades.	61
29.	CF6-50, HPT, Stage 1 Blade (DS René 150) With Ni-Cr-Al-Y/ ZrO_2 -20% Y_2O_3 Duplex TBC Over EA Ni-Cr-Al-Hf Coating.	63
30.	CF6-50, Stage 1 HPT Vanes With Ni-Cr-Al-Y/ ZrO_2 -20% Y_2O_3 Duplex TBC on Selected Areas.	64
31.	CF6-50, Stage 2 HPT Vanes (René 80) With Ni-Cr-Al-Y/ ZrO_2 -20% Y_2O_3 Duplex TBC on Selected Areas.	66
32.	Sketch of CF6-50, Stage 1 Blade Showing Location of Thermocouples.	68
33.	Thermal-Barrier-Coated, CF6-50, Stage 1, MATE II HPT Blades With Thermocouples.	69

LIST OF ILLUSTRATIONS (Continued)

<u>Figure</u>		<u>Page</u>
34.	Thermal Barrier Coating Rig Test Configuration.	70
35.	Planned Cyclic Conditions for Cascade Rig Test of Thermal-Barrier-Coated Blades.	71
36.	Failed Blades After 390 Cycles of Cascade Rig Testing.	73
37.	Cascade Rig Test Blades After Termination of Test (605 Cycles).	74
38.	Photomicrographs of Thermal-Barrier-Coated, René 150, CF6-50, Stage 1 HPT Blades (No. 0395) After 390 Cycles of Cascade Rig Testing.	75
39.	Secondary Electron Image and Elemental X-ray Density Maps of Thermal-Barrier-Coated, CF6-50, Stage 1 HPT Blade (No. 0395) Near the Damaged Region After 390 Cycles of Cascade Rig Testing.	76
40.	Secondary Electron Image and Elemental X-ray Density Maps of Thermal-Barrier-Coated, CF6-50, Stage 1 HPT Blade (No. 0395) Near the Trailing Edge After 390 Cycles of Cascade Rig Testing.	77
41.	Component High Cycle Fatigue Test Results of Thermal-Barrier-Coated Blades at 1200 K (1700° F).	80
42.	Thermal-Barrier-Coated, CF6-50, Stage 2 Blades.	81
43.	CF6-50 Engine Output Versus Time for Endurance Testing "C" Cycle.	82
44.	Photograph Showing Damage to Leading Edge of Thermal-Barrier-Coated Blade After 16 Hours of Engine Checkout.	84
45.	Borescope Photograph Showing Extent of Damage to Leading Edge of Thermal-Barrier-Coated Blade After 476 "C" Cycles.	84
46.	Borescope Photograph of Coating Damage After 27 Hours of Engine Checkout (Blade A2139).	85
47a.	Photos of Engine-Tested (1000 "C" Cycles) CF6-50 Stage 2 Blades (René 80) With and Without TBC, Suction Side.	87
47b.	Photos of Engine-Tested (1000 "C" Cycles) CF6-50 Stage 2 Blades (René 80) With and Without TBC, Pressure Side.	88

LIST OF ILLUSTRATIONS (Continued)

<u>Figure</u>		<u>Page</u>
48.	Chemical Analysis By EDAX of the Greenish Deposits on the Leading Edge, Suction Side of an Engine-Tested, Stage 2 Blade.	90
49a/b.	Photomicrographs of Engine-Tested (1000 "C" Cycles), CF6-50, Stage 2 Blade With TBC (Ni-22Cr-10Al-1Y/ZrO ₂ -20%Y ₂ O ₃ Duplex), 90% and 70% Spans (Blade No. 41, Table XV).	91
49c/d.	Photomicrographs of Engine-Tested (1000 "C" Cycles), CF6-50, Stage 2 Blade With TBC (Ni-22Cr-10Al-1Y/ZrO ₂ -20%Y ₂ O ₃ Duplex), 40% Span and Platform (Blade No. 41, Table XV).	93
50a/b.	Photomicrographs of Engine-Tested (1000 "C" Cycles), CF6-50, Stage 2 Blade With TBC (Ni-22Cr-10Al-1Y/ZrO ₂ -8%Y ₂ O ₃ Duplex), 90% and 70% Spans (Blade No. 42, Table XV).	95
50c/d.	Photomicrographs of Engine-Tested (1000 "C" Cycles), CF6-50, Stage 2 Blades With TBC (Ni-22Cr-10Al-1Y/ZrO ₂ -8%Y ₂ O ₃ Duplex), 40% Span and Platform (Blade No. 42, Table XV).	97
51a/b.	Photomicrographs of Engine-Tested (1000 "C" Cycles), CF6-50, Stage 2 Blade With TBC (Ni-22Cr-10Al-1Y/ZrO ₂ -8%Y ₂ O ₃ Duplex), 90% and 70% Spans (Blade No. 39, Table XV).	100
51c/d.	Photomicrographs of Engine-Tested (1000 "C" Cycles), CF6-50, Stage 2 Blade with TBC (Ni-22Cr-10Al-1Y/ZrO ₂ -8%Y ₂ O ₃ Duplex), 40% Span and Platform (Blade No. 39, Table XV).	102
52.	Secondary Electron Image and Elemental X-Ray Density Maps of Engine-Tested Stage 2 Blade (René 80) with Codep, Vacuum-Plasma-Sprayed Ni-22Cr-10Al-1Y and ZrO ₂ -20%Y ₂ O ₃ Coatings; Leading Edge, Suction Side at 80% Span (Blade No. 41/Table XV).	104
53.	Secondary Electron Image and Elemental X-Ray Density Maps of Engine-Tested Stage 2 Blade (René 80) With Codep, Vacuum-Plasma-Sprayed Ni-22Cr-10Al-1Y and ZrO ₂ -8% Without Y ₂ O ₃ Coatings; Leading Edge, Suction Side at 80% Span (Blade No. 42, Table XV).	105
54.	Secondary Electron Image and Elemental X-Ray Density Maps of Engine-Tested Stage 2 Blade (René 80) With Codep, Vacuum-Plasma-Sprayed Ni-22Cr-10Al-1Y and ZrO ₂ -8% Without Y ₂ O ₃ Coatings; Leading Edge, Suction Side at 80% Span (Blade No. 39, Table XV).	106
55.	Thermal-Barrier-Coated CF6-50 Stage 2 Vanes After Factory Engine Test of 1000 "C" Cycles.	107

LIST OF ILLUSTRATIONS (Concluded)

<u>Figure</u>		<u>Page</u>
56.	Thermal-Barrier-Coated, CF6-50, Stage 2 Vane After 1000 "C" Cycle Factory Engine Test.	108
57a.	Photomicrograph of Engine-Tested (1000 "C" Cycles), CF6-50, Stage 2 Vane With TBC (Ni-22Cr-10Al-1Y/ZrO ₂ -20%Y ₂ O ₃ Duplex); 95% Span.	110
57b.	Photomicrograph of Engine-Tested (1000 "C" Cycles), CF6-50, Stage 2 Vane With TBC (Ni-22Cr-10Al-1Y/ZrO ₂ -20%Y ₂ O ₃ Duplex); 15% Span.	111

LIST OF TABLES

<u>Table</u>		<u>Page</u>
I.	Candidate Coating Systems.	7
II.	Coating Layer Thicknesses Determined by Metallographic Examination.	11
III.	X-ray Diffraction Analysis Results.	12
IV.	Visual Observations of Specimens Exposed at 1255 K (1800° F) and 1366 K (2000° F).	21
V.	High Velocity Dynamic Oxidation Burner Rig Parameters.	23
VI.	Summary of Results of First High Velocity Dynamic Oxidation Test (Total Time = 143 Hours).	24
VII.	Summary of Results of Second High Velocity Dynamic Oxidation Test (Total Time = 97 Hours).	24
VIII.	Summary of High Velocity Dynamic Oxidation Test Results.	27
IX.	Summary of Coating System Ranking From Preliminary Screening Tests.	29
X.	Tensile Bond Test Results.	36
XI.	Summary of Impact Test Results.	37
XII.	Summary of Rankings From Additional Evaluated Tests.	39
XIII.	Bond Coat Process Development Variations.	56
XIV.	Summary of Thermal Test Results of Coated Blades.	59
XV.	Summary of Damage to Thermal-Barrier-Coated, CF6-50, Stage 2 HPT Blades, 1000 "C" Cycle Engine Test.	89

1.0 SUMMARY

This report describes the work performed on the thermal barrier coating development task of the NASA/GE Energy Efficient Engine (E³) Component Development Program. The task consisted of several phases which led to the selection of a thermal barrier coating (TBC) system, development of processes for applying the selected coating to CF6-50 high pressure turbine blades and vanes, laboratory and rig testing of coated specimens and components, and finally, evaluation of thermal-barrier-coated, high pressure turbine (HPT) blades and vanes in CF6-50 factory engine tests.

Eight candidate coating systems, comprised of one bond coat alloy (Ni-22Cr-10Al-1Y), four top coat compositions (ZrO₂-24%MgO, ZrO₂-20%Y₂O₃, HfO₂, and Al₂O₃), and two coating system configurations (duplex and triplex), were compared in laboratory tests and evaluations. The coating systems were evaluated by metallography, X-ray diffraction analysis, tensile bond and bend tests, erosion and impact tests, furnace exposures at 1255 and 1366 K (1800° and 2000° F), thermal cycle [533 to 1310 K (500° to 1900° F)] tests, and high velocity dynamic oxidation [311 to 1366 K (100° to 2000° F)] tests. On the basis of the results of these evaluations, a two-layer (duplex) TBC system consisting of a Ni-22Cr-10Al-1Y bond coat layer and a ZrO₂-20%Y₂O₃ top coat layer was selected for further testing.

The selected coating system was further tested in high cycle fatigue and stress rupture tests at 1255 K (1800° F) on specimens of two blade alloys [René 80 and directionally solidified (DS) René 150] and one vane alloy (X-40) to assess whether the presence of the TBC degrades the mechanical properties of the substrate alloys. Low cycle fatigue tests were run on DS René 150. Comparison of the results from specimens with and without TBC showed no significant effect of the TBC on these mechanical properties.

Procedures were developed for applying the selected TBC to CF6-50 high pressure turbine blades and vanes. The process selected for the blades was application of the Ni-Cr-Al-Y bond coat layer by the vacuum plasma spray (VPS) process and application of the ZrO₂-Y₂O₃ top coat layer by the conventional atmospheric pressure plasma spray process with programmed manipulation of the plasma torch. Special masking for the CF6-50 Stage 1 blade was designed and fabricated to prevent blockage of the film-cooling holes and trailing edge holes present in the airfoil. Both the Stage 1 and 2 vanes were coated in selected areas only. Both coating layers were applied to the vanes by the conventional plasma spray process with manual manipulation of the plasma torch. The ceramic layer of the TBC on all components was hand-polished to a smooth finish prior to the rig and engine testing to reduce aerodynamic friction losses.

The CF6-50 high pressure turbine components coated with the selected TBC were tested in three kinds of tests. Stage 1 blades were tested in a cascade cyclic test rig built especially for the E³ Program, Stage 2 blades were component high cycle fatigue tested to qualify the thermal-barrier-coated blades

for engine testing, and Stage 2 blades and Stage 1 and 2 vanes were run in factory engine tests.

The purpose of the cascade rig test was to examine the durability of the TBC on Stage 1 blades under engine simulative heat flux conditions and to measure the thermal benefit obtained from the TBC. The majority of the blades were instrumented with thermocouples to measure the temperature of the blade/bond coat interface during the test. Problems were encountered during the course of the test when a cooling air supply tube cracked, resulting in leading edge burnout and local melting of some blades. The damaged blades were replaced and the test continued until a negative backflow margin resulted in leading edge burnout of additional blades. The durability of the TBC under the severe test conditions was encouraging since the TBC was found to be in good condition even in areas adjacent to local melting of the substrate.

The component high cycle fatigue testing of fully coated Stage 2 blades at 1200 K (1700° F) showed the average high cycle fatigue strength of the thermal-barrier-coated blades to compare favorably to the strength of uncoated blades, qualifying TBC blades for engine testing.

Several thermal-barrier-coated CF6-50 HPT components were tested in each of two factory engine tests. Twelve fully coated Stage 2 blades were run in the first of these tests. Ten fully coated Stage 2 blades, four partially coated Stage 1 vane pairs, and seven partially coated Stage 2 vane pairs were tested in the second engine test.

The TBC on the 12 thermal-barrier-coated blades which were tested in the first engine test consisted of a 0.13-mm (0.005-in.) thick bond coat layer of Ni-Cr-Al-Y applied by vacuum plasma spraying, and a 0.25-mm (0.010-in.) thick top coat layer of ZrO_2 - Y_2O_3 applied by the conventional arc plasma spray process. Six of the blades were coated at the General Electric Corporate Research and Development (CRD) Center, Schenectady, New York, under NASA Contract NAS3-21727 and had a top coat composition of ZrO_2 -8% Y_2O_3 applied with manual manipulation of the plasma torch. The other six blades were coated at the General Electric Aircraft Engine Business Group (AEBG), Evendale, Ohio, facility and had a top coat composition of ZrO_2 -20% Y_2O_3 applied using programmed mechanical manipulation of the plasma torch.

The first engine test was terminated after 626 endurance cycles due to an engine system failure unrelated to the coated blades. All of the second stage blades were severely damaged when the engine failure occurred, with extensive loss of blade material at the leading edge and blade tip. Considerable impact damage occurred to the suction side of the airfoils near the leading and trailing edges. The bond coat layer of the TBC remained intact over nearly all of the remaining airfoil surface. The ceramic layer was found to be in good condition in areas unaffected by the impact damage.

Ten thermal-barrier-coated CF6-50 Stage 2 blades; four Stage 1 vane pairs; and seven Stage 2 vane pairs underwent 1000 endurance cycles of testing in a second engine test. The blades were fully coated on the platforms and airfoils, and the vanes were coated in selected areas of the airfoils and bands. Three of the blades were coated at GE-CRD under NASA Contract NAS3-21727 as described above. Five of the blades coated at GE-AEBG had a top coat composition of $ZrO_2-20\%Y_2O_3$ and two others had a composition of $ZrO_2-8\%Y_2O_3$. The TBC on the vanes had a top coat layer composition of $ZrO_2-20\%Y_2O_3$. Both coating layers on the vanes were applied by the conventional arc plasma spray process using manual manipulation of the plasma torch.

After completion of the 1000 endurance cycle engine test, the TBC on the blades was in excellent condition on the platforms (except one spalled area on one platform), on the pressure side of the airfoils, and over the greater part of the suction side of the airfoils. Some coating loss occurred from the leading edge above midspan and also from the forward part of the suction side (close to the leading edge) of the airfoils. The coating damage appeared to be caused by particle impingement. The particulate matter may have come from the Stage 1 shrouds which lost some nickel-aluminum material during the test. Adjacent blades without the TBC (Codep coating only) also showed evidence of particle impingement. There was no significant difference in the amount of coating loss or pattern of coating loss from the $ZrO_2-20\%Y_2O_3$ and $ZrO_2-8\%Y_2O_3$ compositions. The performance of the TBC on the blades was very encouraging, but demonstrated the need for improvement in impact damage resistance.

Some coating loss occurred from the outer 1/3 to 2/3 of the airfoil leading edge of every thermal-barrier-coated Stage 2 vane. The abrupt edge of the remaining coating suggests that coating loss was by spalling rather than from impact by particulate matter. In localized areas of the outer band near the leading edge of some of the airfoils, the ceramic layer was missing after 1000 endurance cycles and appeared to have been eroded away by particle impingement. The TBC was in good condition on the other areas of the vanes. The bond coat layer on the vanes was oxidized to a much greater extent than it was on the blades. Variation in coating thickness was much greater on the vanes than on the blades, indicating that further improvements are needed in the application process for coating vanes. The Stage 1 vanes remained in the engine for further testing and were not available for analysis.

The overall performance of the TBC on these HPT components was very encouraging, especially on the Stage 2 blades which were subjected to a centrifugal field and vibratory loads. Further improvement in erosion, impact, and spalling resistance of the coating is needed before the use of TBC's on HPT airfoils is implemented.

2.0 INTRODUCTION

The continuing effort to increase the efficiency of aircraft gas turbine engines has received added impetus in recent years because of the rising cost of fuel. Several generations of superalloys have been developed over the years to permit increases in turbine inlet gas temperatures, but the general temperature limits of alloy materials and the sophisticated cooling schemes required make this increasingly difficult and expensive. An alternate approach for increasing engine efficiency that has received wide interest and attention is the use of insulative coatings to protect the metal surfaces of turbine components from the hot gas stream (References 1 through 7). The use of these coatings, known as thermal barrier coatings, has the potential to increase engine efficiency by permitting increased turbine gas inlet temperatures while maintaining present coolant flows and metal temperatures, or by maintaining current gas inlet temperatures and reducing the present coolant flow requirements thus increasing engine operating efficiency. Alternatively, TBC's may be utilized to reduce metal component operating temperatures and thereby extend part life.

Thermal barrier coatings are presently bill-of-material coatings on certain combustor and afterburner components with extended part life being the realized benefit. However, the use of TBC's on turbine components offers the more desirable benefit of increased engine efficiency. The use of TBC's on turbine components requires much greater coating reliability. The conditions which coatings will be required to endure are much more severe in the high pressure turbine than in the combustor and afterburner. In addition to the extremely high heat fluxes existing in both the stator and rotor components, high mechanical centrifugal stresses are present in rotor components and their coatings. Furthermore, whereas loss of the insulative coating from combustors and afterburners is not especially detrimental to the reliability of those components, loss of such coatings from critical areas of high pressure turbine blades has the potential to shorten component life below that of uncoated parts (Reference 7). This is because the metal temperature in the spalled area increases substantially giving rise to higher localized thermal stresses, thereby significantly reducing part life.

The use of TBC's on HPT components is a high-payoff technology; thus, there is strong motivation to develop reliable TBC's that can be utilized on HPT blades and vanes.

One element in the supporting technology effort of the NASA/GE Energy Efficient Engine (E³) Component Development and Integration Program was the multiphase development of a TBC system and demonstration of its adequacy for E³ application. In the first phase, screening tests were conducted on eight TBC systems with the goal of selecting the three most promising systems for further evaluation. In the second phase, the three systems were further tested with the goal of selecting the single most promising TBC system for engine testing. In subsequent phases of the effort, some potential effects

of the presence of the selected TBC on the properties of typical substrate alloys were investigated, and application processes for coating HPT blades and vanes were developed. Finally, HPT blades and vanes were coated with the selected TBC system and evaluated in rig and factory engine tests. The following sections of this report present the results of this overall effort.

3.0 SELECTION OF A THERMAL BARRIER COATING SYSTEM

The objective of this task was to select a TBC system for application on turbine components and eventual evaluation in a factory engine test. The selection process consisted of conducting preliminary screening tests on eight candidate TBC systems, selecting the best three of these systems and further evaluating them with the aim of selecting the single best TBC system for turbine hardware application.

3.1 CANDIDATE COATING SYSTEM SELECTION

The candidate coating systems which were selected for screening in this program are comprised of four ceramic materials, one metallic bond coat material, and two coating system configurations - duplex (two layers) and triplex (three layers). For the bond coat, which is essential for adherence of the ceramic insulating layer to the substrate, a highly oxidation-resistant alloy which forms a good bond with both the substrate and the ceramic layer was desired. The bond coat alloy chosen for this program was Ni-22Cr-10Al-1Y (all compositions are given in weight percent). This alloy had performed well as a bond coat in previous thermal cycle tests and engine tests of thermal barrier coatings.

The four ceramic insulating materials were chosen based on either General Electric experience in experimental engine and laboratory tests or on NASA test results. Selection criteria included (1) demonstrated ability to survive the gas turbine thermal environment, (2) low thermal conductivity, (3) thermal expansion as close as possible to that of superalloys, and (4) superior resistance to the oxidation/corrosion environment of the gas turbine. The materials selected were Al₂O₃ (Metco 105), ZrO₂-20%Y₂O₃ (Metco 202), ZrO₂-24%MgO (Metco 210), and HfO₂.

Alumina (Al₂O₃) was chosen mainly for its demonstrated adherence in a gas turbine environment as instrumentation patches on airfoils in factory test engines. Although the thermal conductivity of alumina is fairly high compared to that of stabilized zirconia, it is substantially lower than the conductivities of superalloys and could therefore significantly reduce the heat flux into a component. Moreover, alumina has outstanding resistance to oxygen transport and has good erosion resistance. Yttria-stabilized zirconia (ZrO₂-20%Y₂O₃) was chosen because it has low thermal conductivity, relatively high thermal expansion coefficient, and, if fully stabilized, no phase transformations below 2755 K (4500° F). Furthermore, yttria-stabilized zirconia coating patches had survived engine tests on airfoils without observable distress.

Magnesia-modified zirconia (ZrO₂-24%MgO) was also chosen for its low conductivity, high expansion coefficient, and demonstrated utility in the gas turbine environment. Although magnesia-modified zirconia is not phase-stable,

its benefit as a TBC on combustion liners had been demonstrated in field service evaluations. Hafnia (HfO_2) was chosen for its low thermal conductivity and absence of phase transformations up to 1895 K (2950° F). Hafnia also has excellent hot corrosion resistance. Although monoclinic hafnia has a low value of thermal expansion coefficient, the favorable engine experience with alumina coatings (which also have low coefficients) indicated that a close expansion match between the substrate and the ceramic layer may not be necessary to ensure coating durability.

The eight coating systems are listed in Table I. Each of the ceramic insulating materials was evaluated in both duplex (two-layer) and triplex (three-layer) configurations. Duplex coatings (Reference 8) consisted of a Ni-Cr-Al-Y bond coat layer covered directly by a top coat of insulating ceramic. This configuration had been shown to be durable on several components in engine tests, and has an advantage in being easier to apply to complex shapes than triplex or graded coatings. The triplex coatings consisted of a bond coat layer followed by a cermet layer which was a mixture of the bond coat alloy and the ceramic top coat material (approximately 50% by volume of each), and finally, a ceramic top coat layer. The triplex configuration is utilized to reduce interface stresses in thick coatings, and it was felt at the time that triplex coatings might better withstand the stresses which occur in the TBC during engine operation. All coatings were applied by the arc plasma spray process.

Table I. Candidate Coating Systems⁽¹⁾.

<u>Top Coat</u>	<u>Configuration</u> ⁽²⁾	<u>Identification Code</u>
ZrO ₂ -24%MgO	Duplex	MZD
ZrO ₂ -24%MgO	Triples	MZT
ZrO ₂ -20%Y ₂ O ₃	Duplex	YZD
ZrO ₂ -20%Y ₂ O ₃	Triples	YZT
Al ₂ O ₃	Duplex	AD
Al ₂ O ₃	Triples	AT
HfO ₂	Duplex	HD
HfO ₂	Triples	HT

(1) All coating systems had a bond coat alloy of Ni-22Cr-10Al-1Y.

(2) Duplex: bond coat layer covered by top coat.

Triples: bond coat layer covered by mixture of bond coat and top coat materials (50% by volume each), then top coat.

HS 188 alloy was selected as the substrate alloy for this phase of the work. Positive factors in its selection included its availability and cost relative to the vane alloy X-40, a thermal expansion coefficient very similar to that of X-40, and a conservative (greater) thermal expansion mismatch with the candidate ceramic top coat materials relative to their mismatch with the blade alloy René 80 and DS René 150.

3.2 ESTABLISHMENT OF PLASMA SPRAY PARAMETERS

Coatings of each of the four candidate ceramic materials and the bond coat alloy were deposited on HS 188 alloy substrates using at least 10 sets of plasma spray parameters. The parameters which were varied included arc gas and carrier gas compositions and flow rates, powder feed rate, arc power, and spray distance. Each deposit was evaluated for adherence as measured by an ambient temperature bend test and by a thermal shock test. The bend test consisted of bending a 19 mm by 115 mm by 0.76 mm (0.75 in. by 4.5 in. by 0.030 in.) coupon, coated on one surface, over a special mandrel having a varying radius of curvature and noting the largest radius of curvature at which cracking occurred and also noting the amount, if any, of coating loss. The thermal shock test consisted of heating a coated button, 25 mm (1 in.) in diameter by 3.2 mm (0.125 in.) thick to 1366 K (2000° F) for 5 to 10 minutes and then immersing it in a beaker of water. Specimens were visually inspected with a stereo microscope (15X) for evidence of cracking or spalling.

Metallographic evaluation was used to determine deposit uniformity, density, and apparent bonding. Spray parameters were selected for each material based on the results of these evaluations.

3.3 COMPARISON OF CANDIDATE COATING SYSTEMS

Once the spray parameters were established, button and coupon specimens were coated with the eight TBC systems and the coating systems compared in screening tests. The coatings were evaluated by metallography, X-ray diffraction, tensile bond and bend tests, thermal exposure and thermal cycle tests, and high velocity dynamic oxidation tests.

3.3.1 Metallography

The coatings were evaluated metallographically to determine structure, structure uniformity, density (porosity), coating thickness, and apparent bonding. All of the coatings appeared to be well bonded and exhibited uniform structures. Coatings microstructures are shown in Figure 1. The microstructures are typical of plasma-spray-deposited materials; that is, the coatings consisted of elongated splats and numerous pores having a large variety of shapes and sizes. The interface between the substrate and the bond coat layer appears to be clean and free of embedded grit-blast media for all coating systems. The ceramic insulating layer contains on the order of 10% porosity

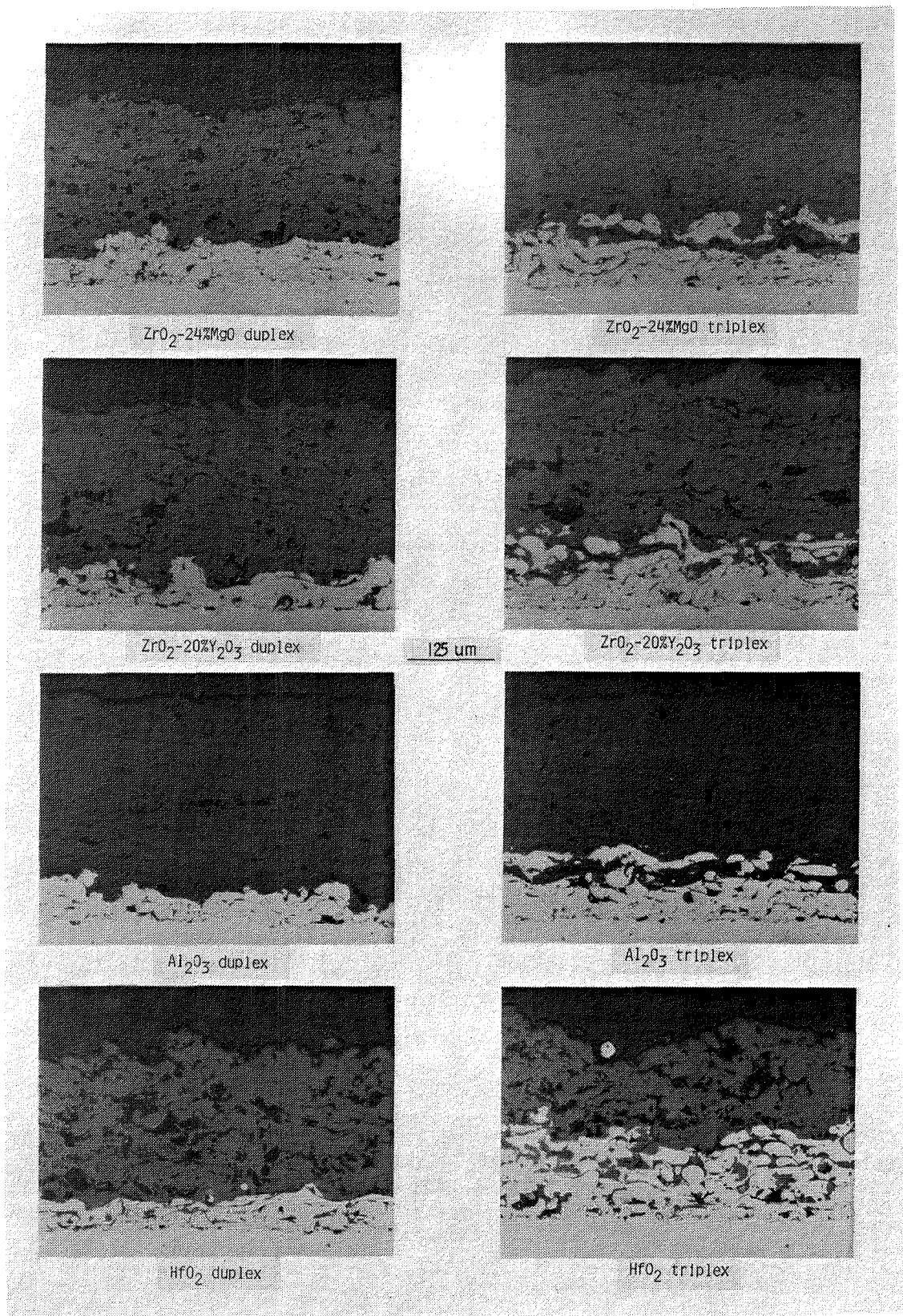


Figure 1. Typical Microstructures of Candidate Coating Systems.

for the zirconia coating systems; the alumina coatings contain less porosity and the hafnia coatings are considerably more porous than the zirconia coatings. Coating thicknesses are listed in Table II. Bond coat layer thickness averaged about 0.05 mm (0.002 in.), the intermediate layer of triplex coatings averaged about 0.06 mm (0.0025 in.), and top coat layers averaged about 0.23 to 0.25 mm (0.009 to 0.010 in.). Bond coats were thinner than the 0.13 (0.005 in.) planned, but intermediate layer thicknesses were near the target thicknesses.

3.3.2. X-ray Diffraction Phase Analyses

X-ray diffraction analyses using Cu K α radiation were performed on specimens in the as-coated condition and after 200 hours exposure at 1255 K (1800° F) and at 1366 K (2000° F). Diffractometer scans were used to analyze the surface phases; Table III lists the phases identified in the eight TBC systems.

The ZrO₂-20%Y₂O₃ coating layers were found to be essentially all cubic phase with a lattice parameter of 5.16Å in the as-coated condition. Neither the phase compositions nor lattice parameter changed during 200 hours of exposure at 1255 K (1800° F). However, after the 200-hour exposure at 1366 K (2000° F), the lattice parameter of the cubic phase decreased slightly to 5.13Å and a very small amount of monoclinic phase was present.

The ZrO₂-24%MgO coating layers were also essentially all cubic phase as-coated, with a lattice parameter of 5.03Å. Exposure of these coatings at 1255 K (1800° F) resulted in a slight increase in lattice parameter to 5.08Å. After 200 hours at 1366 K (2000° F), the primary phase was monoclinic, with a small amount of cubic phase also present.

The alumina coating layers were gamma phase as-coated and after 200 hours of exposure at 1255 K (1800° F); after 200 hours at 1366 K (2000° F), the ceramic layer had transformed to alpha-alumina.

Monoclinic phase was the only phase detected in the hafnia layer as-coated and after 200-hour exposures at 1255 K (1800° F) and 1366 K (2000° F).

3.3.3 Tensile Bond Testing

The adhesive/cohesive strengths of the specimen coating layers were measured (Reference 9). Button specimens in the as-coated condition and after 200 hours at 1255 K (1800° F) and 1366 K (2000° F) were prepared for testing by bonding them with epoxy-resin to 25 mm (1 in.) diameter pull fixtures. Triplicate specimens were then tested at room temperature by applying a tensile stress at a constant rate between 8 to 10 MPa (1200 to 1400 psi) per minute until rupture. The test results are shown in Figure 2.

Table II. Coating Layer Thicknesses Determined by Metallographic Examination.

	Coating Layer Thickness, mm (thousandths of an inch)								
	As-Coated			1255 K (1800° F)/200 hr			1366 K (2000° F)/200 hr		
	Bond	Inter.	Top	Bond	Inter.	Top	Bond	Inter.	Top
ZrO ₂ -20%Y ₂ O ₃ Duplex	0.051(2)	---	0.25(10)	0.051(2)	---	0.24(9.5)	0.063(2.5)	---	0.23(9)
ZrO ₂ -20%Y ₂ O ₃ Triplex	0.051(2)	0.051(2)	0.25(10)	0.063(2.5)	0.063(2.5)	0.24(9.5)	0.051(2)	0.051(2)	0.23(9)
ZrO ₂ -24%MgO Duplex	0.063(2.5)	---	0.22(8.5)	0.051(2)	---	0.20(8)	0.051(2)	---	---
ZrO ₂ -24%MgO Triplex	0.051(2)	0.051(2)	0.22(8.5)	0.051(2)	0.063(2.5)	0.23(9)	0.051(2)	0.063(2.5)	0.23(9)
Al ₂ O ₃ Duplex	0.051(2)	---	0.29(11.5)	0.051(2)	---	---	0.051(2)	---	---
Al ₂ O ₃ Triplex	0.051(2)	0.051(2)	0.23(9)	0.038(1.5)	0.051(2)	---	0.051(2)	0.063(2.5)	---
HfO ₂ Duplex	0.051(2)	---	0.23(9)	0.051(2)	---	0.20(8)	0.051(2)	---	0.23(9)
HfO ₂ Triplex	0.063(2.5)	0.063(2.5)	0.18(7)	0.063(2.5)	0.063(2.5)	0.18(7)	0.063(2.5)	0.063(2.5)	0.18(7)
General: Bond Coat Thickness - Uniform at 0.05 mm (0.002 in.) Intermediate Thickness - Uniform at 0.05 to 0.06 mm (0.002 to 0.0025 in.) Top Coat - Fairly Uniform at 0.24 to 0.25 mm (0.009 to 0.010 in.)									

Table III. X-ray Diffraction Analysis Results.

Coating System	Crystallographic Phase		
	As-Coated	1255 K (1800° F)/200 hr	1366 K (2000° F)/200 hr
ZrO ₂ -20%Y ₂ O ₃ Duplex	Cubic a = 5.16Å	Cubic a = 5.16Å	Cubic ⁽¹⁾ a = 5.153A
ZrO ₂ -20%Y ₂ O ₃ Triplex	Cubic a = 5.16Å	Cubic a = 5.16Å	Cubic ⁽¹⁾ a = 5.149A
ZrO ₂ -24%MgO Duplex	Cubic a = 5.03Å	Cubic a = 5.08Å	Monoclinic ⁽²⁾
ZrO ₂ -24%MgO Triplex	Cubic a = 5.03Å	Cubic a = 5.08Å	Monoclinic ⁽²⁾
Al ₂ O ₃ Duplex	Gamma	Gamma	Alpha
Al ₂ O ₃ Triplex	Gamma	Gamma	Alpha
HfO ₂ Duplex	Monoclinic	Monoclinic	Monoclinic
HfO ₂ Triplex	Monoclinic	Monoclinic	Monoclinic

(1)Very small amount of monoclinic phase also present.

(2)Small amount of cubic phase also present.

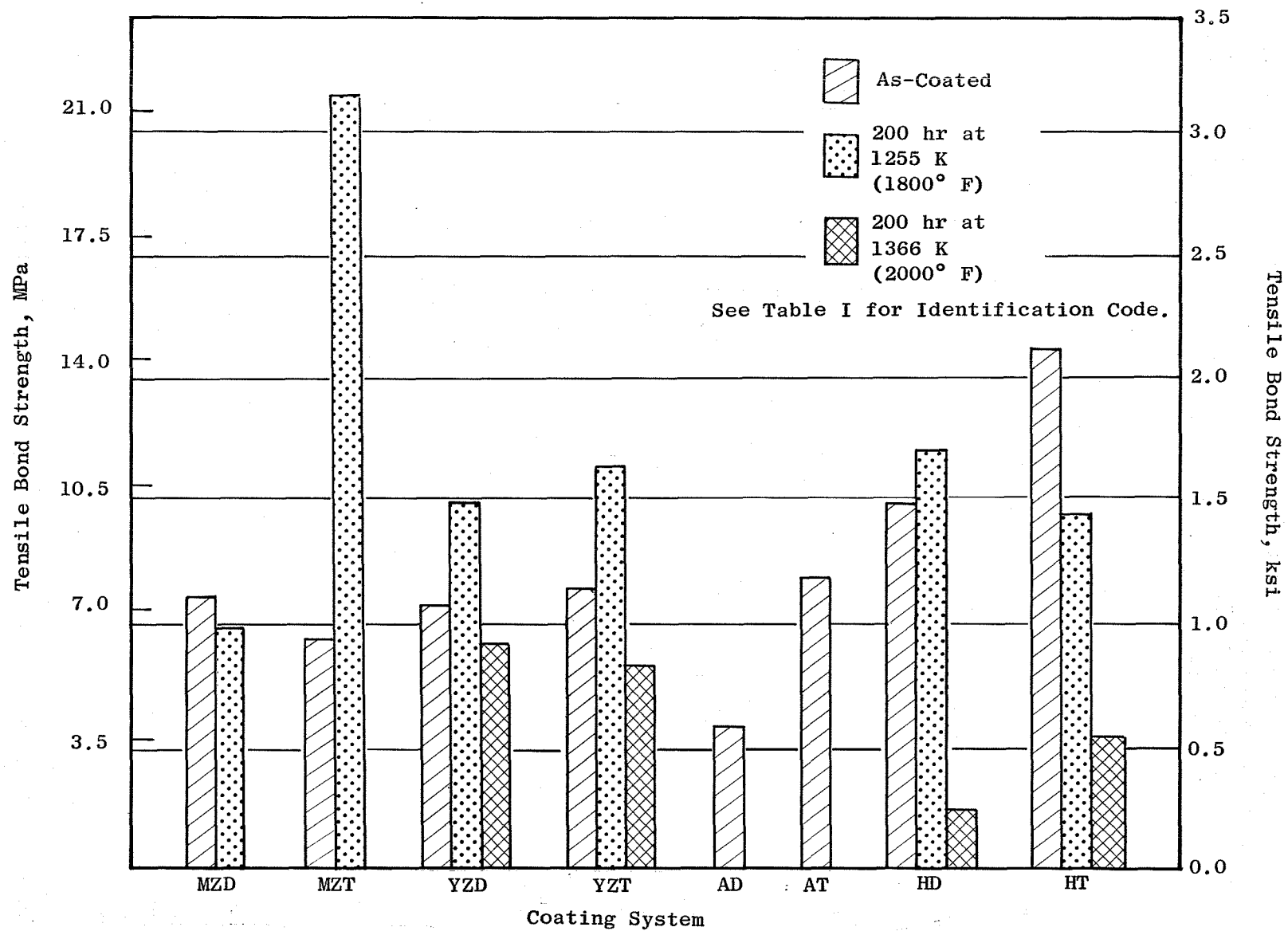


Figure 2. Tensile Bond Strengths in the As-Coated Condition and After 1255 K (1800° F)/200-Hour and 1366 K (2000° F)/200-Hour Exposures (Average of Three Specimens).

The adhesive/cohesive strengths of the $ZrO_2-20\%Y_2O_3$ and $ZrO_2-24\%MgO$ coating systems in the as-coated condition were about 7 MPa (1 ksi), similar to the values obtained by Levine (Reference 10) for a $ZrO_2-12\%Y_2O_3$ TBC. The strengths of the Al_2O_3 coating systems were about the same or lower. The HfO_2 as-coated specimens exhibited an average strength of about 12.5 MPa (1.8 ksi). In most cases, the strengths were higher after the 200-hour exposure at 1255 K (1800° F). However, after a 200-hour exposure at 1366 K (2000° F), the strengths were lower in all cases. Generally, failure of the duplex coating systems occurred in the ceramic layer just above the interface between the ceramic layer and the bond coat layer. In the triplex coating systems, the failure often occurred partially in the ceramic layer and partially in the intermediate (blend) layer of the coating.

3.3.4 Bend Testing

Ambient temperature bend tests were conducted as one means of assessing the durability of the candidate coating systems. Test specimens, 25 mm by 100 mm by 1.6 mm (1 in. by 4 in. by 0.062 in.) and coated on one surface, were bent around a 12.7 mm (0.5 in.) diameter mandrel and the coatings ranked based on the extent of top coat spallation. Although the severity of the test is such that all ceramic coatings crack, the extent to which they spall can be used as a measure of durability and bonding shear strength of the coating. Some of the specimens were exposed to 1255 K (1800° F) or 1366 K (2000° F) for 200 hours before bend testing.

Extensive loss of the ceramic layer of the coating occurred during the testing of specimens which had been exposed at 1366 K (2000° F). In general, there was greater loss of coating from specimens exposed at 1255 K (1800° F) than from as-deposited specimens. Also, there was a tendency toward less coating loss from triplex coating systems than from duplex coatings. The bend test results are summarized in Figure 3. The HfO_2 duplex coating system fared the best, followed by $ZrO_2-20\%Y_2O_3$ duplex and triplex systems and $ZrO_2-24\%MgO$ duplex.

3.3.5 Erosion Testing

Some amount of abrasive particulate matter passes through aircraft turbine engines during their operation, and it is therefore important that components and their coatings be resistant to particulate erosion. The resistance of the candidate coating systems to particulate erosion was measured in laboratory tests. In these tests, the surface of coated specimens was impacted with alumina grit discharged from a 4.8 mm (0.1875 in.) diameter nozzle positioned at an angle of 20° to the surface, 51 mm (2 in.) from the coating surface. The air pressure was maintained at 105 Pa (15 psig) during the 30-second test. Approximately 160 grams of SS White No. 3 alumina grit was used for each test. These test conditions were chosen to prevent penetration of the ceramic layer during the test on the basis of preliminary test results. On the few occasions when penetration did occur, the test was terminated as soon as the underlying metal in the bond or intermediate coating was observed and the weight loss data were normalized to 30 seconds.

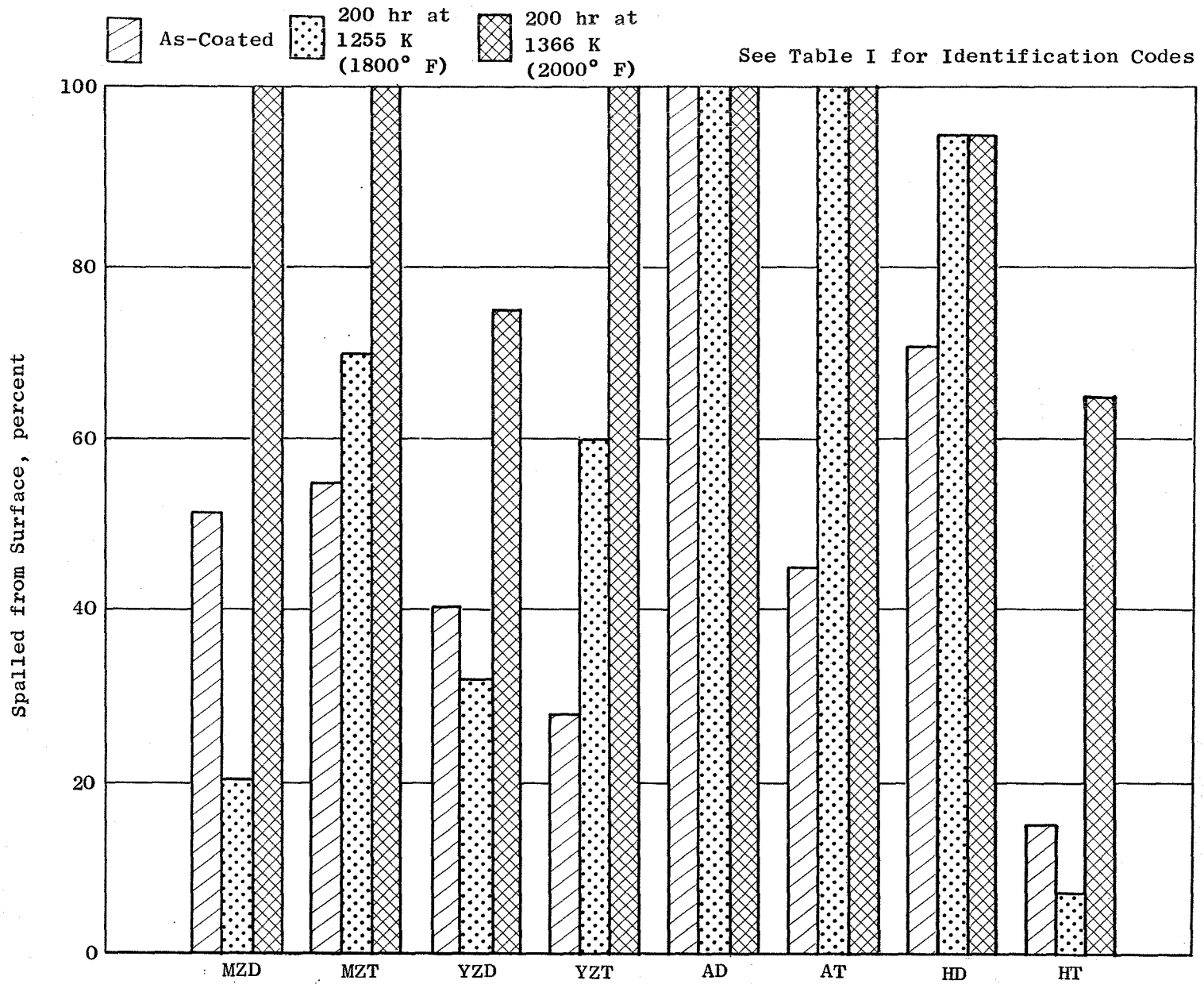


Figure 3. Bend Test Results Showing Extent of Coating Spallation in the As-Coated Condition and After 1255 K (1800° F)/200-Hour and 1366 K (2000° F)/200-Hour Exposures (Average of Three Exposures).

The test severity was calibrated using Ti-6Al-4V panels which were eroded at intervals between coating tests. The calibrations showed that the erosion severity was essentially unchanged throughout the testing.

The erosion test results are shown in Figure 4. In the as-deposited condition, Al₂O₃ coatings were the most erosion resistant followed by ZrO₂-20%MgO, HfO₂, and finally ZrO₂-20%Y₂O₃ being the least resistant. After thermal exposure for 200 hours at 1255 K (1800° F), both of the Al₂O₃ coating systems spalled and were unsuitable for erosion testing. All other coatings, with the exception of the HfO₂ triplex system, had greater erosion resistance after thermal exposure at 1255 K (1800° F) than before. ZrO₂-24%MgO coatings, which had the best erosion resistance of specimens exposed at 1255 K (1800° F), eroded at about four times the rate of Codep-coated René 80. The erosion resistance of HfO₂ and ZrO₂-20%Y₂O₃ improved further as a result of thermal exposure for 200 hours at 1366 K (2000° F), but the ZrO₂-24%MgO coatings spalled and were not tested.

3.3.6 Thermal Cycle Testing

Thermal-barrier-coated button specimens 25 mm (1 in.) in diameter by 3.2 mm (0.125 in.) thick and coated on one side were thermal cycled between natural gas-fired heating stations and cold air jet cooling stations in the test rig shown in Figure 5. The specimens were supported on fixtures which periodically advanced the specimens to the next test station. Specimens were heated to a temperature of 1310 K (1900° F) in approximately 30 seconds, held at that temperature for a period of 60 seconds, and then cooled to about 420 K (300° F) in 60 seconds. A schematic of the temperature cycle is shown in Figure 6. Testing was interrupted periodically and the specimens were removed for visual examination for coating damage and photographing when necessary to document changes in the coating condition.

The test results are shown in Figure 7, where percent coating loss is plotted as a function of number of thermal cycles. The ZrO₂-24%MgO and HfO₂ duplex systems exhibited the least coating loss, with both the ZrO₂-20%Y₂O₃ duplex and triplex coating systems also showing good resistance to thermal cycling. Overall, the duplex coating systems showed better resistance to thermal cycling than the triplex systems. The obvious exceptions were the Al₂O₃ duplex coating specimens which lost most of their coating after relatively few thermal cycles. Triplex coatings with Al₂O₃ and ZrO₂-24%MgO ceramic layers underwent on the order of a 20% loss in 3000 cycles and loss from the HfO₂ triplex coatings was approximately 35%.

3.3.7 Furnace Exposure Testing

Coated specimens were exposed to high temperature oxidation at 1255 K (1800° F), and 1366 K (2000° F). The specimens, 25 mm (1 in.) diameter buttons and 25 mm by 100 mm by 1.6 mm (1 in. by 4 in. by 0.062 in.) panels, which were coated on one side only, were supported by a 41 cm by 75 cm (16 in. by

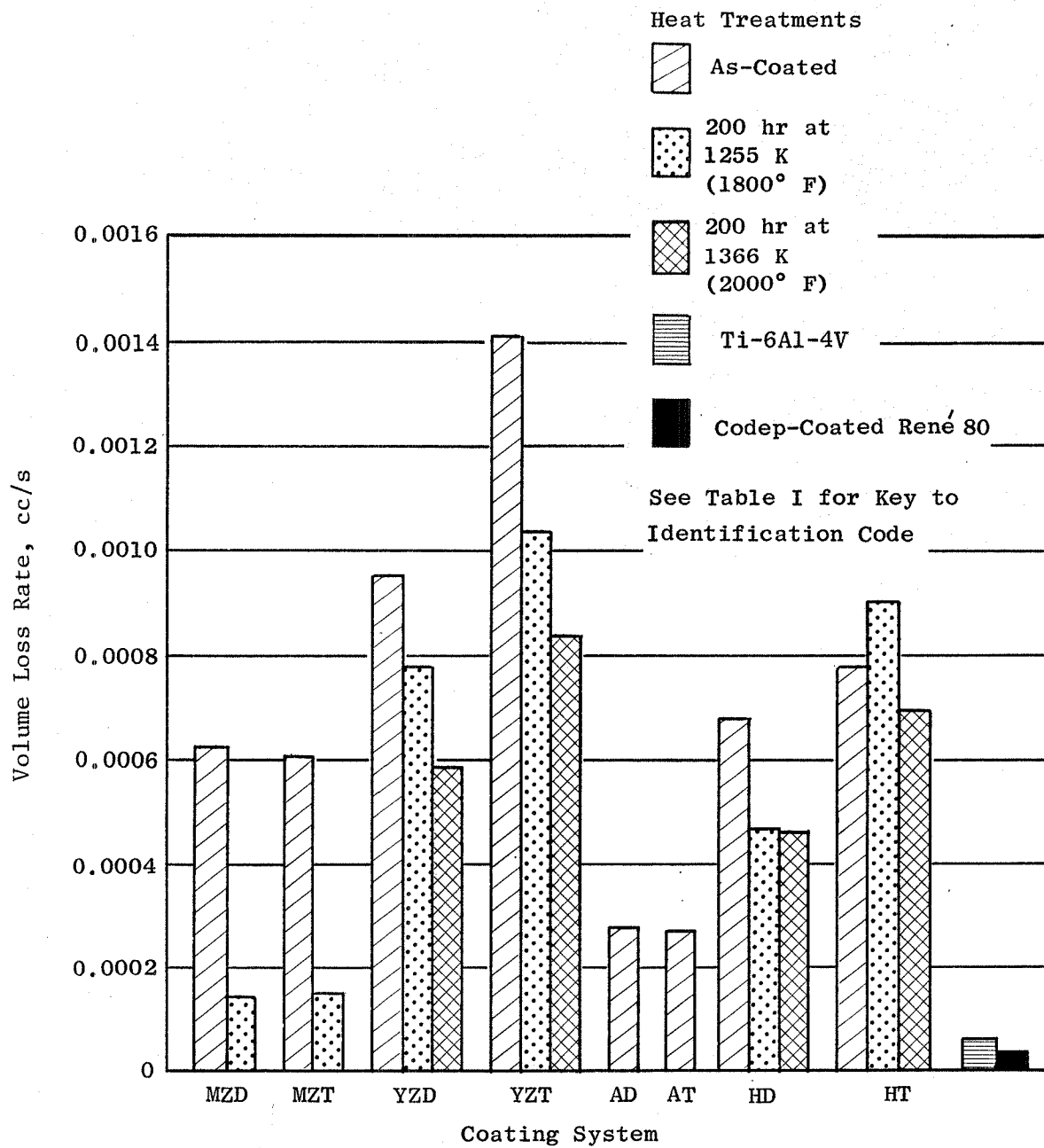


Figure 4. Erosion Test Results (Average of Two Specimens).

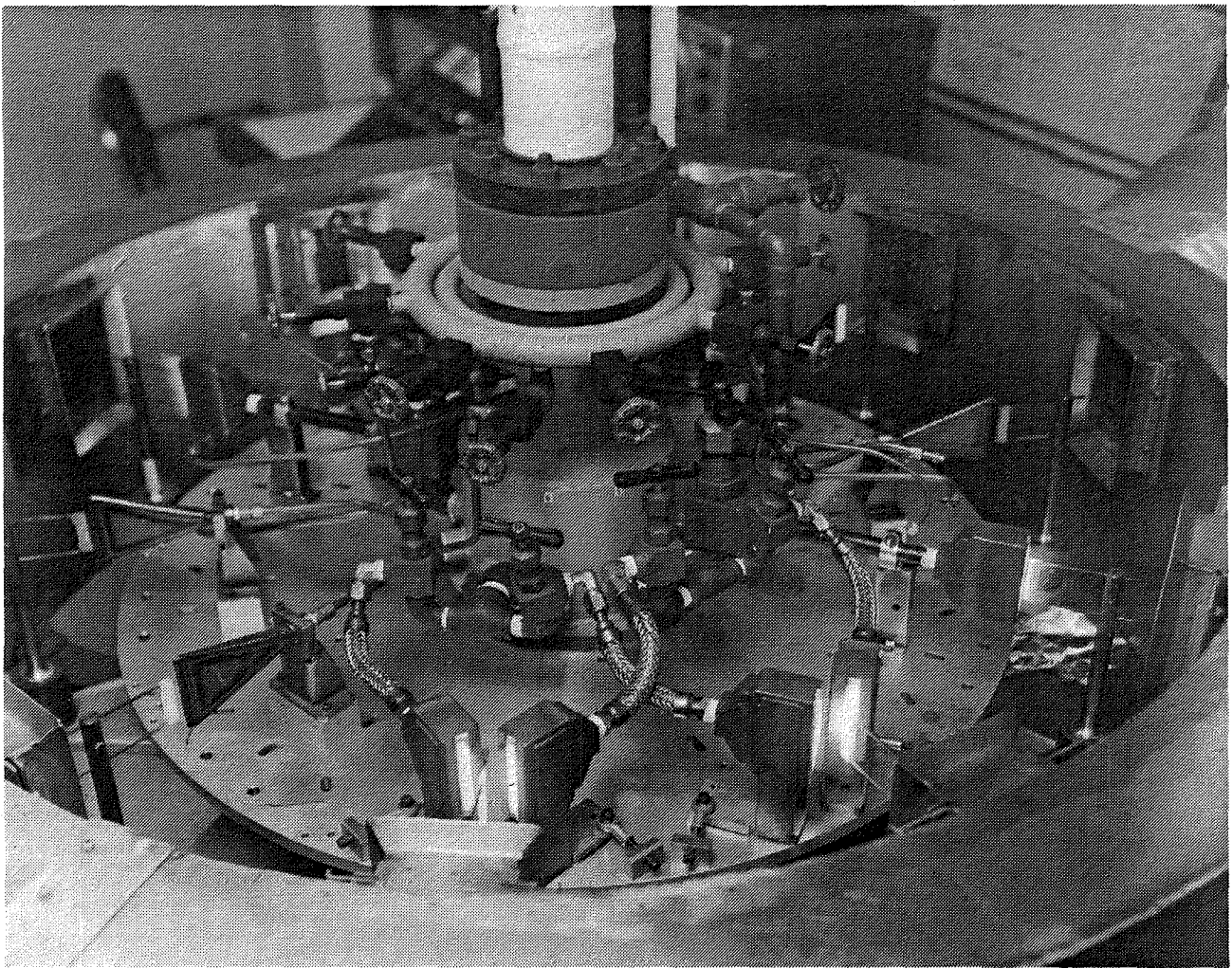


Figure 5. Thermal Shock Test Rig.

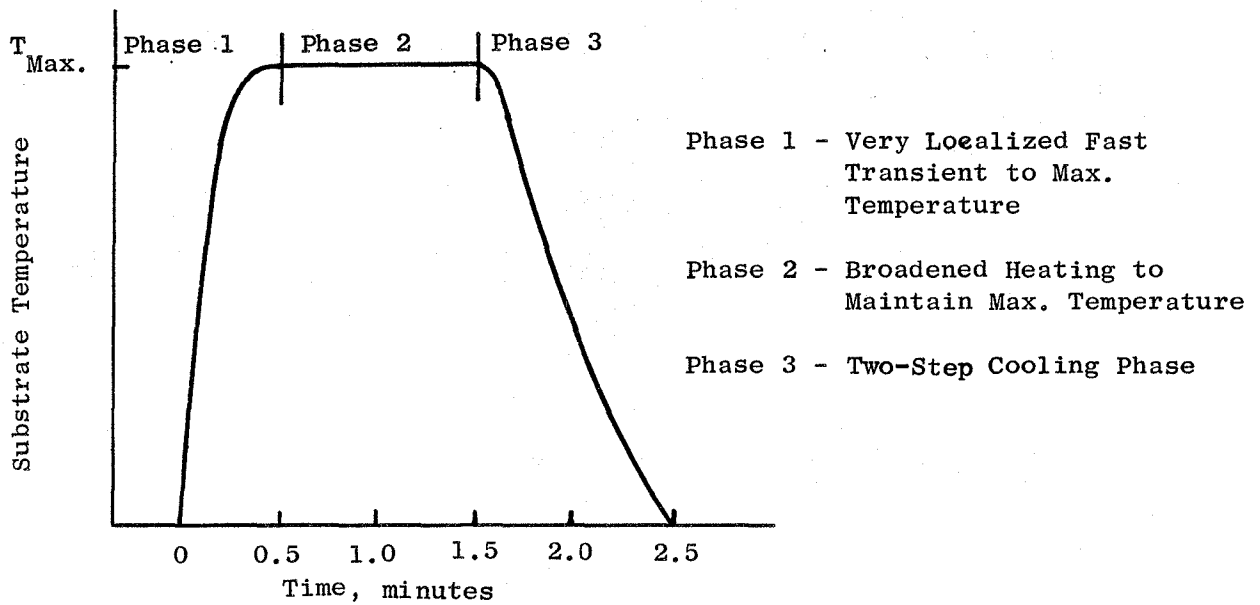


Figure 6. Thermal Cycle for Thermal Shock Testing.

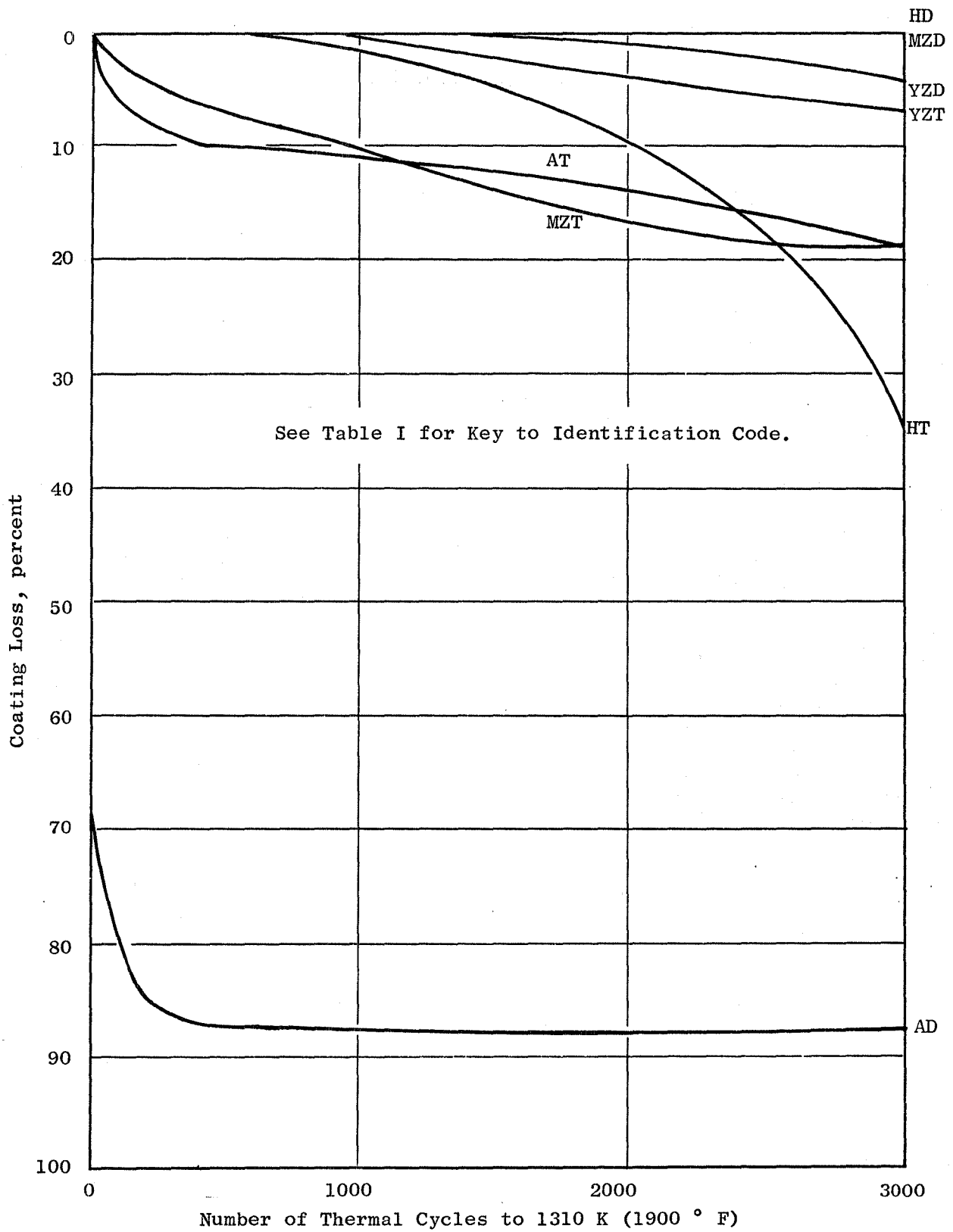


Figure 7. Thermal Cycle Test Results.

29 in.) double shelf rack of Inconel 718 in the test furnace. During the exposure at 1255 K (1800° F), the specimens were maintained at test temperature for 200 hours, cooled and examined. Visual observations of these coatings are recorded in Table IV. Both the duplex and triplex Al₂O₃ coatings were spalled after thermal exposure at 1255 K (1800° F). The three other coating systems, ZrO₂-24%MgO, ZrO₂-20%Y₂O₃ and HfO₂, were well bonded and displayed no evidence of deterioration.

The specimens exposed at 1366 K (2000° F) were cooled to room temperature and examined after accumulated times of 50, 100, and 200 hours. All of the alumina coatings had spalled at the first inspection time of 50 hours, and these specimens were removed from test. All of the other coatings were intact after 50 hours. The ZrO₂-24%MgO coatings became somewhat discolored during the 1366 K (2000° F) exposure. After 50 and 100 hours, only the edges of the coating were affected; but after 200 hours, all of the surface of the coating was noticeably affected. The ZrO₂-24%MgO coatings, both duplex and triplex, also underwent some coating loss after 200 hours. A spalled chip from a ZrO₂-24%MgO duplex coating was examined by energy dispersive X-ray analysis (EDAX); the inner surface of the chip (next to the bond coat) showed the expected elements but the outside (brown) surface clearly had a significant amount of chromium present. The spalled alumina had also exhibited a pinkish hue, suggesting contamination. The source of the contamination was believed to be spalled oxide scale from the Inconel furnace rack. Subsequent thermal exposures were performed on zirconia firebrick covered with a layer of spun alumina.

All of the panel specimens which were coated with triplex coating systems exhibited bending after exposure at 1366 K (2000° F), with the coated side of the specimen being on the convex side of the bend. The amount of bend increased with test time at 1366 K (2000° F). After 50 hours, slight bending of approximately 3 mm (0.125 in.) at the center of a 100 mm (4 in.) long panel was observed, increasing to about 6 mm (0.250 in.) after 100 hours and 9 mm (0.375 in.) after 200 hours at 1366 K (2000° F). Results are shown in Figure 8. This bending appears to be associated with the oxidation of metal particles (and resultant increase in volume) in the blend layer of triplex coatings.

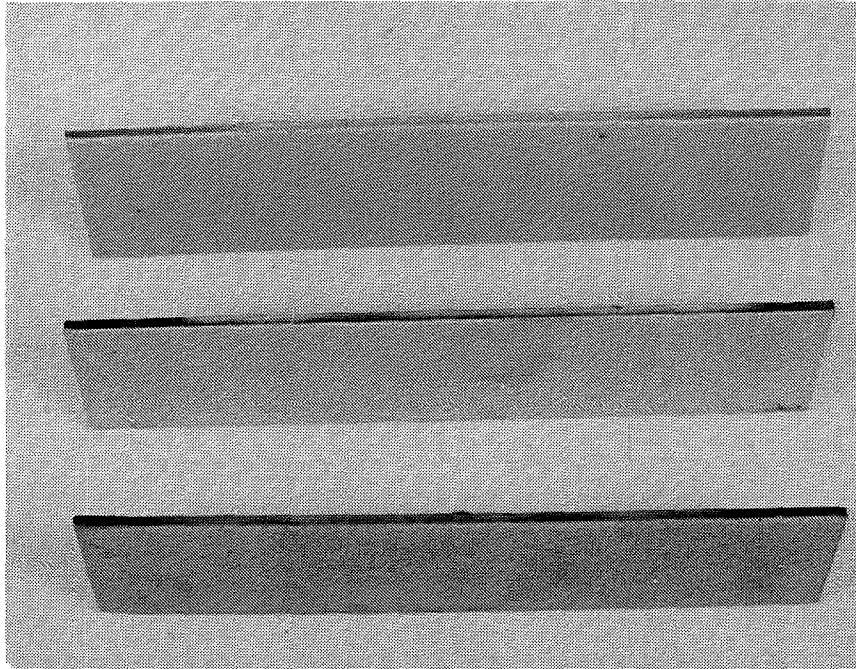
3.3.8 High Velocity Dynamic Oxidation Testing

A test was conducted to compare the durabilities of the eight candidate coating systems under conditions of high velocity, hot gas dynamic oxidation. The test was conducted in a burner rig in which the combustor was mounted vertically and the hot gas vented directly upwards into a stainless steel, heavily insulated stack. The specimen holder was connected to a horizontal hydraulic drive shaft that drove the specimens in and out of the hot gas stream. A slipring mounted to the drive shaft of the 1725 rpm specimen drive motor allowed continuous monitoring of a thermocouple embedded in a dummy specimen. The fuel was JP-5 (MIL-J-5634F) containing 0.047% sulfur. Specimens were 6.3 mm (0.25 in.) diameter by approximately 100 mm (4 in.) long rods, rounded on one end. The majority of the specimens were René 80, but some Hastelloy X specimens were included as well.

Table IV. Visual Observations of Specimens Exposed at 1255 K (1800° F) and 1366 K (2000° F).

Coating ⁽¹⁾ System	1255 K (1800° F)/200 hr	1366 K (2000° F)/50 hr	1366 K (2000° F)/100 hr	1366 K (2000° F)/200 hr	Ranking
MZD	OK	Good adherence No bending Edges slightly discolored	Edge chipping on buttons Browning of edges	Spalling at edges 40% spalled Browning of surface	6
MZT	OK	Good adherence Slight bend (3 mm at center) Edge slightly discolored	Slight edge chipping on button Browning on edge Bending (6 mm at center)	Spalling on one side of 10% Browning of surface Bending (6 mm at center)	5
YZD	OK	Good adherence No color change No bending	Good adherence No color change No bending	Good adherence No color change No bending	1
YZT	OK	Good adherence No color change Slight bend (3 mm at center)	Slight edge cracking on buttons Bend (6 mm at center)	Good adherence No color change Bend (9 mm at center)	3
AD	Spalled off completely at bond coat interface	Spalled off Pinkish color Removed from test No bending - FAILED	---	---	---
AT	Spalled off slightly at Al ₂ O ₃ layer	Spalled off Pinkish color Removed from test No bending - FAILED	---	---	---
HD	OK	Good adherence No bending	Good adherence Flat	Good adherence No color change Flat	1
HT	OK	Good adherence Bending (3 mm at center)	Good adherence Bending (6 mm at center)	Good adherence No color change Bending (9 mm at center)	3

(1) See Table I for key to identification code.

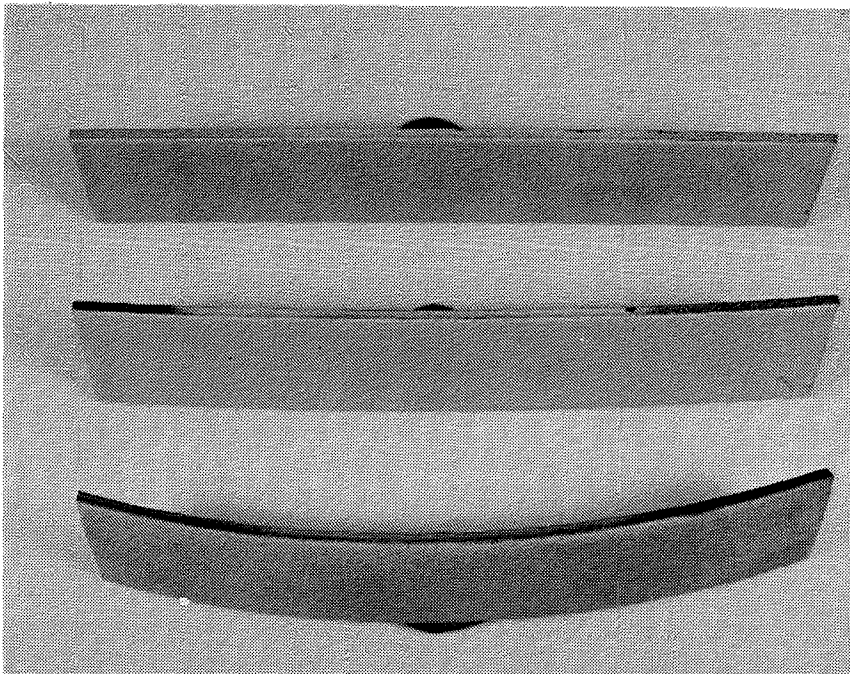


As-Coated

200 Hours at 1255 K
(1800° F)

200 Hours at 1366 K
(2000° F)

DUPLEX COATINGS



As-Coated

200 Hours at 1255 K
(1800° F)

200 Hours at 1366 K
(2000° F)

TRIPLEX COATINGS

Figure 8. Bend Test Results of Thermal-Barrier-Coated Specimens with $ZrO_2-20\%Y_2O_3$ Top Coat.

Two tests were conducted under the test conditions shown in Table V, and the results are shown in Tables VI and VII. Failure was defined as the appearance of spalled areas on the thermal-barrier-coated specimen such that discontinuous and nonuniform coating protection remained. Some of the specimens were not removed after coating failure occurred, but were allowed to continue in order to evaluate the degree of protection afforded by the underlying intermediate and/or bond coat layers.

Table V. High Velocity Dynamic Oxidation Burner Rig Parameters.

Specimen Surface Temperature	1366 K \pm 30 (2000° F \pm 50)
Flame Temperature	1615 K (2450° F)
Airflow	5.2 kg/min (11.4 lb/min)
Fuel Flow	0.2 kg/min (0.4 lb/min)
Air-Fuel Ratio	28.5
Air Velocity	625 m/sec (2050 ft/sec)
Mach Number	0.84
Cycle	55 minutes at 1366 K (2000° F) 5 minutes cooldown to ~300 K (~100° F)

In the first test (Table VI) which lasted 143 cycles (1 hour/cycle), the baseline specimen, No. 25, was a René 80 pin with a Codep B coating. This specimen survived all 143 hours of cyclic testing without failure. Figure 9 shows in bar chart form the exposure to which each specimen was subjected. The coating with the longest life in this test (other than the baseline) was specimen No. 19, a Hastelloy X specimen coated with the ZrO₂-20%Y₂O₃ duplex coating system. This specimen survived 107 cycles without coating failure.

A total of 15 specimens (Table VII) were tested during the second burner rig test. Figure 10 shows the test schedule. The specimen with the longest life in this test was a René 80 specimen coated with the ZrO₂-20%Y₂O₃ duplex TBC coating system.

Table VIII presents a summary of the results of the high-velocity dynamic oxidation tests. The ZrO₂-20%Y₂O₃ duplex coating system proved to be the most durable coating system with specimens averaging 92 hours to failure. This was considerably longer than any of the other systems, the next best coating systems being the ZrO₂-24%MgO duplex and triplex systems with average lives of 68 and 64 hours, respectively.

Table VI. Summary of Results of First High Velocity Dynamic Oxidation Test (Total Time = 143 Hours).

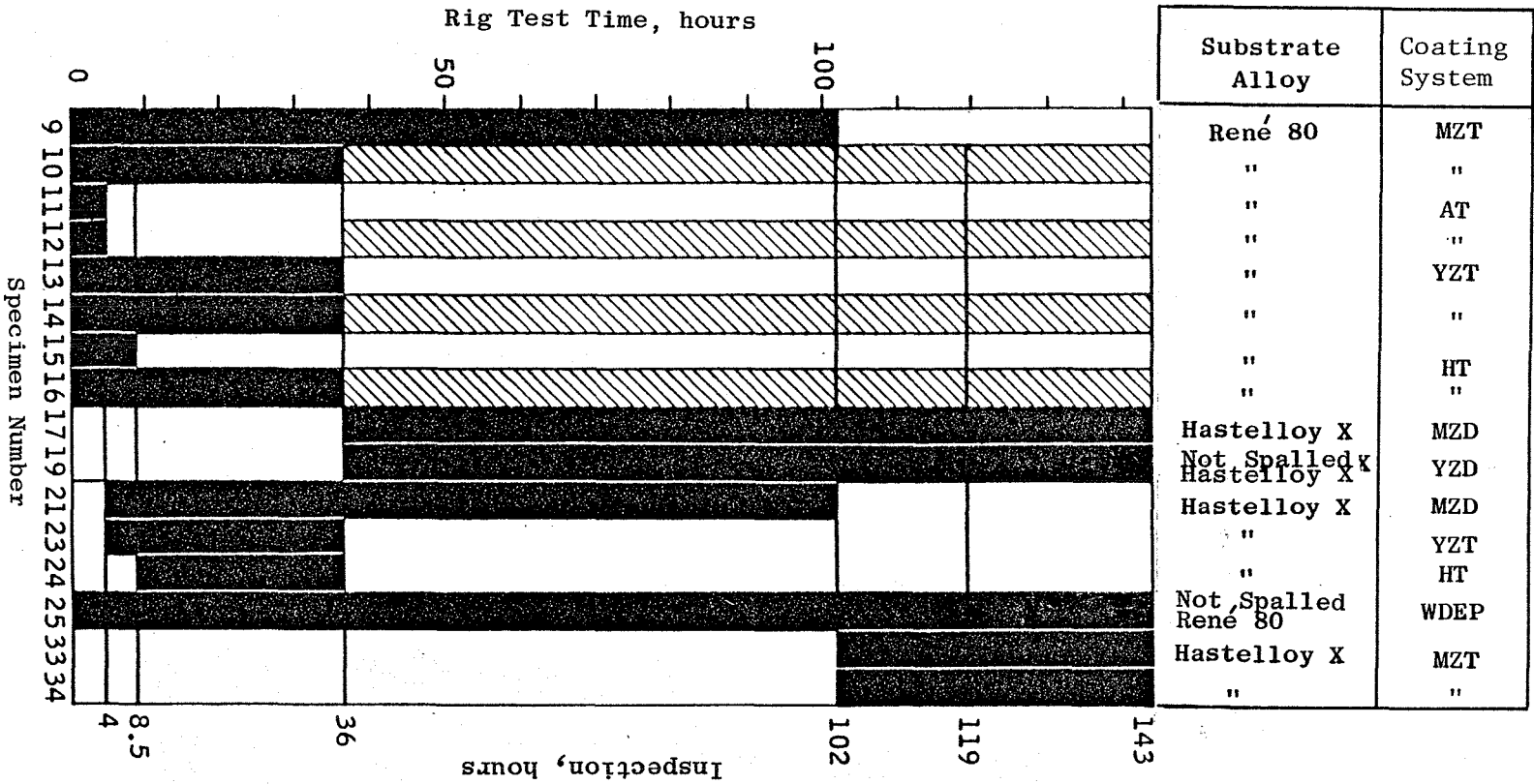
Specimen	Coating System	Substrate Alloy	Cycles to Failure	Weight Change at Failure (mg)	Total Cycles Exposed
9	ZrO ₂ -24%MgO Triplex	René 80	102	-265	102
10	ZrO ₂ -24%MgO Triplex	René 80	36	---	143
11	Al ₂ O ₃ Triplex	René 80	4	-732	4
12	Al ₂ O ₃ Triplex	René 80	4	-811	111
13	ZrO ₂ -20%Y ₂ O ₃ Triplex	René 80	36	-146	36
14	ZrO ₂ -20%Y ₂ O ₃ Triplex	René 80	36	-34	143
15	HfO ₂ Triplex	René 80	8	-1612	8
16	HfO ₂ Triplex	René 80	36	-650	143
17	ZrO ₂ -24%MgO Duplex	Hastelloy X	107	-251	107
19	ZrO ₂ -20%Y ₂ O ₃ Duplex	Hastelloy X	>107	(+8)*	107
21	ZrO ₂ -24%MgO Triplex	Hastelloy X	98	-247	98
23	ZrO ₂ -20%Y ₂ O ₃ Triplex	Hastelloy X	32	-264	32
24	HfO ₂ Triplex	Hastelloy X	28	-1243	28
25	Codep	Hastelloy X	>143	(+8)*	143
33	ZrO ₂ -24%MgO Triplex	Hastelloy X	41	-24	41
34	ZrO ₂ -24%MgO Triplex	Hastelloy X	41	-84	41

*Weight change at end of testing

Table VII. Summary of Results of Second High Velocity Dynamic Oxidation Test (Total Time = 97 Hours).

Specimen	Coating System	Substrate Alloy	Cycles to Failure	Weight Change at Failure (mg)	Total Cycles Exposed
1	ZrO ₂ -24%MgO Duplex	René 80	71	-221	71
2	ZrO ₂ -24%MgO Duplex	René 80	71	---	97
3	Al ₂ O ₃ Duplex	René 80	4	-341	4
4	Al ₂ O ₃ Duplex	René 80	4	-428	30
5	ZrO ₂ -20%Y ₂ O ₃ Duplex	René 80	71	-14	71
6	ZrO ₂ -20%Y ₂ O ₃ Duplex	René 80	97	-10	97
7	HfO ₂ Duplex	René 80	24	-1635	24
8	HfO ₂ Duplex	René 80	4	-1033	30
26	Codep	René 80	>97	(+8)*	97
27	ZrO ₂ -24%MgO Duplex	Hastelloy X	44	---	67
28	ZrO ₂ -24%MgO Duplex	Hastelloy X	44	---	93
29	ZrO ₂ -24%MgO Duplex	Hastelloy X	67	-35	67
30	ZrO ₂ -24%MgO Duplex	Hastelloy X	73	-28	73
31	ZrO ₂ -24%MgO Duplex	Hastelloy X	>26	(+19)*	26
32	ZrO ₂ -24%MgO Duplex	Hastelloy X	>26	(+17)*	26

*Weight change at end of testing

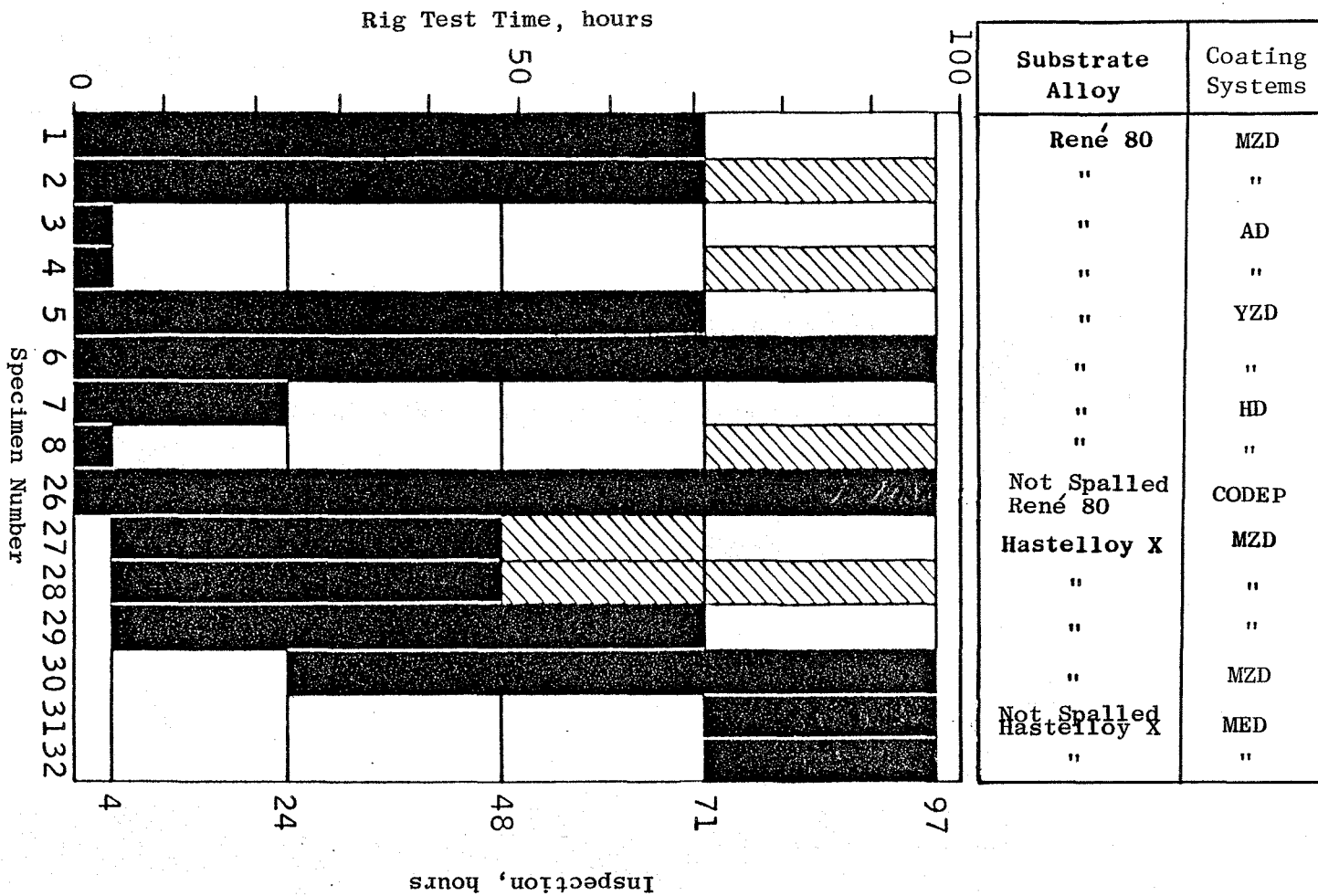


See Table I for Identification Code.

- Cycles to Failure
- ▨ Continued Exposure After Failure

Figure 9. First High Velocity Dynamic Oxidation Test Schedule.

Figure 10. Second High Velocity Dynamic Oxidation Test Schedule.



See Table I for Identification Code.

- Cycles to Failure
- ▨ Continued Exposure After Failure

Table VIII. Summary of High Velocity Dynamic Oxidation Test Results.⁽¹⁾

Coating System	No. of Specs. Tested ⁽²⁾	Time (hours) to Failure		
		Earliest	Longest	Average
ZrO ₂ -20%Y ₂ O ₃ Duplex	3	71	>107 ⁽³⁾	92
ZrO ₂ -20%Y ₂ O ₃ Triplex	3	32	36	35
ZrO ₂ -24%MgO Duplex	9	44	107	68
ZrO ₂ -24%MgO Triplex	5	36	102	64
HfO ₂ Duplex	2	4	24	14
HfO ₂ Triplex	3	8	36	24
Al ₂ O ₃ Duplex	2	4	4	4
Al ₂ O ₃ Triplex	2	4	4	4

(1) One hour cycle [55 min at 1366 K (2000° F) in Mach 0.8 JP-5 flame, 5 min air blast].

(2) Each coating tested on two René 80 pins; remainder of specimens Hastelloy X.

(3) Coating did not fail.

3.3.9 Selection of Three Coating Systems

Three coating systems were selected, based on the results of the preliminary screening tests, for further evaluation. The results of these tests are summarized in Table IX where the coating systems are ranked based on the results of the bend tests, erosion tests, thermal exposure tests, thermal cycle tests, and high velocity dynamic oxidation tests. The three coating systems having the best average ranking (lowest number) were ZrO₂-Y₂O₃ duplex, ZrO₂-MgO duplex, and HfO₂ duplex.

The alumina coating systems, both duplex and triplex, ranked low because of their early and extensive spalling in thermal exposure tests, thermal cycle tests, and high velocity dynamic oxidation tests. The other triplex coating systems ranked lower than their duplex counterparts primarily because of their poorer durabilities in thermal exposure, thermal cycling, and high velocity tests, although the HfO₂ triplex system was somewhat better than the HfO₂ duplex system in the latter test.

The three selected coating systems, all duplex coatings, have ceramic top coat materials of ZrO₂-24%MgO, ZrO₂-20%Y₂O₃, and HfO₂. The bond coat alloy for all coatings was Ni-Cr-Al-Y.

3.4 ADDITIONAL EVALUATION OF THREE COATING SYSTEMS

The three thermal barrier coating systems selected on the basis of the screening test results were further evaluated with the goal of selecting the coating system having the most potential for use on turbine airfoils. As stated above, the selected systems, all duplex coatings with Ni-22Cr-10Al-1Y bond coats, had ceramic coating layers of (1) magnesia-modified zirconia (ZrO₂-24%MgO), (2) yttria-stabilized zirconia (ZrO₂-20%Y₂O₃), and (3) hafnium oxide (HfO₂). These three TBC systems were applied to four substrate alloys which are used in the engine components of interest: the nickel-base alloy DS René 150 and René 80, and cobalt-base X-40 and HS 188 alloys.

All coatings were applied by the arc plasma spray process. Bond coats were deposited to a nominal thickness of 0.13 mm (0.005 in.) and the ceramic top coat layers were applied to a nominal thickness of 0.25 mm (0.010 in.). Extensive metallographic observations were made on all three coating systems. The three systems were evaluated in thermal shock testing, high cycle fatigue, thermal exposure, tensile bond, and impact testing. The results of these tests are described below.

3.4.1 Thermal Cycle Testing

In thermal cycle testing, 25 mm (1 in.) diameter button specimens coated on one side were thermal cycled between 1319 K (1900° F) and about 420 K (300° F) as described in Section 3.3.6. Test results, showing percent coating loss as a function of number of thermal cycles, are shown in Figure 11.

Table IX. Summary of Coating System Ranking From Preliminary Screening Tests.

Coating System	Ranking					
	Bend Test ⁽¹⁾	Erosion ⁽²⁾	Thermal Exposure ⁽³⁾	Thermal Cycling ⁽⁴⁾	High Velocity Dynamic Oxidation ⁽⁵⁾	Average
ZrO ₂ -Y ₂ O ₃ Duplex	2	7	1	3	1	2.8
ZrO ₂ -Y ₂ O ₃ Triplex	4	8	3	4	4	4.6
ZrO ₂ -MgO Duplex	3	3	6	1	2	3.0
ZrO ₂ -MgO Triplex	5	3	5	5	3	4.2
HfO ₂ Duplex	6	5	1	1	6	3.8
HfO ₂ Triplex	1	6	3	7	5	4.4
Al ₂ O ₃ Duplex	8	1	7	8	7	6.2
Al ₂ O ₃ Triplex	6	1	7	5	8	5.4

(1)Least coating loss (Figure 3).

(2)Lowest erosion loss (Figure 4).

(3)Ranking from Table IV.

(4)Least coating loss in 3000 cycles (Figure 7).

(5)Highest average time to failure (Table VIII).

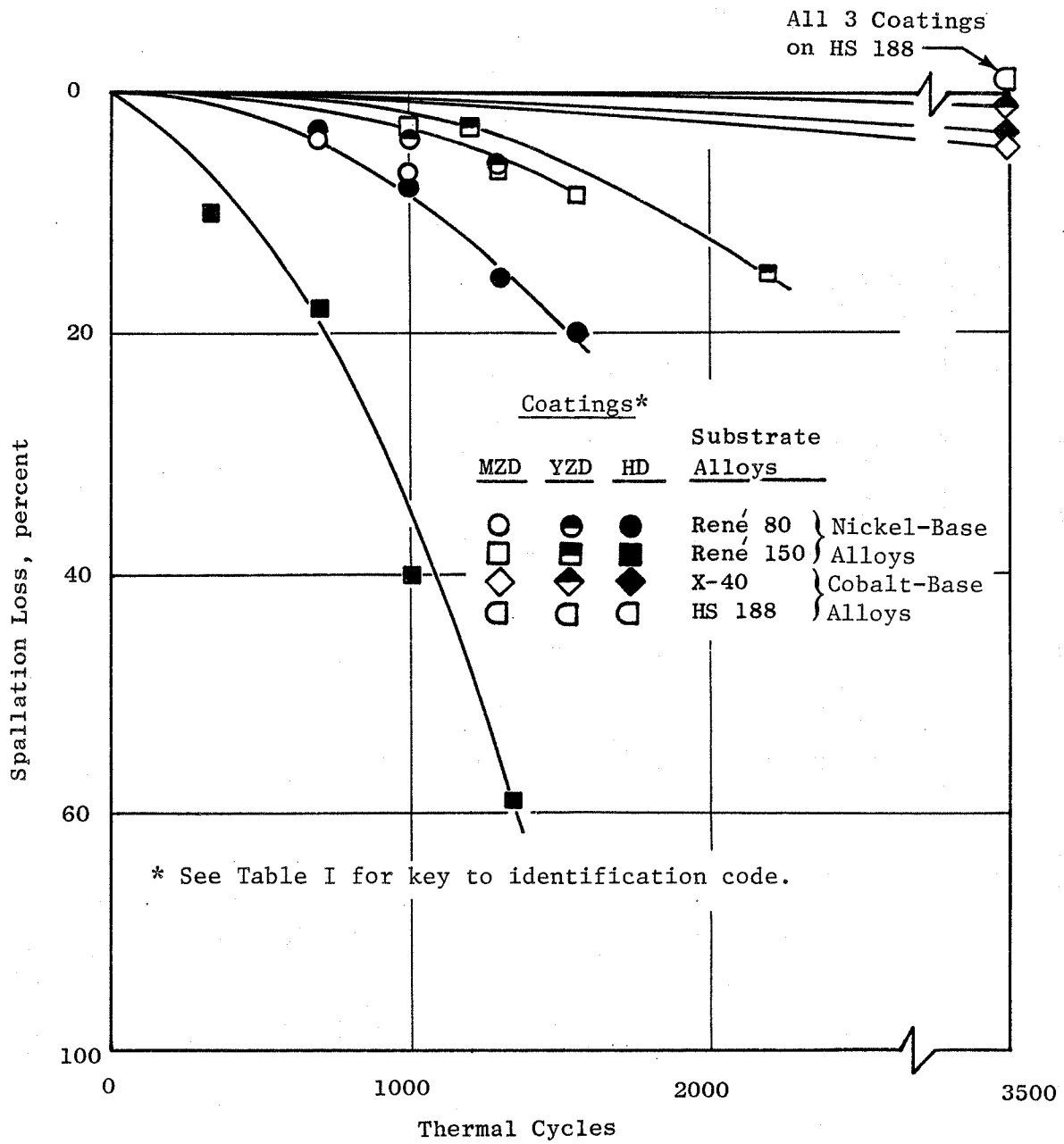


Figure 11. Thermal Cycle Test Results.

All three coating systems performed well when tested on HS 188 and X-40 alloy substrates (cobalt-base alloys). Essentially no coating loss occurred from HS 188 specimens and only minor amounts of coating loss occurred from X-40 specimens in 3500 cycles of testing. In contrast, significant amounts of coating loss occurred from the nickel-base alloy specimens, René 80 and DS René 150. The ZrO₂-Y₂O₃ coatings lost the least amount of coating irrespective of substrate composition; ZrO₂-MgO coating loss was not much greater than the loss from ZrO₂-Y₂O₃ coatings. The greatest effect of the substrate on coating life was noted for HfO₂ coatings.

The coatings did not perform best (as measured by the amount of coating loss in thermal cycle and thermal exposure tests) on substrates with which they had the least thermal expansion mismatch. As shown in Figure 12, the thermal expansion mismatch between ZrO₂-Y₂O₃ and alloy HS 188 is greater than the mismatch between ZrO₂-Y₂O₃ and DS René 150, yet the performance of ZrO₂-Y₂O₃ was better on alloy HS 188 than on DS René 150. This also held true for ZrO₂-MgO and HfO₂ coatings.

Based upon these results, the following conclusions were reached:

1. The ZrO₂-20%Y₂O₃ coating exhibited the best thermal cycle resistance of all three candidate top coat materials.
2. Substrate markedly affects thermal cycle behavior, with the cobalt-base specimens losing much less coating than specimens of the nickel-base alloys René 80 and DS René 150.

3.4.2 High Cycle Fatigue Testing

René 80 and DS René 150 test specimens coated with the three candidate coating systems were high cycle fatigue (HCF) tested at an indicated temperature 1255 K of (1800° F) with an A ratio (alternating stress/mean stress) of 0.95. Uncoated specimens also were tested. Both coated and uncoated specimens prior to test are shown in Figure 13. In these tests, the specimens were heated to test temperature by induction heating, and temperature was measured using a calibrated Ircon radiation pyrometer. A small area of the TBC was covered with Pyromark^R (R - Tempil Division, Big Three Industries, Inc.) which has a known emittance, and the radiation pyrometer was adjusted to this emittance value. The specimens were held at test temperature for approximately 1 hour prior to testing to equalize the temperature distribution along the grips and load train. After the soak at test temperature, the load train was secured to the specimen and the static and dynamic loads applied. Tests were run to specimen failure or 10⁷ cycles.

Subsequent to the testing, temperature calibration runs were made using runout specimens which were drilled axially to accommodate a thermocouple. Surface temperatures of the uncoated specimens measured optically agreed with bulk temperatures measured with the thermocouple. However, for specimens with thermal barrier coatings, the bulk temperature as measured with the thermocouple was about 30 K (50° F) higher than the optical (surface) temperature

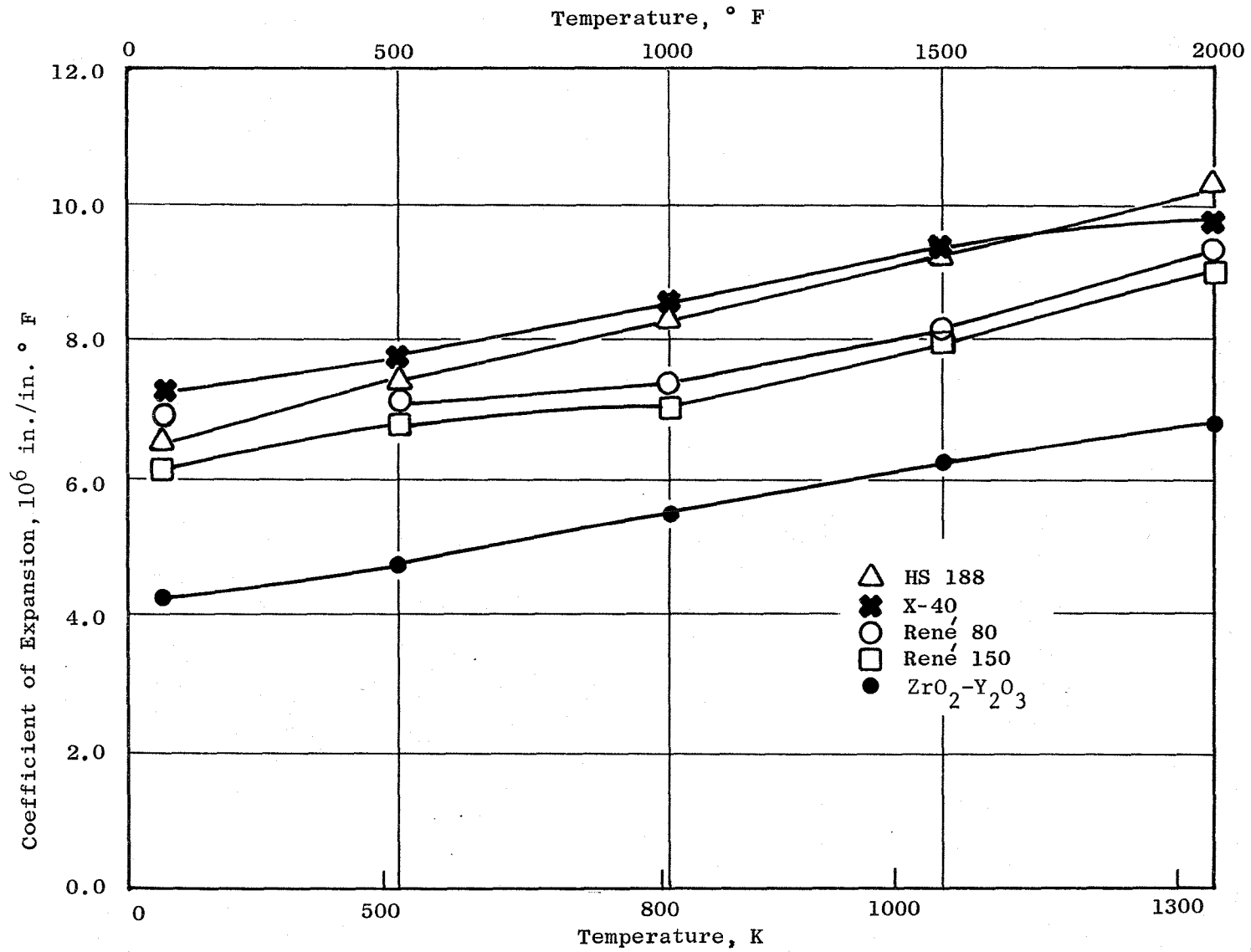


Figure 12. Thermal Expansion of Substrate Alloys and $\text{ZrO}_2\text{-Y}_2\text{O}_3$.

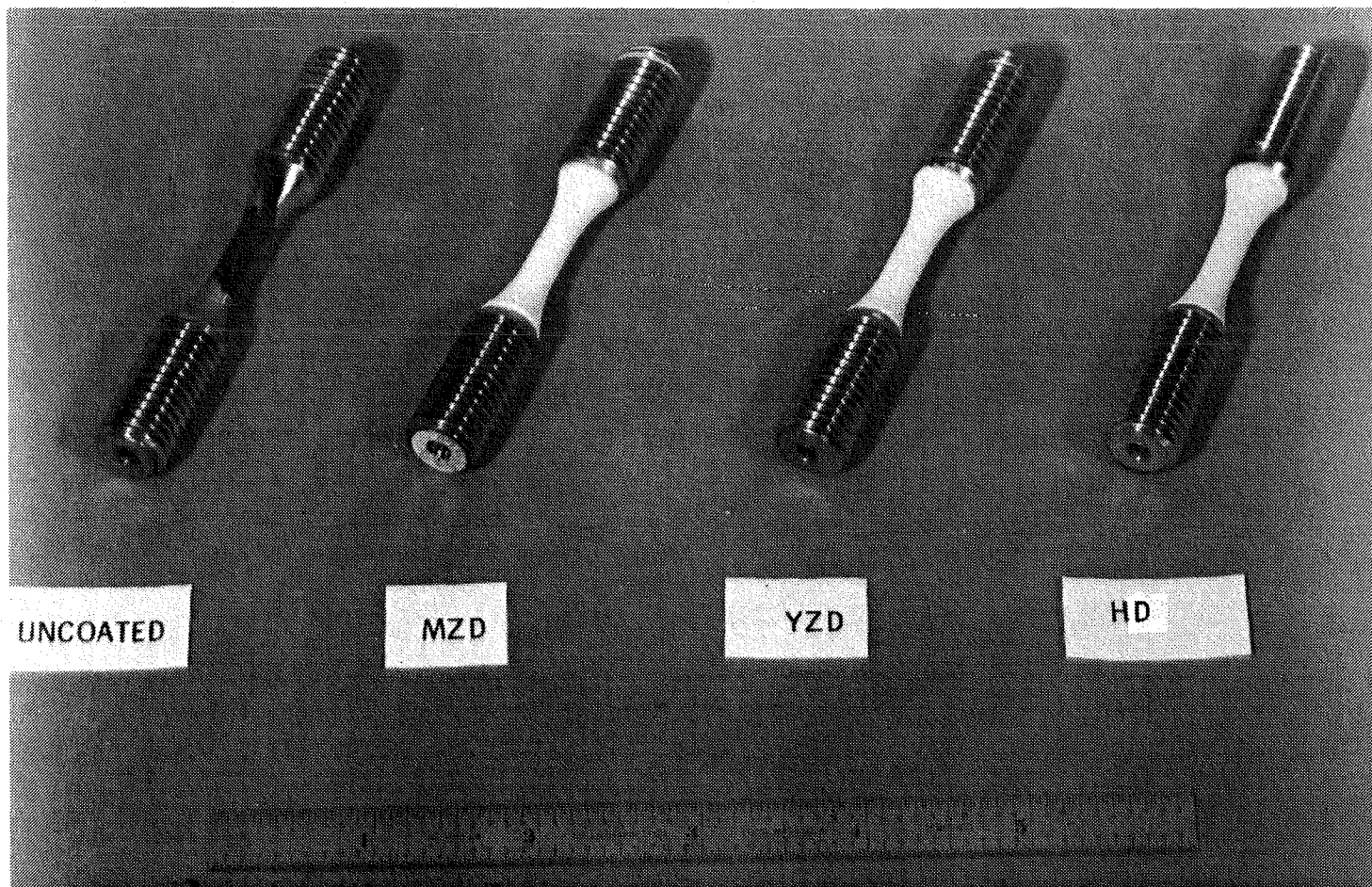


Figure 13. DS René 150 High Cycle Fatigue Specimens Coated with Candidate TBC Systems.

of the coating surface. This difference can be attributed to the fact that heat was generated inductively in the metal (under the TBC) and the TBC served to retard heat loss from the specimen surface. Thus a temperature drop occurred through the coatings with the outer surface of the TBC being cooler than the bulk temperature of the specimens. Since test temperatures had been adjusted to 1255 K (1800° F) based on surface temperature, the bulk temperature of the thermal-barrier-coated specimens was actually 1280 K (1850° F).

Results of the high cycle fatigue test are shown in Figure 14. The HCF strength of the thermal-barrier-coated alloys tested at a metal temperature of 1280 K (1850° F) appears to be approximately 3.5 MPa (5 ksi) lower than that of the same alloy uncoated and tested at 1255 K (1800° F). The 3.5 MPa (5 ksi) difference in strength is very close to the difference attributable to a 30 K (50° F) difference in test temperature, thus the presence of TBC's on high cycle fatigue test specimens does not appear to have any detrimental effect on fatigue strength of René 80 or DS René 150 at this temperature.

3.4.3 Furnace Exposure Testing

Button specimens of the four substrate alloys coated with the three selected TBC systems were exposed to high temperature oxidation at 1255 K (1800° F) and 1366 K (2000° F) for times of 500 and 250 hours, respectively. No changes were detectable in the specimens after the 1255 K (1800° F) exposure except for a slight discoloring near the edges of ZrO₂-24%MgO coatings. After the 1366 K (2000° F) exposure, the ZrO₂-24%MgO and HfO₂ coatings spalled from the DS René 150 substrate. Although extensive oxidation was noted on the edges of René 150 substrates, no spallation of the ZrO₂-20%Y₂O₃ coating was evident.

3.4.4 Tensile Bond Testing

Tensile bond tests were conducted on duplicate specimens in the as-coated condition and on specimens which had been exposed for 500 hours at 1255 K (1800° F) and 250 hours at 1366 K (2000° F). These tests were conducted as described in Section 3.3.3. Results of the tests are presented in Table X. The adhesive/cohesive strengths of coated HS 188 alloy specimens were consistent with the strengths obtained from preliminary testing of these coatings. Coating strengths after the 1255 K (1800° F) exposure were not significantly different from as-coated strengths. However, the 250-hour exposure at 1366 K (2000° F) resulted in significant changes in most cases, with the ZrO₂-20%Y₂O₃ coating system showing the best overall behavior. The ZrO₂-20%Y₂O₃ coating was the only coating system that retained some bond strength on all four substrate alloys after the 1366 K (2000° F) exposure.

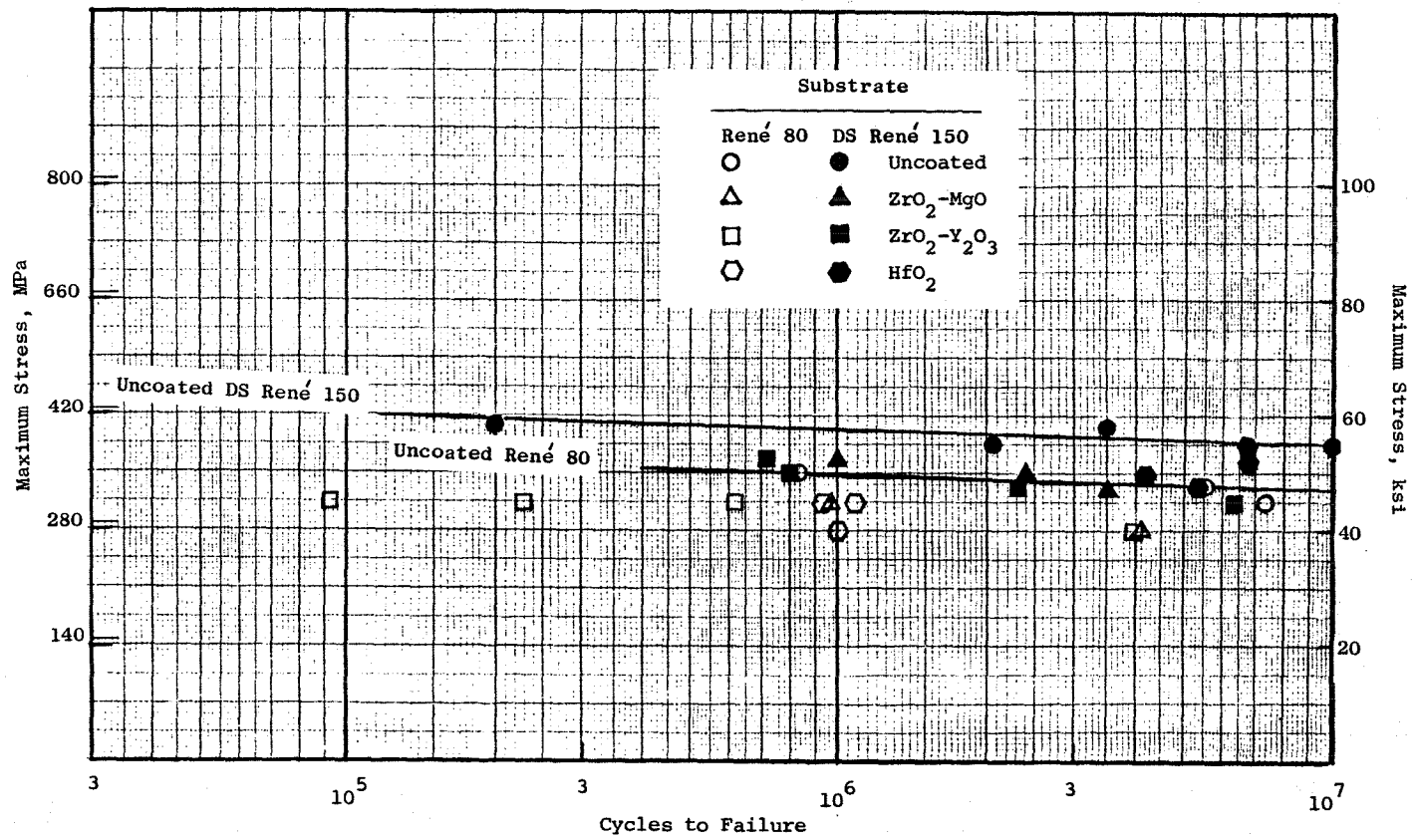


Figure 14. High Cycle Fatigue Test Results on Uncoated 1255 K (1800° F) and Thermal-Barrier-Coated 1280 K (1850° F) Specimens.

Table X. Tensile Bond Test Results.

Coating System/Substrate	Tensile Bond Strength - MPa, ksi		
	As-Coated	After 1255 K (1800° F)/500 hours Exposure	After 1366 K (2000° F)/250 hours Exposure
<u>ZrO₂-24%MgO</u>			
René 80	13.3 (1.9)	15.4 (2.2)	5.6 (0.8)
DS René 150	13.3 (1.9)	16.1 (2.3)	*
X-40	12.6 (1.8)	13.3 (1.9)	7.0 (1.0)
HS 188	10.5 (1.5)	14.7 (2.1)	16.8 (2.4)
<u>ZrO₂-20%Y₂O₃</u>			
René 80	11.9 (1.7)	8.4 (1.2)	1.4 (0.2)
DS René 150	8.4 (1.2)	10.5 (1.5)	6.3 (0.9)
X-40	11.2 (1.6)	9.1 (1.3)	9.1 (1.3)
HS 188	11.2 (1.6)	10.5 (1.5)	10.5 (1.5)
<u>HfO₂</u>			
René 80	17.5 (2.5)	11.2 (1.6)	*
DS René150	15.4 (2.2)	15.4 (2.2)	*
X-40	14.7 (2.1)	9.8 (1.4)	4.9 (0.7)
HS 188	13.3 (1.9)	7.7 (1.1)	5.6 (0.8)
*Not tested; coating spalled during exposure.			

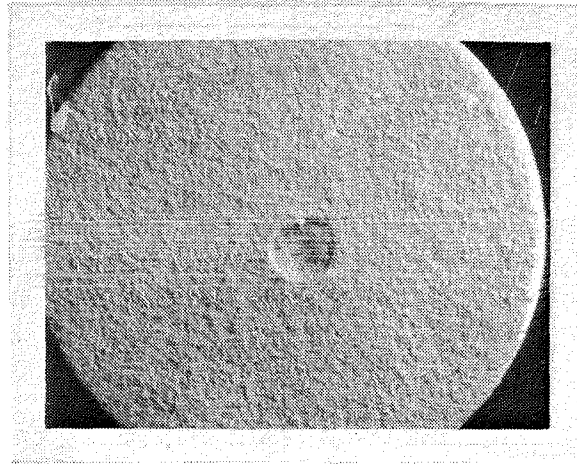
3.4.5 Impact Testing

The ability of the selected TBC systems to withstand ballistic impact was measured in laboratory tests. Thermal-barrier-coated button specimens were impacted at room temperature with spherical steel projectiles 4 mm (0.175 in.) in diameter. Impact tests were performed at 20° and 90° incidence angles to produce a moderate amount of coating damage. The nominal projectile energy was 1.35 J (1.0 ft-lb) for the 90° incidence angle tests, and 5.4 J (4.0 ft-lb) for the 20° angle tests. Typical coating damage which resulted from the impacts is shown in Figure 15. A summary of the impact conditions and the resulting coating losses is given in Table XI.

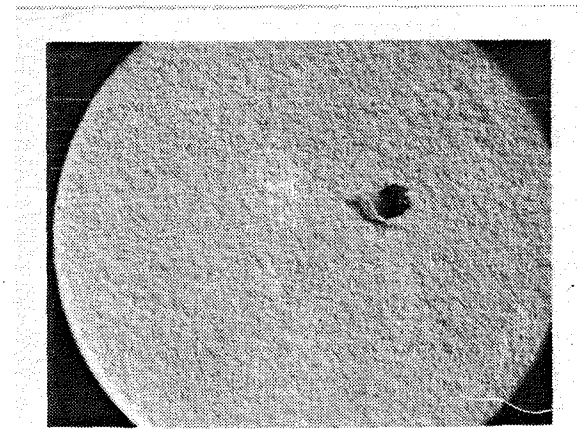
Table XI. Summary of Impact Test Results.(1)

Coating System	Substrate Alloy	Impact Angle, degrees	Energy, J (ft-lb)	Area Spalled, mm ² (in. ²)
ZrO ₂ -24%Mgo	X-40	90	1.27 (0.94)	36 (0.055)
	René 80	90	1.36 (1.00)	46 (0.071)
	René 150	90	1.40 (1.03)	24 (0.037)
	HS 188	90	1.38 (1.02)	3 (0.004)
ZrO ₂ -20%Y ₂ O ₃	X-40	90	1.26 (0.93)	19 (0.030)
	René 80	90	1.34 (0.99)	6 (0.010 & 0.019)(2)
	René 150	90	1.38 (1.02)	12 (0.019)
	HS 188	90	1.36 (1.00)	7 (0.011)
HfO ₂	X-40	90	1.37 (1.01)	19 (0.029)
	René 80	90	1.36 (1.00)	58 (0.090)
	René 150	90	1.36 (1.00)	15 (0.023)
	HS 188	90	1.37 (1.01)	1 (0.002)
ZrO ₂ -24%Mgo	X-40	20	5.42 (4.00)	5 (0.008)
	René 80	20	5.50 (4.06)	3 (0.004)
	René 150	20	5.60 (4.13)	5 (0.008)
	HS 188	20	5.38 (3.97)	3 (0.004)
ZrO ₂ -20%Y ₂ O ₃	X-40	20	5.50 (4.06)	6 (0.009)
	René 80	20	5.45 (4.02)	4 (0.009)
	René 150	20	5.52 (4.07)	4 (0.006)
	HS 188	20	5.38 (3.97)	5 (0.007)
HfO ₂	X-40	20	5.57 (4.11)	3 (0.005)
	René 80	20	5.44 (3.99)	3 (0.005)
	René 150	20	5.41 (3.99)	3 (0.005)
	HS 188	20	5.44 (4.01)	3 (0.005)

(1) 4 mm (0.175 in.) diameter spherical steel projectile; room ambient temperatures.
(2) Secondary impact.



90°



20°

Figure 15. Typical Features of TBC Specimens After Impact at 90° and 20° Incidence Angles.

The impacted specimens were subsequently subjected to thermal cycle testing between approximately 420 K (300° F) and 1310 K (1900° F) in the manner described in Section 3.3.6. Figures 16 through 18 show the appearance of the coatings and coating damage after various numbers of thermal cycles.

From the results of the impact testing and subsequent thermal cycles, it was concluded that the amount of damage sustained by the coatings from ballistic impact was greater for the ZrO₂-24%MgO coatings than for the other two coating systems. It was also concluded that the size of the impact-damaged area did not grow during subsequent thermal cycling of the coated specimen between 420 K (300° F) and 1310 K (1900° F), and that the impact-damaged area did not act as an initiation site for further spalling.

3.4.6 Summary of Additional Evaluation

Based on the results of the thermal cycle, high cycle fatigue, thermal exposure, tensile bond and impact testing, it was concluded that the duplex yttria-stabilized zirconia (ZrO₂-20%Y₂O₃) coating system had the best overall performance of the three coating systems evaluated (see Table XII). This coating system exhibited the least amount of coating loss in thermal cycle testing in the as-coated condition, as well as after impact testing. The ZrO₂-20%Y₂O₃ coating system also showed the least spallation and least deterioration in bond strength after thermal exposure at 1255 K (1800° F) and 1366 K (2000° F).

Table XII. Summary of Rankings for Additional Evaluation Tests.

Coating System	Ranking				
	Normal(1) Exposure	Thermal(2) Cycling	High Cycle(3) Fatigue	Impact(4)	Average
ZrO ₂ -20%Y ₂ O ₃ Duplex	1	1	1	1	1.0
ZrO ₂ -24%Mgo Duplex	2	2	1	1	1.5
HfO ₂ Duplex	2	3	1	1	1.75

(1) Least coating loss during thermal exposure
 (2) Least coating loss (Figure 11)
 (3) Least effect of TBC on substrate HCF strength (Figure 14)
 (4) Least coating damage (Table XI)

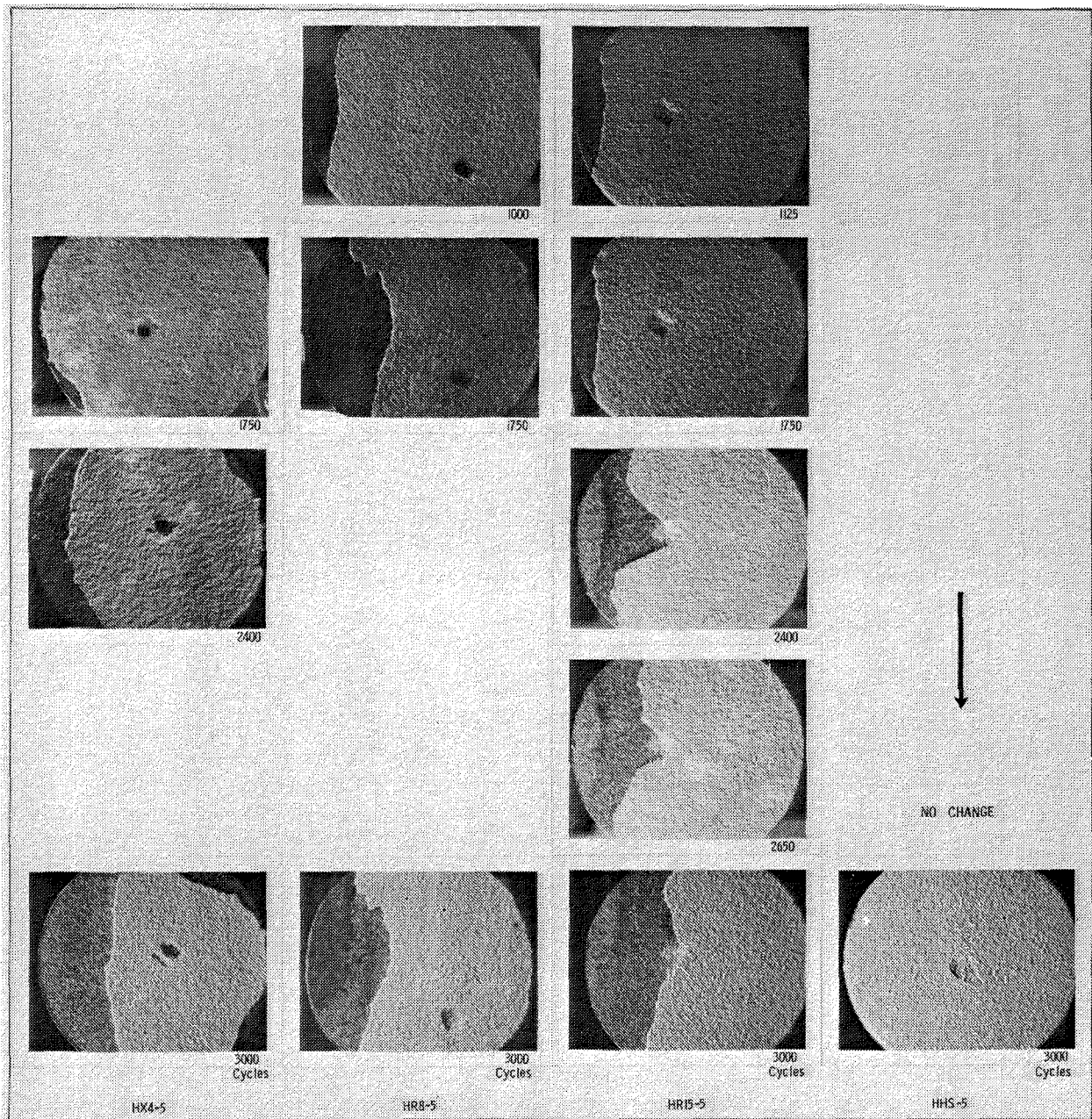


Figure 16. Results of Thermal Cycle Testing of HfO₂ TBC with Ballistic Impact Damage (20° Impact Angle).

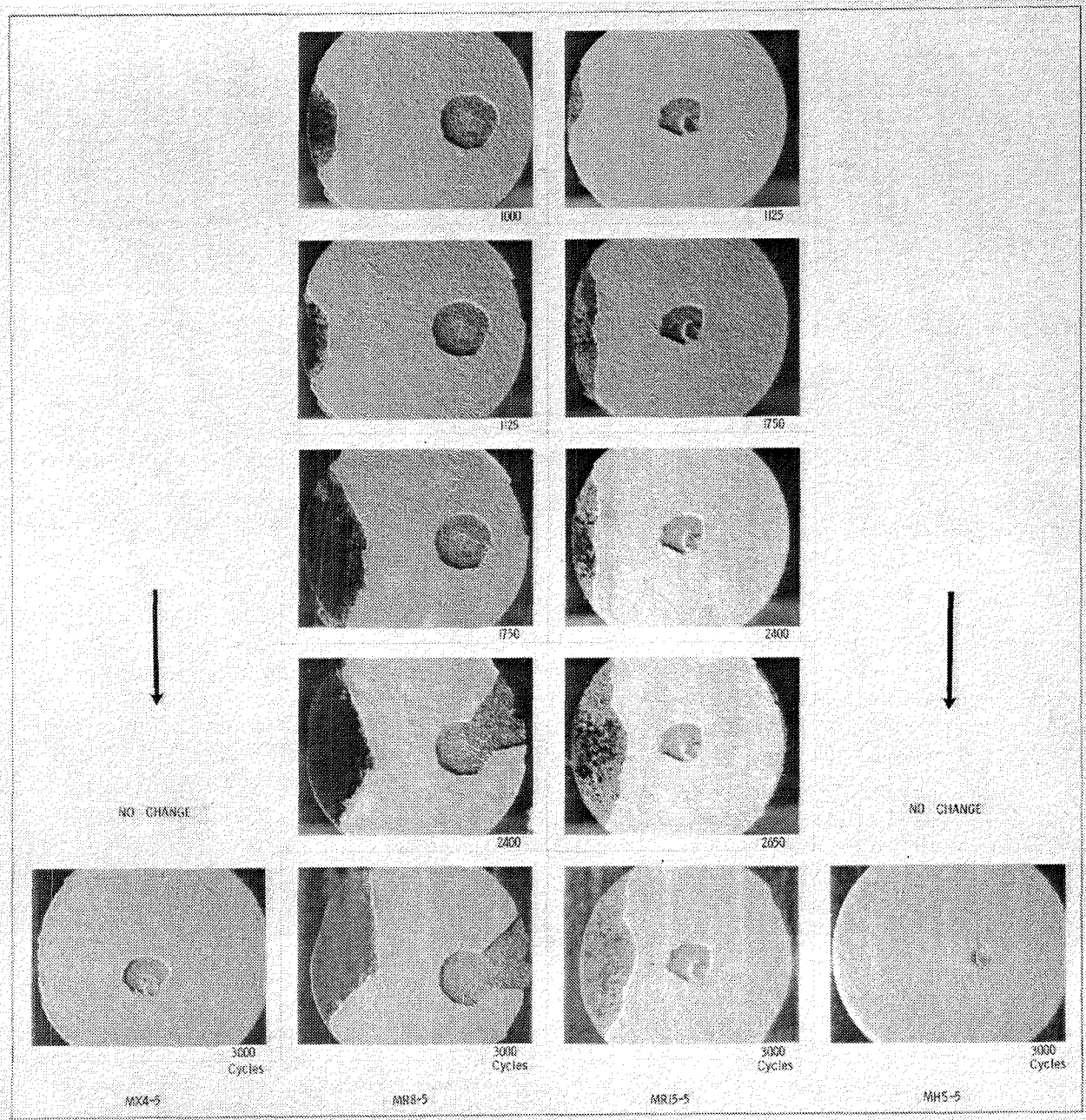


Figure 17. Results of Thermal Cycle Testing of $ZrO_2-24\%MgO$ TBC with Ballistic Impact Damage (20° Impact Angle).

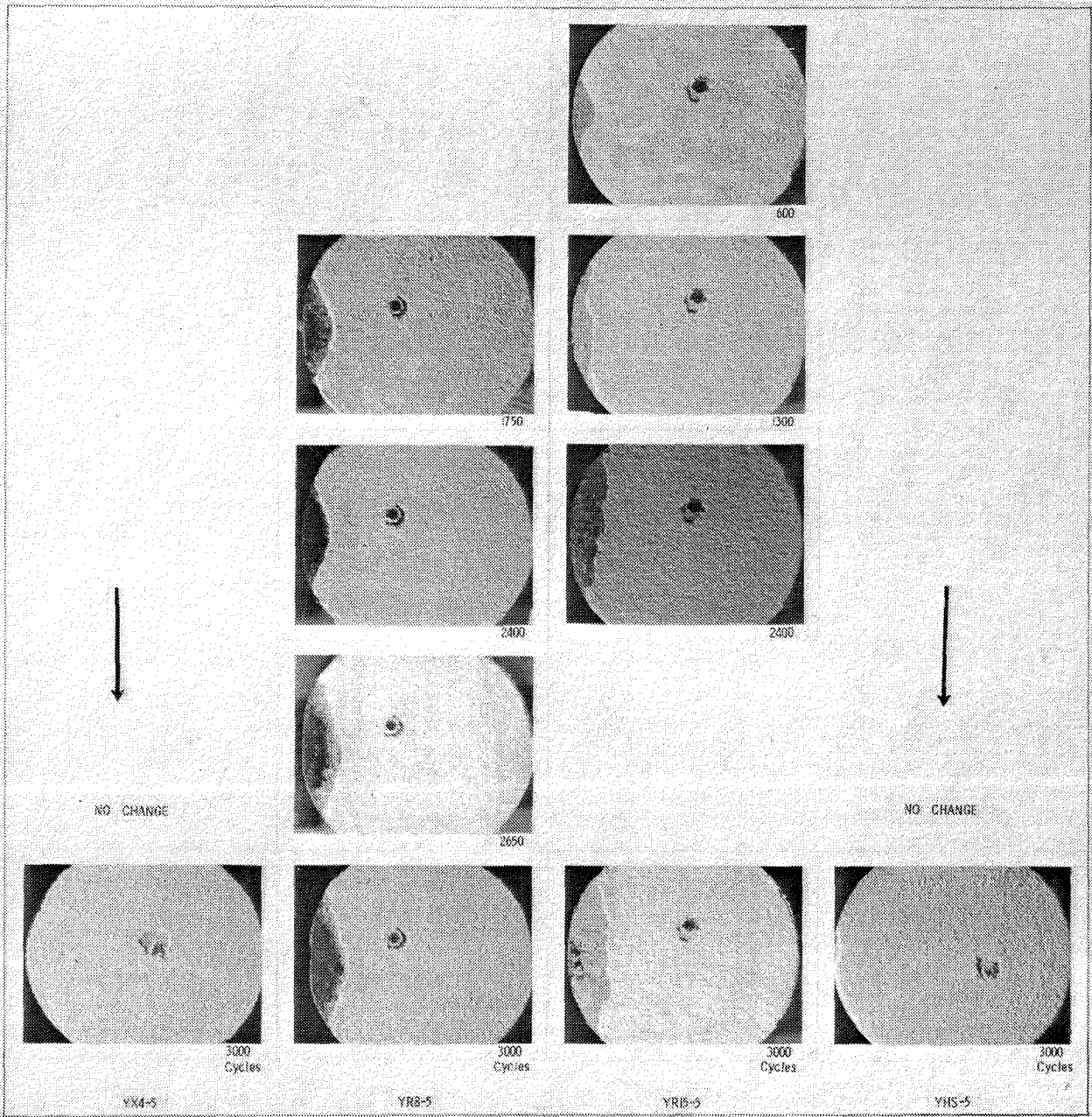


Figure 18. Results of Thermal Cycle Testing of $ZrO_2-20\%Y_2O_3$ TBC with Ballistic Impact Damage (20° Impact Angle).

3.5 COMPARISON OF ZrO₂-20%Y₂O₃ TBC WITH NASA TBC

The selected TBC system, ZrO₂-20%Y₂O₃/Ni-Cr-Al-Y duplex, was compared to another (NASA) TBC system, ZrO₂-8%Y₂O₃/Ni-Cr-Al-Y duplex (Reference 11), in several tests. Specimens of three substrate alloys (X-40, DS René 150, and HS 188) were coated at NASA-Lewis with the ZrO₂-8%Y₂O₃ TBC system. Nominal total coating thickness (bond coat plus top coat) was 0.38 mm (0.015 in.).

It should be noted that, while the two coating systems compared here are referred to by their composition (that is, ZrO₂-20%Y₂O₃ and ZrO₂-8%Y₂O₃), other significant differences exist between the two coatings. These differences include ceramic powder characteristics and coating process variables and may influence coating durability as much or more than stabilizer content.

The ZrO₂-8%Y₂O₃-coated specimens were evaluated in thermal exposure, tensile bond, impact, and thermal cycle tests identical to those previously described.

3.5.1 Thermal Cycle Testing

Coated specimens were thermally cycled between approximately 420 K (300° F) and 1310 K (1900° F) as described earlier. Some of the specimens were impact-tested prior to thermal cycling to evaluate the effect of impact damage on coating loss during subsequent thermal cycling. The results of the thermal cycle tests are given in Figures 19 through 21.

Average coating loss as a function of thermal cycles for the ZrO₂-20%Y₂O₃ and ZrO₂-8%Y₂O₃ TBC systems on three substrate alloys is shown in Figure 19. The results of this testing are consistent with the earlier results in that the least amount of coating loss occurred from HS 188 alloy specimens followed by X-40 specimens, and the greatest amount of coating loss occurred from DS René 150 specimens. For specimens of a given substrate alloy, the amount of coating loss that occurred during thermal cycling was about the same for the ZrO₂-20%Y₂O₃ and ZrO₂-8%Y₂O₃ TBC systems.

Figure 20 shows the results of a thermal cycle test of DS René 150 specimens which had been coated with the electroplate aluminide (EA) Ni-Cr-Al-Hf environmental coating prior to application of the two TBC's. (EA Ni-Cr-Al-Hf coating was to be used under the TBC on CF6-50, DS René 150, Stage 1 blades to protect those areas that were not covered by TBC.) Only one specimen with each coating system is represented in the data; thus the significance of the curves is limited. Keeping this limitation in mind, the curve suggests that the two coating systems behave similarly when applied over EA Ni-Cr-Al-Hf environmental coating.

The effect of thermal cycling on ZrO₂-20%Y₂O₃ and ZrO₂-8%Y₂O₃ TBC systems subjected to ballistic impact prior to testing is compared in Figure 21. Again, very little difference in the behavior of the two coating systems is apparent. Overall, thermal cycle testing did not show either coating system to be superior to the other.

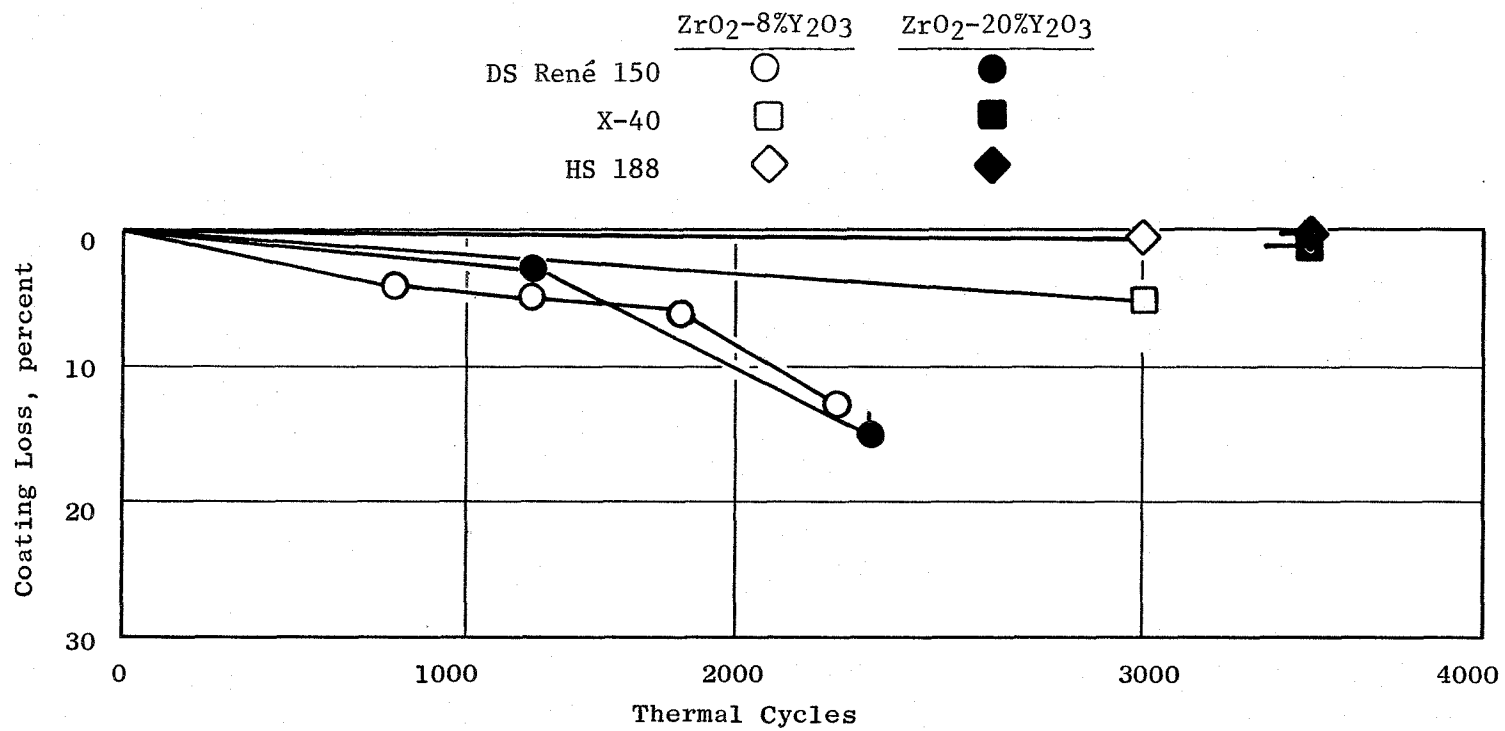


Figure 19. Comparison of Test Results on ZrO₂-8%Y₂O₃ and ZrO₂-20%Y₂O₃ TBC's.

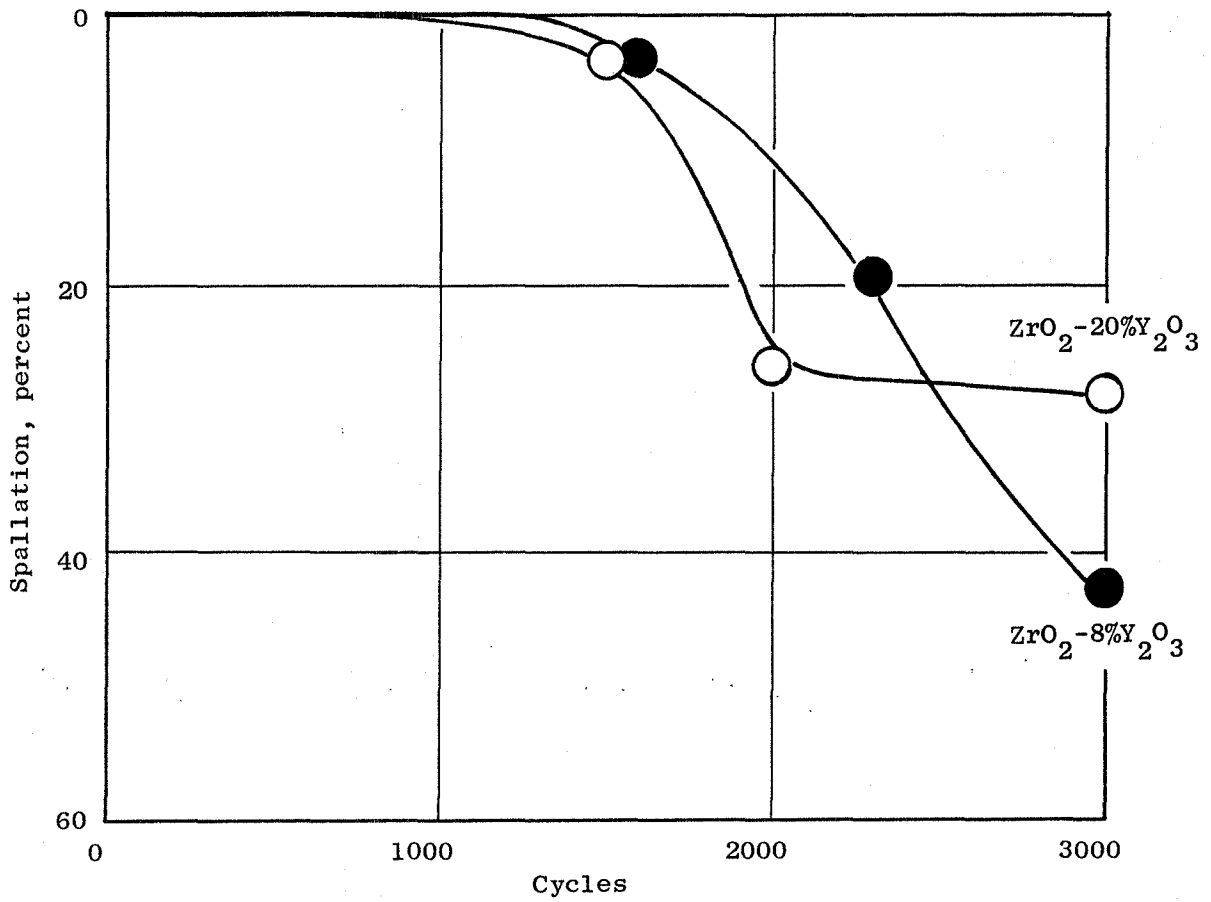


Figure 20. Thermal Cycle Test Results for ZrO₂-8%Y₂O₃ and ZrO₂-20%Y₂O₃ Coatings on EA Ni-Cr-Al-Hf-Coated DS René 150 Specimens.

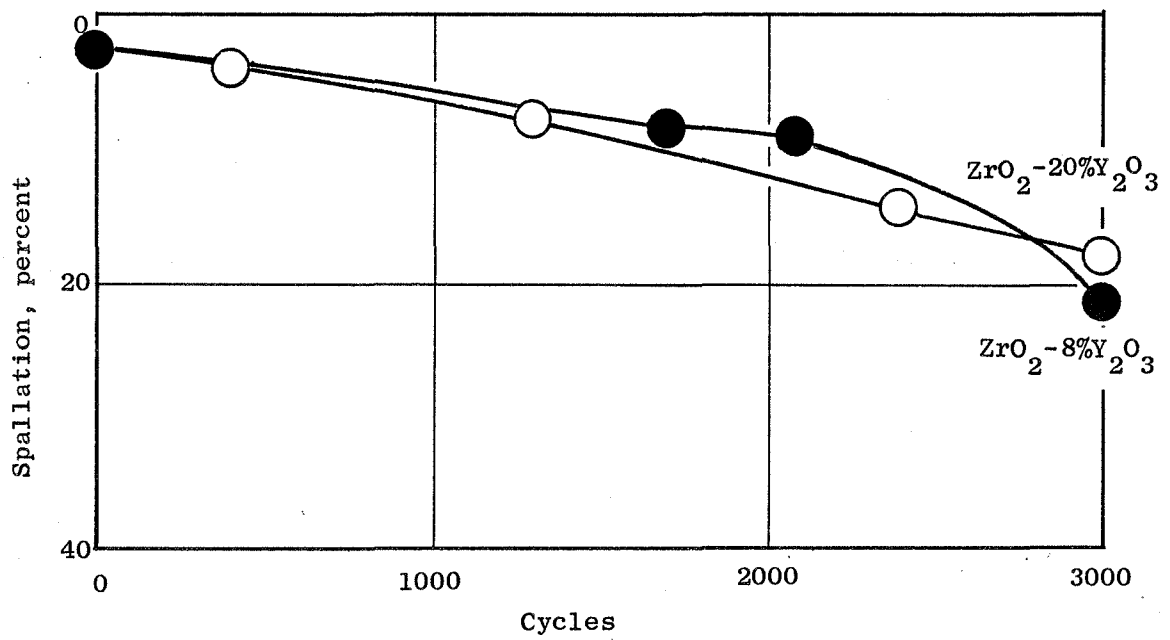


Figure 21. Thermal Cycle Test Results for $ZrO_2-8\%Y_2O_3$ and $ZrO_2-20\%Y_2O_3$ Coatings on DS René 150 Specimen After 90° Incidence Impact.

3.5.2 Thermal Exposure Testing

Specimens coated with the $ZrO_2-8\%Y_2O_3$ coating system were exposed for 250 hours at 1366 K (2000° F). Test procedures were as described earlier. Examination of the specimens at the conclusion of the 250-hour exposure revealed some loss of coating from the DS René 150 substrates. Little or no coating was lost from the X-40 and HS 188 alloy substrates.

3.5.3 Tensile Bond Testing

Bond strengths were measured on specimens which had been tested in thermal exposure at 1366 K (2000° F) for 250 hours, and on specimens which had been thermal cycle tested. Tensile bond strengths of the $ZrO_2-8\%Y_2O_3$ specimens were on the order of 17.5 MPa (2.5 ksi); bond strengths of $ZrO_2-20\%Y_2O_3$ specimens were found earlier to be on the order of 10.5 MPa (1.5 ksi).

3.5.4 Impact Testing

Impact tests were performed on coated 25 mm (1 in.) diameter button specimens at room temperature as described earlier. Impact angles were 20° and 90° and projectile energies were 5.4 and 1.4 J (4 and 1 ft-lb), respectively. The impacted specimens were then subjected to thermal cycling tests. The amount of impact damage sustained by the $ZrO_2-8\%Y_2O_3$ coated specimens was quite similar to that sustained by the $ZrO_2-20\%Y_2O_3$ coated specimens. The behavior of these specimens in thermal cycling was described above.

3.5.5 Metallography

Figure 22 shows the optical metallographs on as-received $ZrO_2-8\%Y_2O_3$ coating supplied by NASA. The top coat was about 0.20 mm (0.008 in.) thick, and the bond coat was about 0.076 mm (0.003 in.) thick. Examination of the top coat at the higher magnification revealed the presence of an elongated second phase occupying about 10% of the area. Scanning electron microscope (SEM) analysis of the top coat region, Figure 23, reveals the overall nature of the top coat. The specimen was gold-coated prior to SEM examination to prevent excessive flashing. To more thoroughly evaluate the composition of this region, an energy dispersive analysis by X-ray (EDAX) was made. As seen in Figure 23, the ceramic coating consisted of two phases: (1) a zirconium-rich phase containing yttrium, and (2) an yttrium-rich phase containing silicon.

3.5.6 Summary

The testing which was performed did not show a significant difference in the durabilities of the two coatings, $ZrO_2-8\%Y_2O_3$ prepared by NASA-Lewis and $ZrO_2-20\%Y_2O_3$ prepared by GE. Because of GE's much larger experience base in applying the latter coating, $ZrO_2-20\%Y_2O_3/Ni-Cr-Al-Y$ duplex TBC was selected as the coating system that was to be used in the remainder of the program.

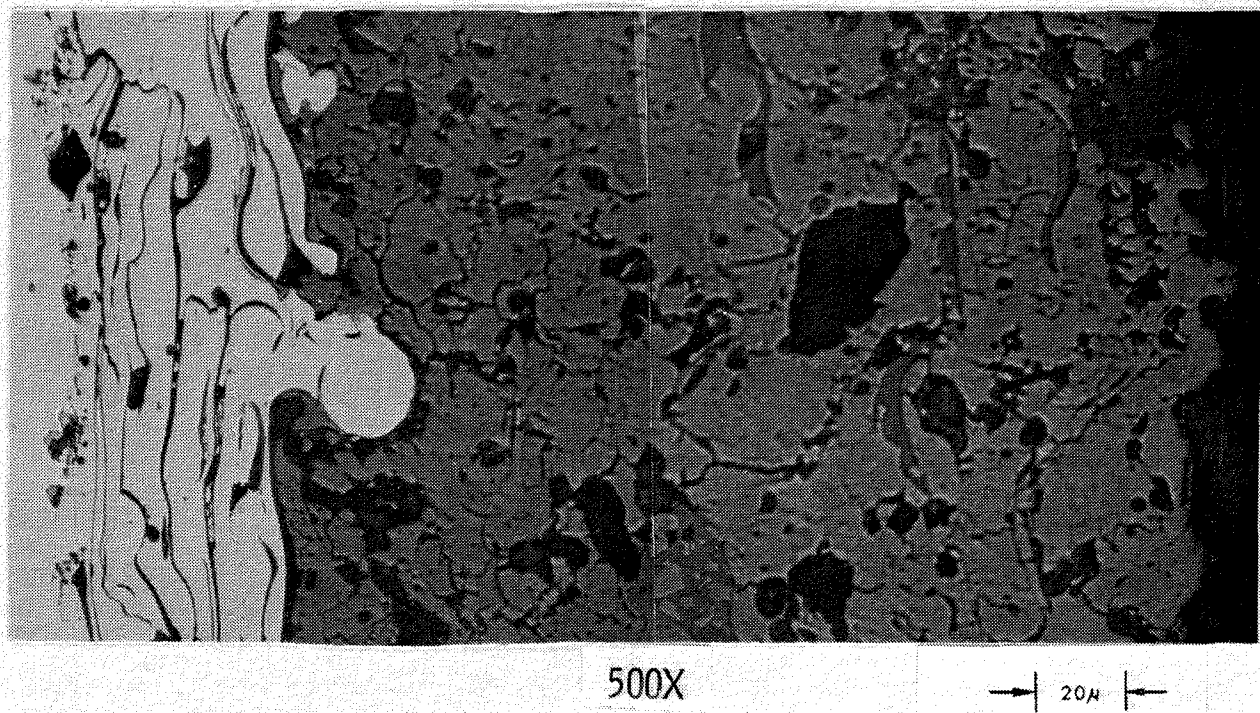
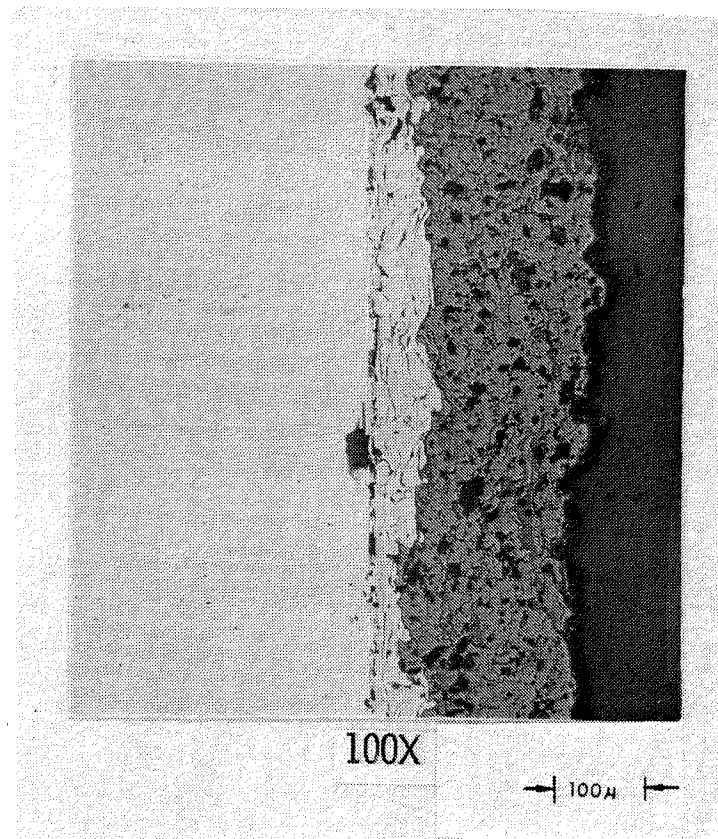


Figure 22. Microstructure of $ZrO_2-8\%Y_2O_3$ TBC.

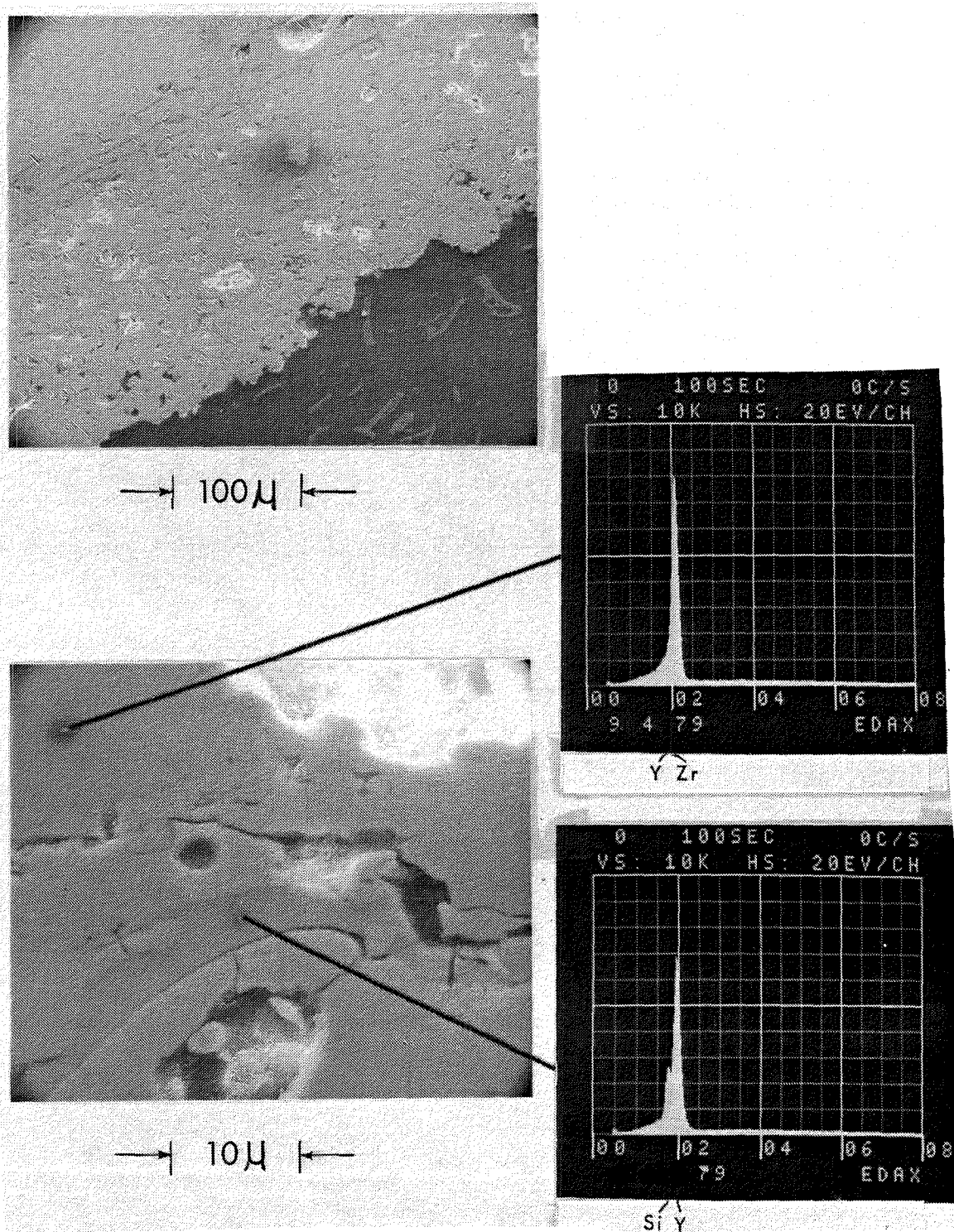


Figure 23. Scanning Electron Micrograph and EDAX Results on $ZrO_2-8\%Y_2O_3$ TBC.

4.0 EVALUATION OF TBC EFFECT ON MECHANICAL PROPERTIES OF SUBSTRATE ALLOYS

In order to assess whether the presence of a TBC degrades the mechanical properties of the substrate alloys, test specimens with and without the selected TBC were tested at 1255 K (1800° F) in low cycle fatigue, high cycle fatigue, and stress rupture tests, and the results compared. Test specimens of three substrate alloys, X-40, René 80, and DS René 150, were prepared and given the standard alloy heat treatments and the normal environmental coatings: Codep on X-40 and René 80, and EA Ni-Cr-Al-Hf on DS René 150. (In the earlier high cycle fatigue tests of thermal-barrier-coated specimens, the TBC was applied directly over the substrate.) Half of the specimens were then coated with the selected duplex thermal barrier coating system. On the X-40 and René 80 specimens, the TBC consisted of a nominal 0.063 mm (0.0025 in.) thick Ni-Cr-Al-Y bond coat layer and a 0.19 mm (0.0075 in.) thick ZrO₂-20%Y₂O₃ top coat. The TBC on the DS René 150 specimens consisted of a nominal 0.13 mm (0.005 in.) thick bond coat layer and a 0.38 mm (0.015 in.) thick top coat layer.

It was noted in previous high cycle fatigue testing of thermal-barrier-coated specimens which were heated inductively that the bulk temperature of the specimens was substantially higher than the temperatures at the coating surface. This occurs because (1) with inductive heating, the heat is generated under the TBC in the metal specimen, and (2) a temperature drop occurs across the coating thickness because of its low thermal conductivity. Since the specimen temperature during testing was monitored by sighting a radiation pyrometer on a Pyromark spot on the coating surface, the magnitude of the difference between bulk metal temperature and coating surface temperature for the thermal-barrier-coated specimens had to be determined to ensure that specimens with and without TBC were tested at the same substrate temperature [1255 K (1800° F)]. This applied to high and low cycle fatigue specimens which were heated and gripped in similar manners. The stress rupture specimens, however, were heated in a radiant furnace and developed a uniform temperature throughout.

Three specimens were specially prepared by embedding a thermocouple in the metal substrate before the TBC was applied. These specimens were then placed in the testing machines, heated, and the substrate temperature as indicated by the thermocouples was compared to the ceramic surface temperatures measured with a radiation pyrometer. For the specimens with a TBC consisting of 0.063 mm (0.0025 in.) bond coat and 0.19 mm (0.0075 in.) top coat, the ceramic surface was 56 K (100° F) cooler than the metal substrate for LCF specimens and 28 K (50° F) cooler for the HCF specimens. With the TBC consisting of 0.13 mm (0.005 in.) bond coat and 0.38 mm (0.015 in.) top coat, the temperature differences were found to be 100 K (180° F) for LCF specimens and 67 K (120° F) for HCF specimens. The temperature differences between the LCF and HCF specimens are related to physical shape and size differences. Temperature measurement corrections for the thermal-barrier-coated specimens were made accordingly; thus all tests were run at a substrate temperature of 1255 K (1800° F).

The results of the mechanical testing are shown in Figures 24 through 26. For each test and each alloy, the data points for specimens with and without TBC fall within the same scatter band. The presence of the TBC system apparently did not have any significant effect on the high cycle fatigue, low cycle fatigue, and stress rupture properties of the three substrate alloys tested.

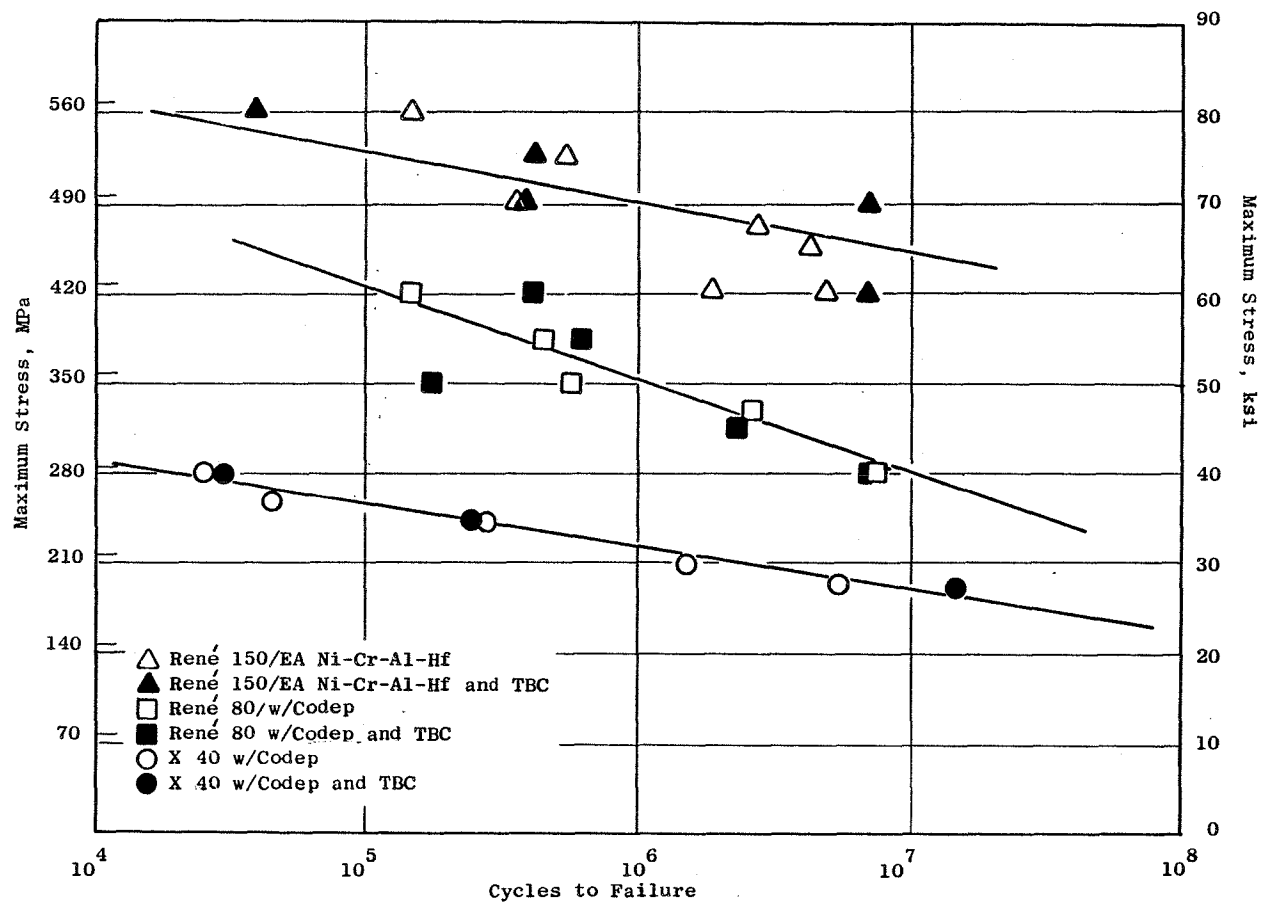


Figure 24. Results of 1255 K (1800° F), High Cycle Fatigue Testing Comparing Specimens With and Without Thermal Barrier Coating.

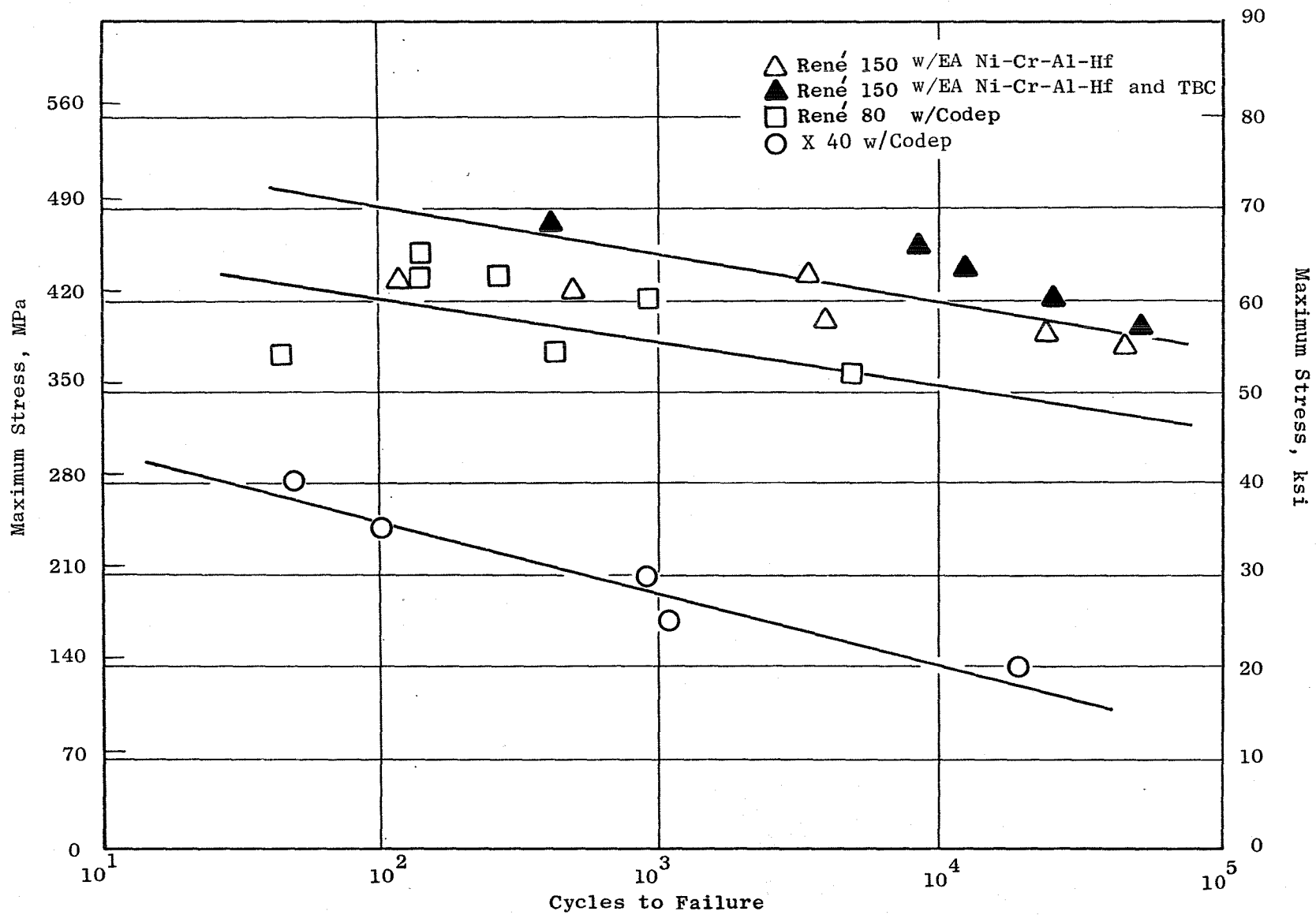


Figure 25. Results of 1255 K (1800° F), Low Cycle Fatigue Testing Comparing Specimens With and Without Thermal Barrier Coating.

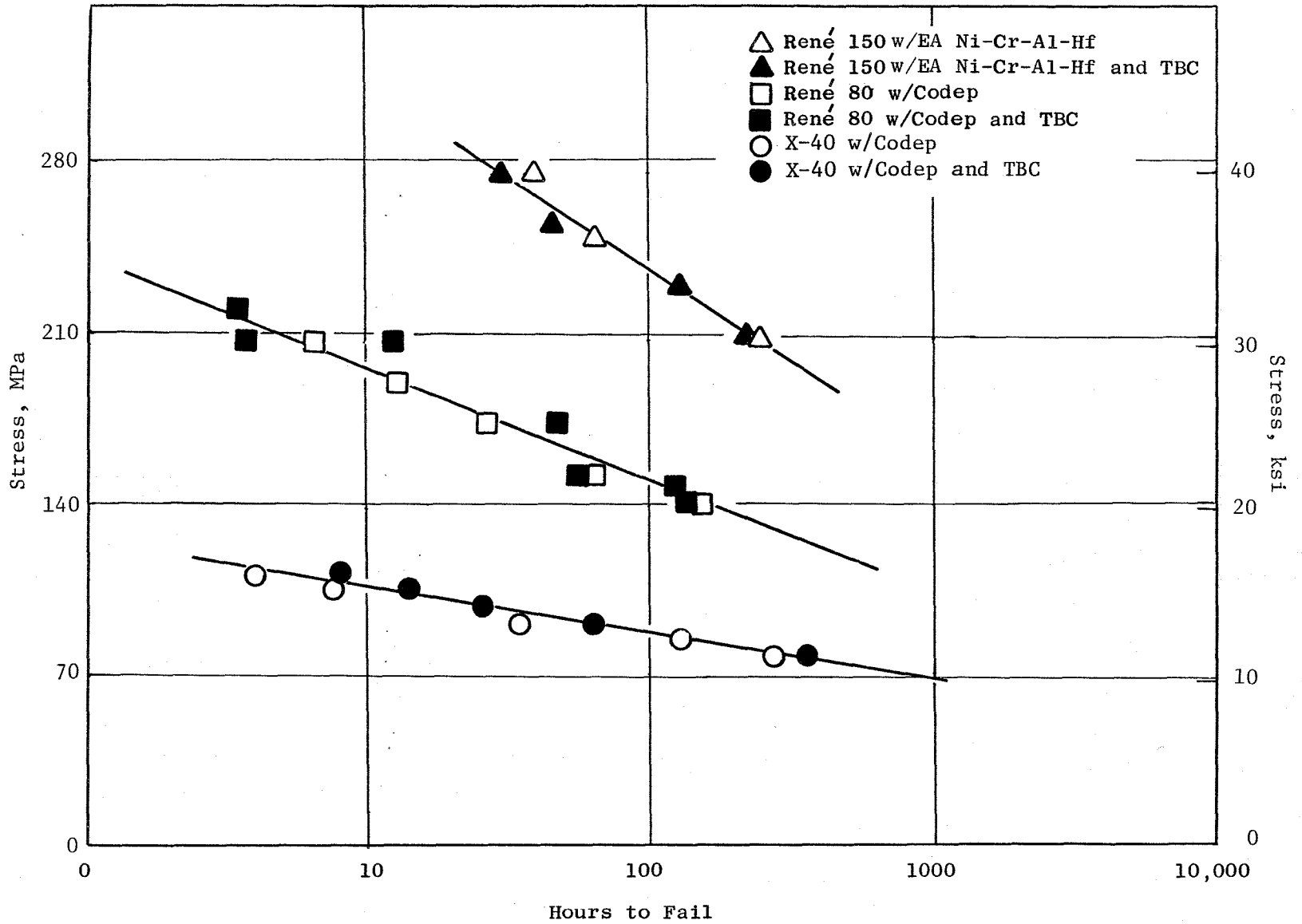


Figure 26. Results of 1255 K (1800° F), Stress Rupture Testing Comparing Specimens With and Without Thermal Barrier Coating.

5.0 APPLICATION OF TBC TO TURBINE COMPONENTS

The objective of this effort was to establish processes for reproducibly applying the selected TBC system to selected high pressure turbine blades and vanes. Because of the complex shapes of these components and the line-of-sight nature of the plasma spray process, it is extremely difficult to obtain coatings of uniform thickness and structure when the coating is applied by manually manipulating the spray gun. It is especially difficult to accomplish this repeatedly. Thus emphasis was placed on establishing a mechanized, and preferably an automated, process for applying the bond and top coat layers to HPT blades.

5.1 DEVELOPMENT OF PROCEDURES FOR COATING BLADES

The initial effort to develop procedures for coating blades was started before the final TBC system was selected. $ZrO_2-24\%MgO$ was used as the top coat material in the early work. Initially, reject CF6-50 Stage 1 blades without cooling holes were coated by conventional plasma spray processes. During coating, the blades were supported vertically in a special fixture and rotated at a constant angular velocity in front of the plasma torch while it was traversed up and down the blade. The Ni-Cr-Al-Y bond coat layer was applied to blades using such a procedure. Two procedures were employed to apply the ZrO_2-MgO top coat. In one, the top coat was sprayed with the plasma torch at a 45° angle to the blade stacking axis for two passes, then at a 90° angle during the final pass. In the second procedure, the plasma torch was maintained at an angle of 45° to the stacking axis during all passes.

Evaluation of coatings applied by the two procedures indicated that the procedure utilizing two incidence angles produced a more uniform coating. However, a detailed metallographic examination of coatings produced by both procedures revealed excessive buildup of bond coat and top coat on the concave side of the airfoils, and revealed a much thinner coating on the convex side. The nonuniformity of the coating on airfoils rotated at a constant angular velocity in front of the plasma torch is attributable to the fact that the impingement angle, torch-to-substrate distance, and impingement time are different for each point on the airfoil. These results accentuated the need for a more fully automated process for coating turbine blades.

The second approach taken was to apply the bond coat and top coat layers to Stage 1 blades using the automated manipulating equipment which is a part of the GE Manufacturing Technology Laboratory's vacuum plasma deposition facility. A large number of reject blades were coated using this equipment. Bond coats were applied both at low pressure (approximately 0.1 atmosphere) and at atmospheric pressure. All top coats were applied at atmospheric pressure.

First, nine Stage 1 blades were coated with the Ni-Cr-Al-Y bond coat in an iterative manner, again rotating the blade in front of the plasma torch.

After each series of blades was coated, the blades were sectioned at two air-foil span heights and the coating thickness measured. Rather uniform bond coats were obtained after several iterations.

Next, 18 Stage 1 blades were coated in a series of 6 runs. No attempt was made to mask the cooling holes in these blades. Process variations in these coating series are shown in Table XIII. Coatings were applied to EA Ni-Cr-Al-Hf-coated blades and Codep-coated blades; some blades were grit-blasted and others were mildly cleaned (vapor honed) prior to TBC application. The bond coats were deposited in the vacuum plasma spray (VPS) equipment at a pressure of about 6.7 k Pa (50 Torr) using two procedures: (1) the blade positioned on a stalk and rotated while being moved in and out of the plasma spray, and (2) the blade, again mounted on a stalk, pre-positioned by the computer at given rotation angles and radially traversed in and out of the plasma spray. In five of the six series, the blades were preheated to approximately 1200 K (1700° F.) In both procedures, the blade motion and plasma gun position were computer controlled.

Table XIII. Bond Coat Process Development Variations.

Parameter	Standard	Variations
Environmental Coating	Codep EA Ni-Cr-Al-Hf	--
Surface Preparation	Grit blast	None, vapor hone
Application Temperatures	1200 K (1700° F)	Cold, ~475 K (~400° F)
Chamber Pressure	6.7 kPa (50 Torr)	0.1 MPa (760 Torr)
Application Motion	Rotation	Radial traverse
Substrate Alloy: René 80 Bond Coat Alloy: Ni-Cr-Al-Y Bond Coat thickness: 0.08 to 0.13 mm (0.003 to 0.005 in.)		

A $ZrO_2-20\%Y_2O_3$ top coat layer was applied to these specimens using the manipulator in the VPS facility, but the coatings were applied at atmospheric pressure. Only the radial traverse procedure was employed for depositing the top coat. In this procedure, the blade was rotated to selected angles and moved through the plasma. A total of seven blades were coated, again in an iterative manner; the number of plasma gun passes across the surface was increased each iteration. Figure 27 shows five of these blades. By metallographic examination, it was determined that 27 passes gave a top coat thickness of approximately 0.11 mm (0.0045 in.), hence the programmer was set to repeat the initial 27 passes to produce an overall top coat thickness of 0.23 mm (0.009 in.) Included with this series was one blade with a $ZrO_2-6.2\%Y_2O_3$ top coat. Visual examination of the blades after coating revealed spallation of the top coat from the blades with the bond coat applied cold.

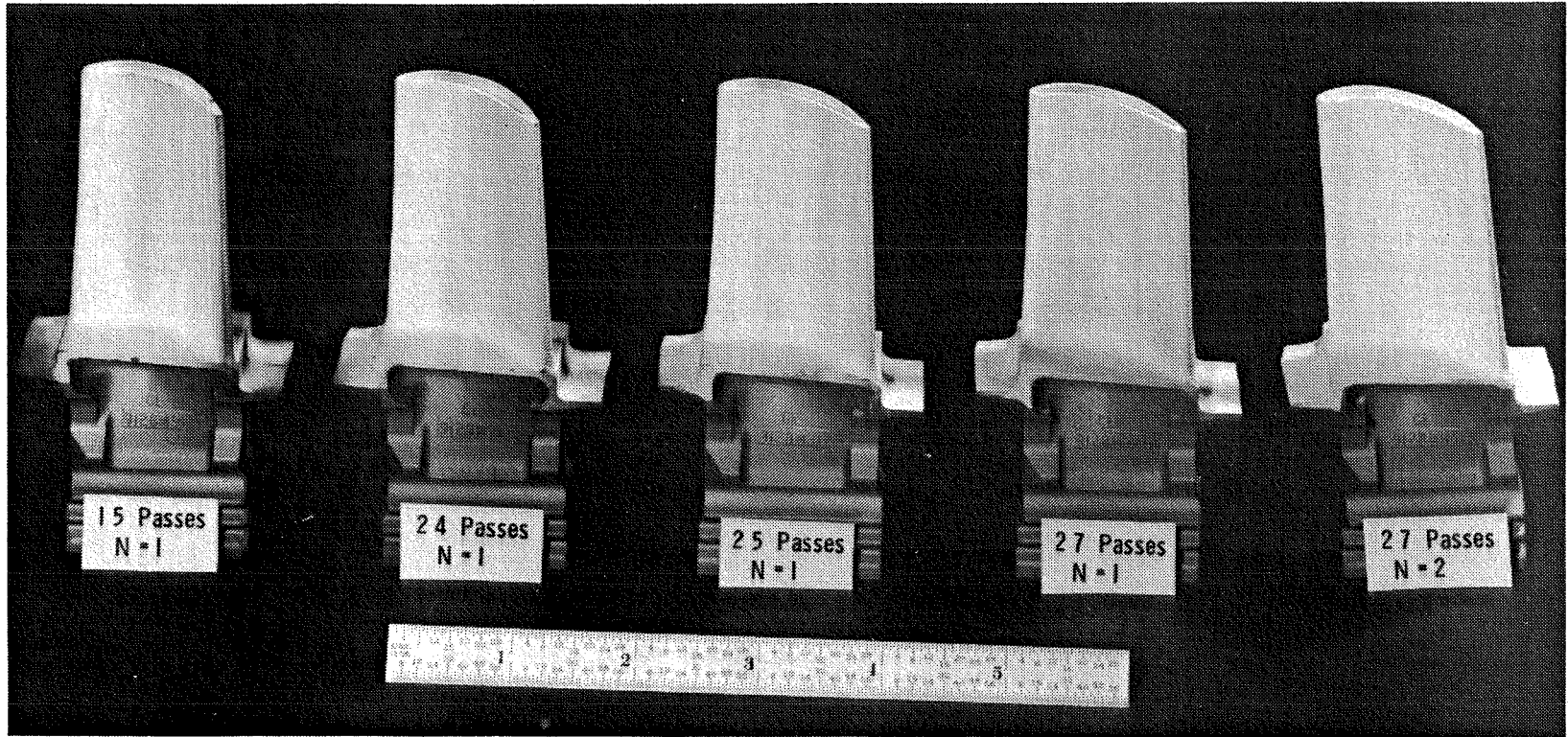


Figure 27. CF6-50, Stage 1 Blades With Increasing Number of Coating Passes of $ZrO_2-20\%Y_2O_3$ Ceramic Layers.

The coated blades were evaluated by thermal exposure at 1366 K (2000° F). The results from this testing showed early (after 100 hours) spallation of the top coat layer from the blade with the $ZrO_2-6.2\%Y_2O_3$ top coat. The EA Ni-Cr-Al-Hf coated specimen with a grit-blast surface preparation exhibited the greatest spallation resistance.

Using the VPS equipment to apply the zirconia top coat layer at atmospheric pressure had a number of disadvantages. One of these pertained to maneuverability of the plasma torch. Since the equipment was designed for low pressure operation under which conditions the plasma is much longer than it is at atmospheric pressure [about 40 cm (16 in.) compared to about 15 cm (6 in.)], it was necessary to use an extension nozzle on the plasma torch to apply the zirconia layer at atmospheric pressure. The use of this extension restricted the maneuverability of the plasma torch.

When a computer-controlled robot for manipulating a plasma torch for conventional atmospheric pressure plasma spraying became available, use of the VPS manipulator for applying ceramic layers was discontinued. A series of Stage 1 and Stage 2 blades was coated to evaluate the use of the computer-controlled robot for applying the zirconia top coat. Specimens also were coated to compare the durabilities of coatings applied using various processes for applying the bond coat and top coat layers. Ni-Cr-Al-Y bond coat was applied to the blades by three methods, and a $ZrO_2-20\%Y_2O_3$ top coat was applied by two methods. Bond coat application methods included the VPS method described above as well as the same general method in another low pressure plasma facility. The third method for applying the bond coat was the conventional atmospheric plasma spray process. The zirconia top coat layer was applied by the conventional plasma spray process, manually and with the computer-controlled robot manipulation of the plasma torch.

The durabilities of the coatings applied by the various process methods were compared by subjecting the coated blades to thermal shock treatments of increasing severity. First, the coated blades underwent three thermal cycles in vacuum from 1366 K (2000° F) to 533 K (500° F) after which the coatings were examined visually. They then underwent a static air quench from 1366 K (2000° F) followed by a water quench from 1255 K (1800° F), and again visually examined. Finally, the coated blades were exposed to 1310 K (1900° F) for 250 hours with five cycles to room temperature. Comments on the conditions of the coating after these various treatments are summarized in Table XIV, along with relative rating values based on coating durability during these treatments. The coatings thus rated may be ranked as follows:


	<u>Bond Coat Process</u>	<u>Top Coat Process</u>
Best	VPS 1	Robot 1
	VPS 2	Robot 1
	Conventional 3	Manual 3
Worst	VPS 2	Manual 2

Table XIV. Summary of Thermal Test Results of Coated Blades.

	Process (1)		Evaluation Results			
	Bond Coat	Top Coat	After 3 Vacuum (2) Thermal Cycles	After Air and (3) Water Quench	After 250 hours (4) 1310 K (5 cycles to RT)	Rank(5)
Stage 1 Blades	VPS 1	ROB 1(6)	Gunmetal grey OK	Manila yellow OK	Cream OK	10
	VPS 1	ROB 1(6,7)	Gunmetal grey OK	Manila yellow OK	Cream OK	10
	CONV 3	MAN 3	Gunmetal grey OK	Manila yellow OK	Cream spall at L/E Spall midspan L/E	8
	VPS 2	MAN 2	Gunmetal grey Extensive spall FAILED			0
	VPS 2	ROB 1	Gunmetal grey OK	Manila yellow OK	Cream delam of tip L/E	9
	VPS 2	ROB 1(7)	Gunmetal grey OK	Manila yellow OK	Cream V slight cracking T/E tip	9+
	VPS 1	ROB 1	Gunmetal grey OK	Manila yellow OK	Cream OK	10
	VPS 1	ROB 1	Gunmetal grey OK	Manila yellow OK	Cream slight cracking at T/E tip	9
Stage 2 Blades	VPS 1	ROB 1	Gunmetal grey OK	Manila yellow OK	Cream spall at T/E root	9
	VPS 1	ROB 1	Gunmetal grey OK	Manila yellow OK	Cream spall at T/E root	8
	VPS 1	ROB 1(7)	Gunmetal grey OK	Manila yellow OK	Cream spall at T/E root	9
	VPS 2	ROB 1	Gunmetal grey OK	Manila yellow OK	Cream OK	10
	VPS 2	ROB 1	Gunmetal grey OK	Manila yellow OK	Cream OK	10
	YPS 2	ROB 1	Gunmetal grey OK	Manila yellow OK	Cream OK	10
	VPS 2	MAN 2	Gunmetal grey Crack at tip	Light orange Extensive spall FAILED		1
	CONV 3	MAN 3	Gunmetal grey OK	Manila yellow OK	Cream spall at L/E and T/E	8
<p>(1) CONV = Conventional (atmospheric pressure) plasma spray process VPS = Vacuum plasma spray process MAN = Manual manipulation of plasma torch ROB = Robot manipulation of plasma torch 1,2,3 = Plasma spray facility identification</p> <p>(2) Thermal cycles in vacuum from 1366 K (2000° F) to 533 K (500° F).</p> <p>(3) Air quench from 1366 K (2000° F), followed by water quench from 1255 K (1800° F).</p> <p>(4) Thermal exposure for 250 hours at 1310 K (1900° F) with 5 cycles to room temperature.</p> <p>(5) 10 = best.</p> <p>(6) DS René 150 blades; all others René 80.</p> <p>(7) Surface of ceramic layer polished before testing.</p>						

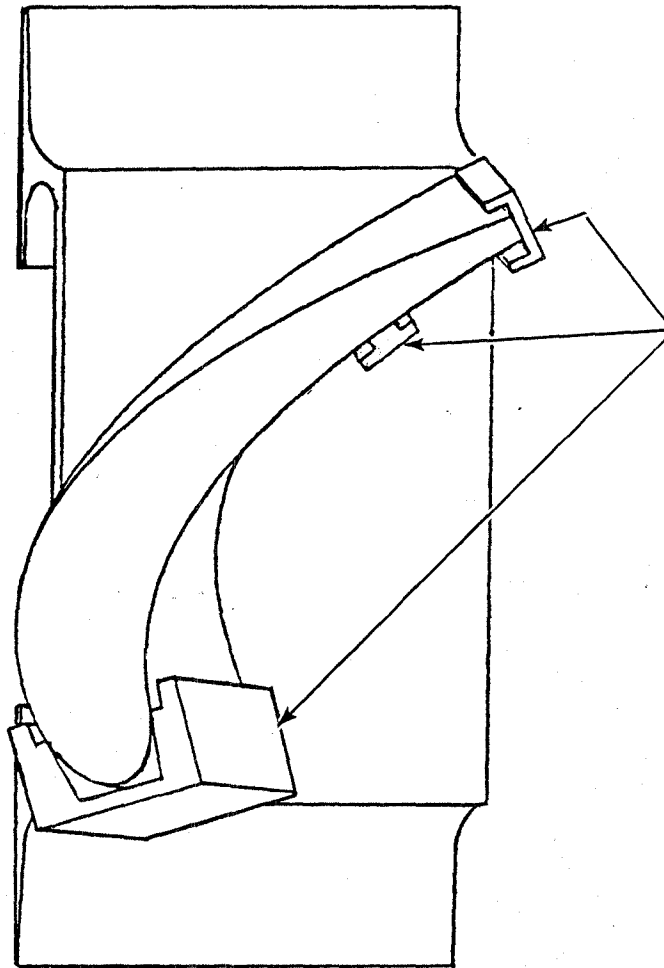
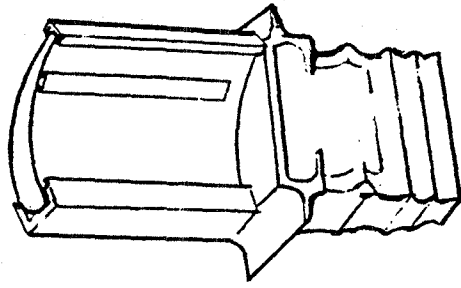
On the basis of these results, bond coat application by vacuum plasma deposition (VPS 1) and top coat application using the computer-controlled robot were selected as the processes for coating HPT Stage 1 and 2 blades. Manipulator programs for the two blade geometries were finalized by coating and evaluating a large number of reject blades in an iterative process. A few blades were coated, then cut up and the coating thickness and structure evaluated metallographically at selected span heights. Adjustments were made to the manipulator programs and the process repeated until acceptable thickness and structure uniformity were attained. This was accomplished for Stage 1 and 2 CF6-50 HPT blades.

5.2 MASKING PROCEDURES

Three of the four HPT components to which thermal barrier coatings were to be applied for rig or engine testing could not be coated over their entire surfaces. Stage 1 blades and vanes both have a large number of film cooling holes in the gas path surfaces. It was therefore necessary to leave selected areas of the components uncoated because there was no established method for applying TBC's without blocking cooling holes and no method available within the standard CF6-50 manufacturing process for drilling holes through TBC's. Stage 2 vanes are cast as a pair of airfoils in common bands, making it impractical to apply coatings to all surfaces by a line-of-sight process. Thus Stage 2 vanes also were coated only in selected areas.

Since the blades are preheated to about 1200 K (1700° F) prior to application of the bond coat by VPS, a temperature considerably above the temperature limit of the welding tape which is commonly used for masking parts coated by the conventional plasma spray process, a method compatible with the high preheat temperature was required for masking selected areas of the Stage 1 blade. Early effort was aimed at identifying a release agent that could be applied to the surface of the blade to prevent adhesion of the TBC. Some mold release agents were examined for use as spray-on masks. Blades were coated with the release agents, the solvent baked out at about 533 K (500° F), and the agent removed from areas on which TBC was desired using a minigrit blaster. After the TBC was applied to the blades, the coating over the release agent could be removed. Most of the work was done with Formkote T50 (E/M Lubricants, Inc., North Hollywood, California), a graphite-base release agent. Removing the unwanted TBC was found to be very tedious, particularly the Ni-Cr-Al-Y bond coat.

Another approach undertaken was the use of a metal (Hastelloy X) mask. Mask components, shown in the sketch in Figure 28, were fitted to the blade to prevent spray powders from depositing on the area around the cooling air holes. The mask components were designed in such a way that the coatings were feathered down to the uncoated (masked) regions. This was of great advantage in obtaining relatively smooth transitions between the coated and uncoated surfaces.



Masking to Keep Film
Cooling Holes and
Trailing Edge Holes
Free of Coating

Figure 28. Sketch of Metal Marks Used in Coating of CF6-50,
Stage 1 HPT Blades.

The metal masks were found to be very effective and were used when applying bond coats to all Stage 1 blades coated for rig testing. The buildup of Ni-Cr-Al-Y on the mask components was removed periodically by acid stripping. The primary drawback associated with the use of the metal mask was that it prevented the use of the reverse transfer arc procedure to clean the blade surface after preheat and immediately before application of the Ni-Cr-Al-Y bond coat by the VPS process; the arc tended to jump to the edges of the mask. However, no difficulties were encountered with bonding of the Ni-Cr-Al-Y bond coat to the substrate.

Once the bond coat layer had been applied to the Stage 1 blades, the ceramic top coat layer was applied without the use of masks. The ceramic layer did not adhere well to the regions of the blades which had been masked during application of the bond coat and therefore were free of bond coat, and the ceramic layer was readily removed from those areas using a minigrit blaster. A Stage 1 blade, coated by using these procedures, is shown in Figure 29.

Welding tape was used to mask the vanes. The bond coat and top coat layers were applied to these components using the conventional arc plasma process; therefore, the parts remained cool enough for welding tape to be used.

5.3 PROCEDURES FOR COATING VANES

As indicated earlier, Stage 1 and 2 vanes were not coated with TBC over their entire flowpath surfaces but were coated only in selected areas.

In the production of Stage 1 vanes, vanes are cast individually and then welded together to form pairs prior to machining, application of Codep environmental coating, and the other manufacturing processes. The vane pairs which were to be coated with TBC were engine quality machined vanes. They were separated into single vanes, the TBC applied, and the vanes rejoined by welding to re-form pairs. The TBC applied to the Stage 1 vanes was 0.13 mm (0.005 in.) of Ni-Cr-Al-Y bond coat and 0.25 mm (0.010 in.) of $ZrO_2-20\%Y_2O_3$ top coat; both layers were applied by the conventional arc plasma spray process. The sprayed ceramic surface was subsequently smoothed by hand-polishing with 400 grit paper under flowing water. The vanes were then rewelded to re-form pairs. Examination of the coating after welding revealed no coating damage or loss. Two coated Stage 1 vane segments, prior to rewelding, are shown in Figure 30.

One vane pair was exposed to a series of thermal cycles of increasing severity to determine the durability of the TBC. This consisted of three vacuum quenches from 1366 K (2000° F) to 533 K (500° F), a 1366 K (2000° F) static air quench to room temperature, and a water quench from 1255 K (1800° F). Examination showed no TBC spallation. Finally, this vane pair was exposed to 1310 K (1900° F) for 250 hours in air with five cycles to room temperature for examination of the coating. No detectable deterioration of the TBC was evident.

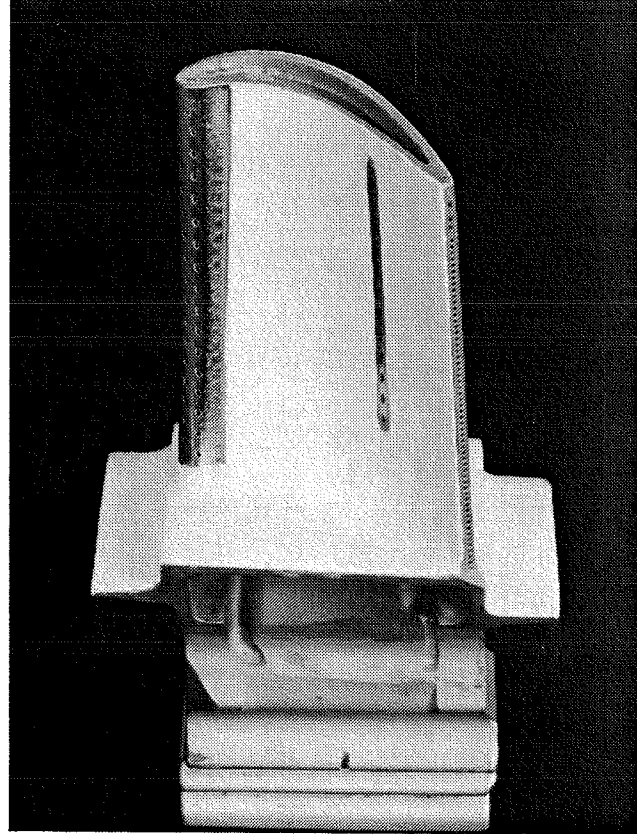
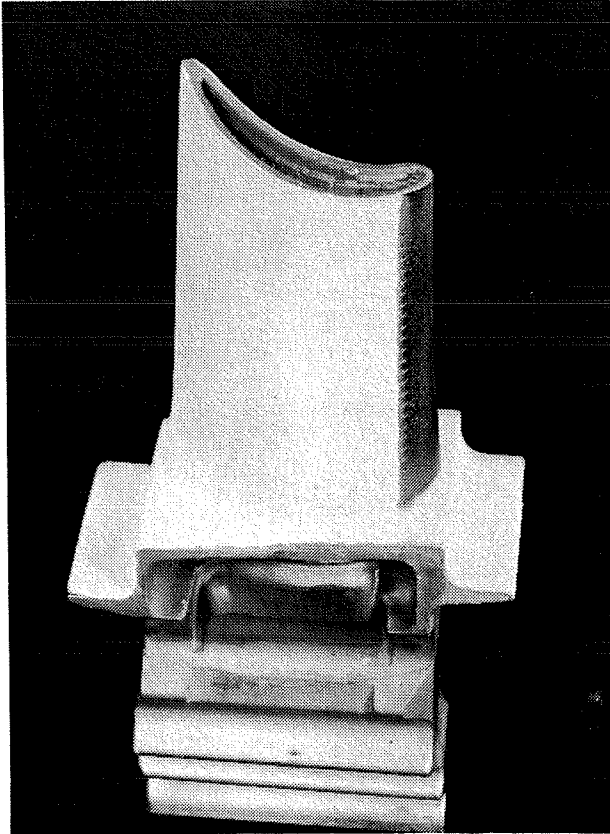


Figure 29. CF6-50 HPT, Stage 1 Blade (DS René 150) With Ni-Cr-Al-Y/ZrO₂-20%Y₂O₃ Duplex TBC Over EA Ni-Cr-Al-Hf Coating.

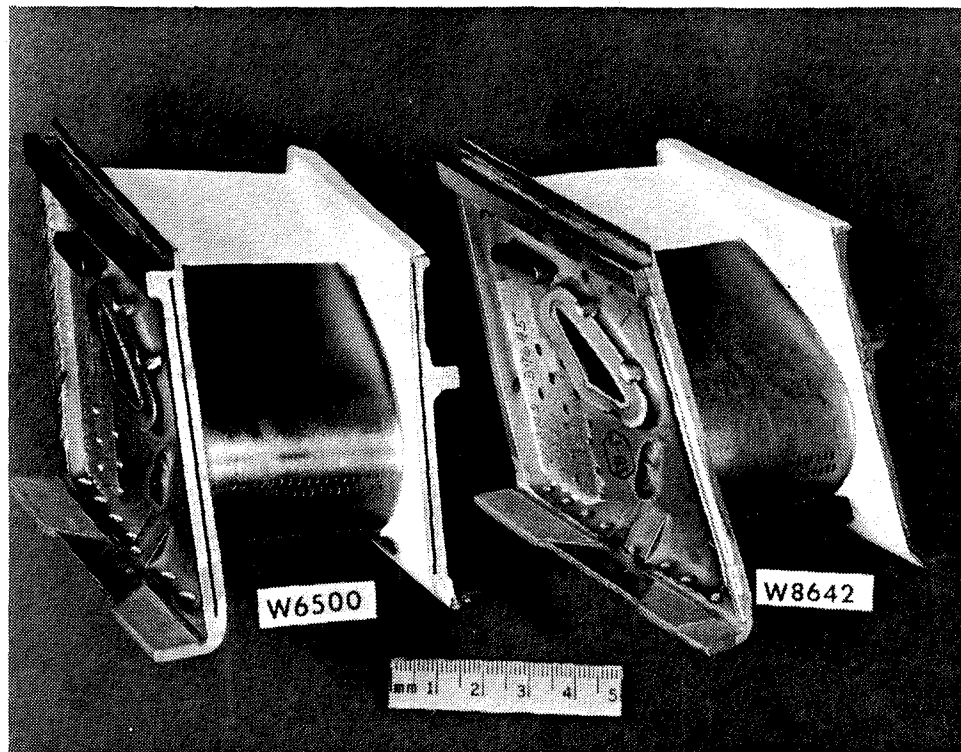
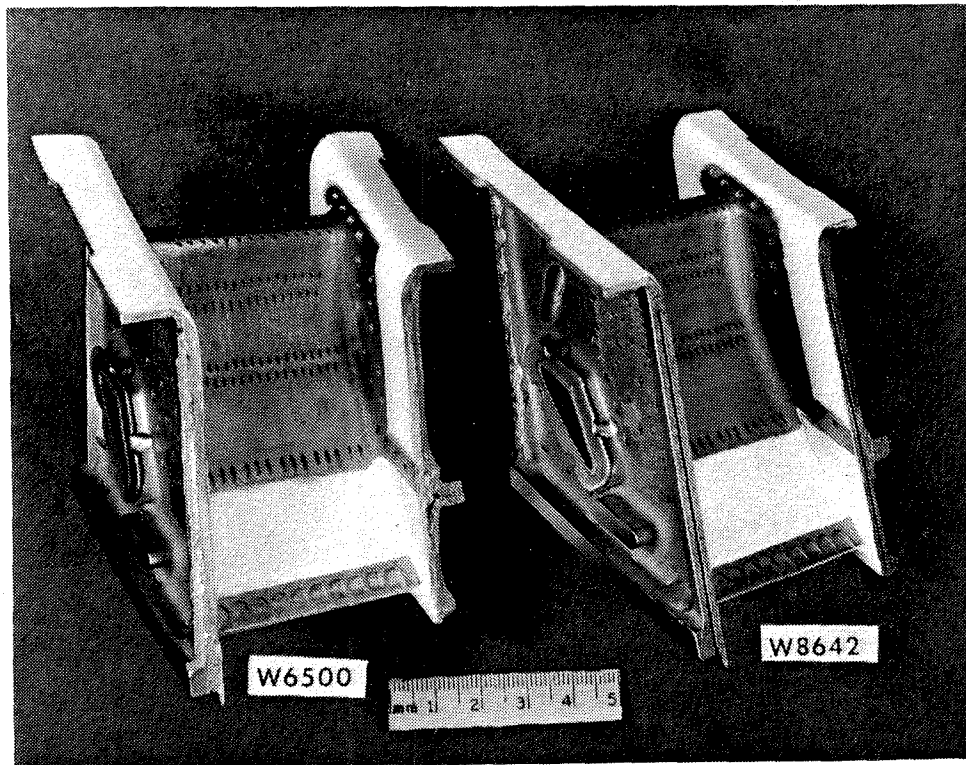


Figure 30. CF6-50, Stage 1 HPT Vanes With Ni-Cr-Al-Y/ZrO₂-20%Y₂O₃ Duplex TBC on Selected Areas.

Stage 2 HPT vanes, which are cast as pairs, were coated with TBC in selected areas governed primarily by component geometry. Areas were selected on the basis of accessibility and thermal stress considerations. The coating was identical to that applied to the Stage 1 vanes except that the ceramic layer thickness was 0.30 mm (0.012 in.). Figure 31 shows several coated Stage 2 vanes.

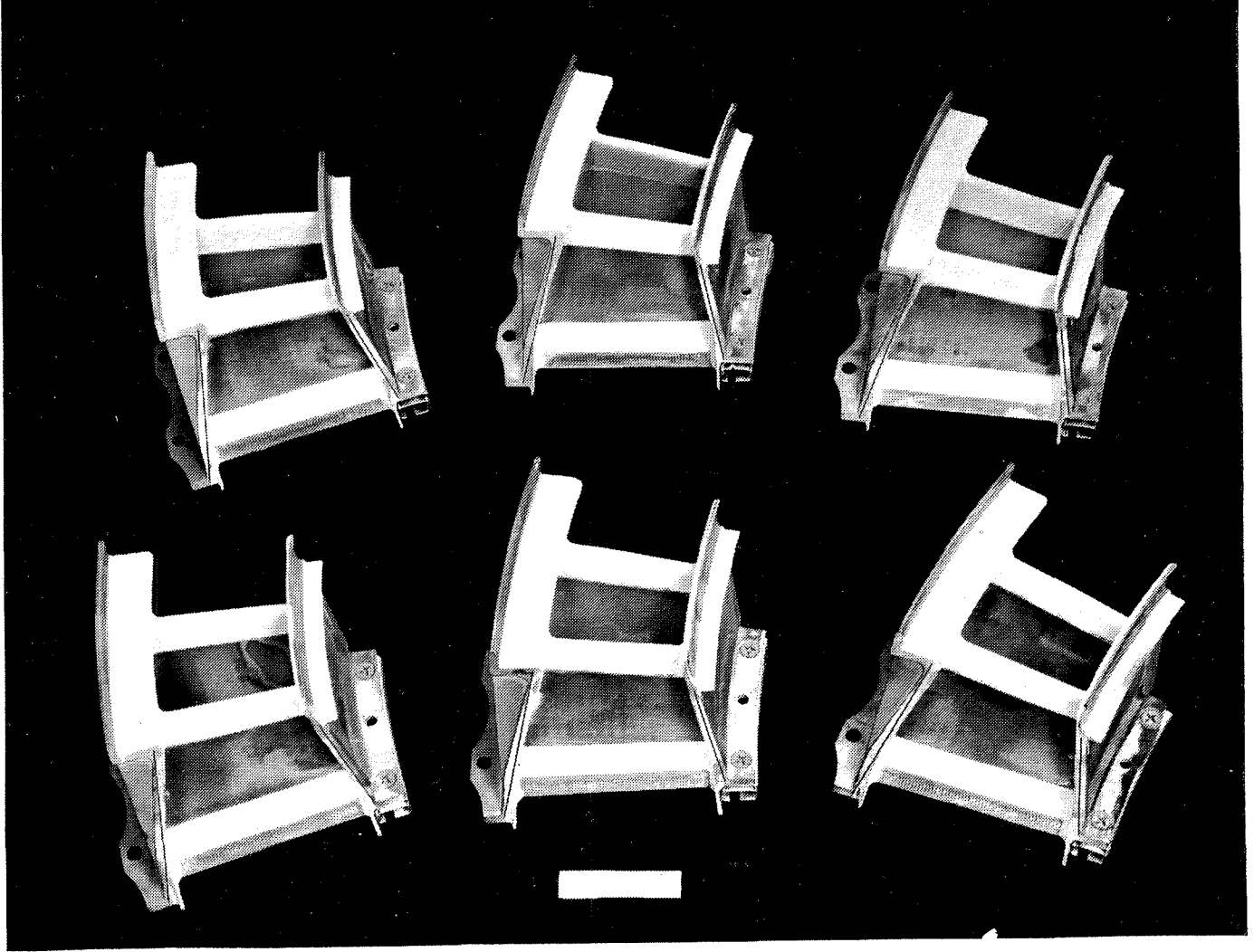


Figure 31. CF6-50, HPT, Stage 2 Vanes (René 80) With Ni-Cr-Al-Y/ZrO₂-20%Y₂O₃ Duplex TBC on Selected Areas.

6.0 TESTING OF THERMAL BARRIER COATED COMPONENTS

High pressure turbine components coated with thermal barrier coatings were tested in three kinds of tests. CF6-50, Stage 1 MATE II (NASA Contract NAS3-20074) HPT blades coated with TBC were tested in a cascade cyclic test rig; coated CF6-50, Stage 2 blades were component high cycle fatigue tested in order to qualify thermal-barrier-coated blades for engine testing; and finally, a number of coated CF6-50 Stage 2 blades and Stage 1 and 2 vanes were run in factory engine tests. These tests and their results are described below.

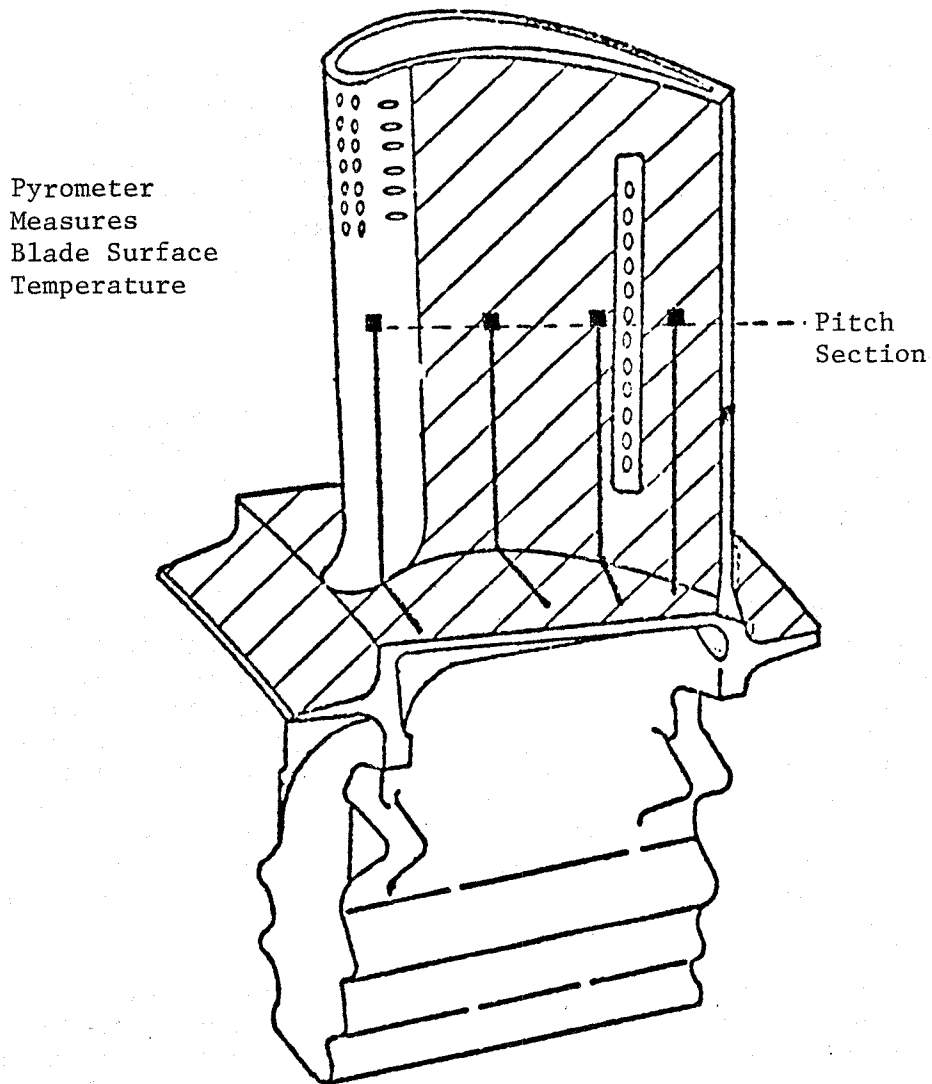
6.1 CASCADE RIG TEST

Thermal-barrier-coated, DS René 150, CF6-50 Stage 1 HPT blades were tested in a cascade cyclic test rig to assess the durability of the TBC under engine simulative heat flux conditions and to measure the thermal benefit obtainable from the TBC. René 150, Stage 1 HPT blades used for the test were coated with EA Ni-Cr-Al-Hf environmental coating prior to application of the TBC. A total of nine blades were used. Six of these blades were instrumented with eight thermocouples each, four on the pressure side and four on the suction side of the airfoil as shown in Figure 32 to measure the temperature at the blade/bond coat interface during the cascade rig test. These blades were coated with the thermal barrier coating system comprised of Ni-Cr-Al-Y bond coat and ZrO₂-20%Y₂O₃ ceramic coat. The thickness of the ceramic layer on the convex sides of all blades was 0.20 mm (0.008 in.). The thickness of the ceramic layer on the concave side of the airfoils was 0.41 mm (0.016 in.) on six blades and 0.20 mm (0.008 in.) on the other three blades; two thicknesses were used to aid in determining the effectiveness of the TBC in reducing the metal temperature of the blades. Figure 33 shows the instrumented and thermal-barrier-coated Stage 1 blades used in the cascade rig testing.

The test rig is shown schematically in Figure 34. Six blades were tested simultaneously in the rig, each with thermocouples. A pyrometer was used to measure ceramic surface temperature. A modified J79, low smoke, single-can combustor was used to provide a hot streak to the cascade package. Combustor airflow was discharged into the combustion transition liner where the flow transitioned from circular to rectangular streamlines.

The blades under test in the cascade were cooled by an external system; blade coolant temperature was controlled automatically, and a manual control valve provided individual blade coolant flow control that was preset prior to the start of testing. Air stream temperature into the cascade was sensed by a traversing temperature rake. The planned temperature and pressure cycle is shown in Figure 35.

The blades were examined after 200 cycles of testing under normal hot gas temperature and pressure and inlet cooling air temperature. The thermal barrier coating on all blades was intact without any evidence of deterioration or



Blade Instrumentation
For Rig Test

Pressure Side - 4 Thermocouples

Suction Side - 4 Thermocouples

Thermocouples Measure Temperature
at Bond and Metal Substrate
Interface

Figure 32. Sketch of CF6-50, Stage 1 Blade Showing Location of Thermocouples.

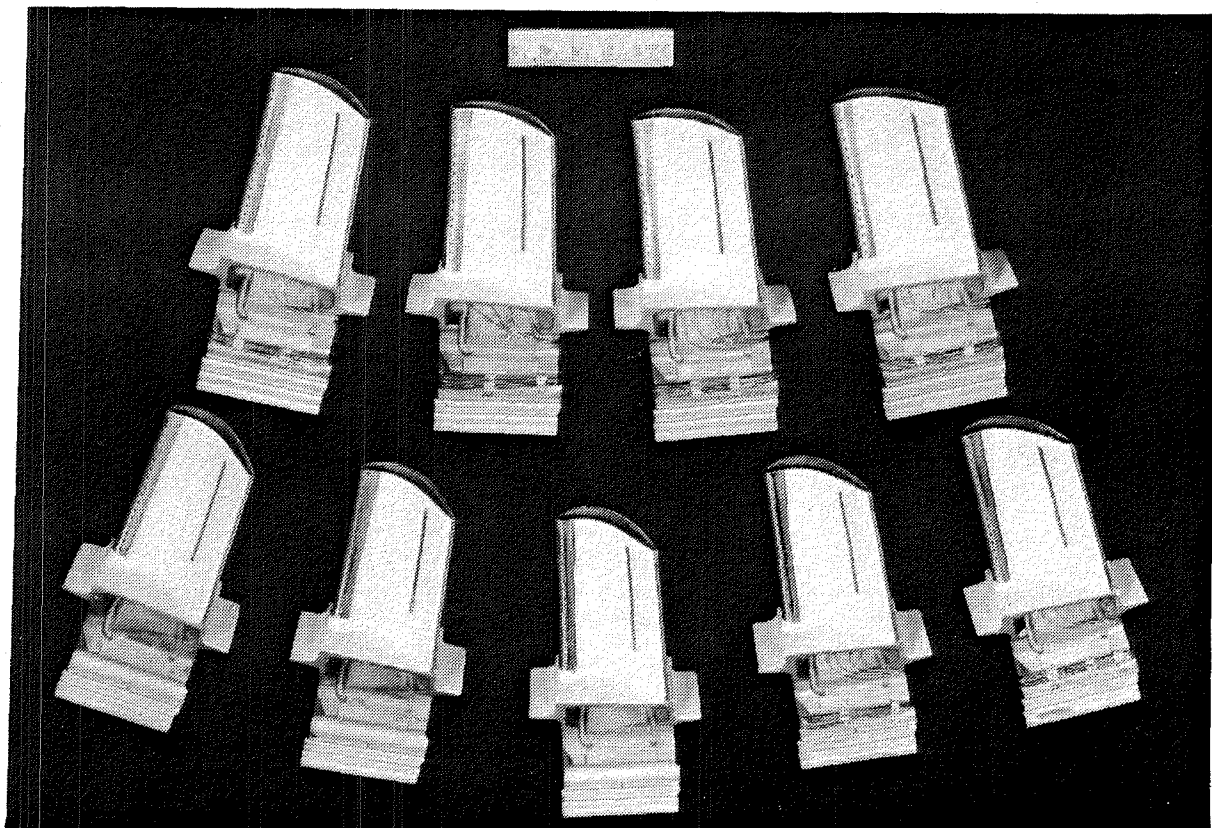


Figure 33. Thermal-Barrier-Coated, CF6-50, Stage 1, MATE II HPT Blades With Thermocouples.

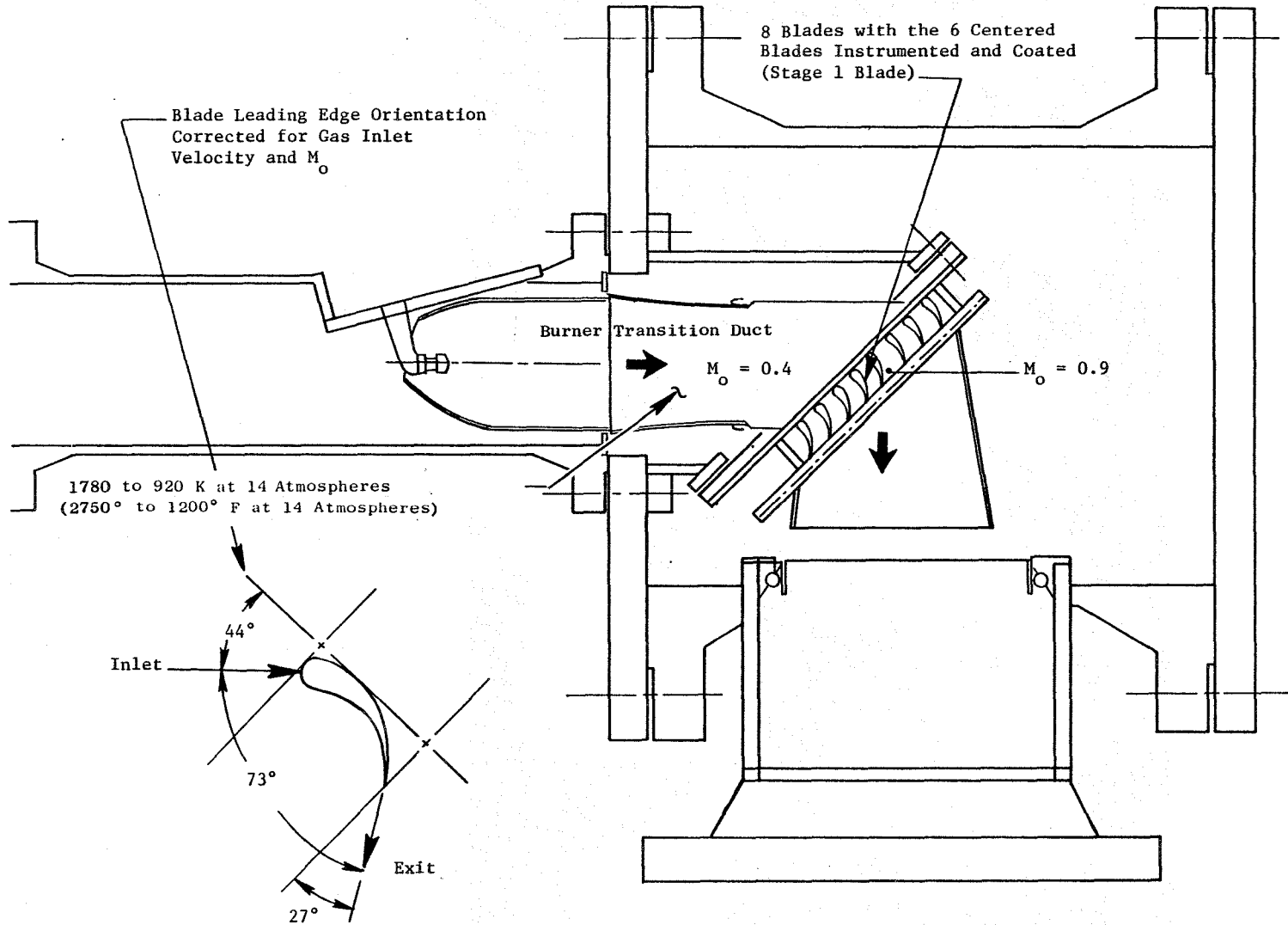


Figure 34. Thermal Barrier Coating Rig Test Configuration.

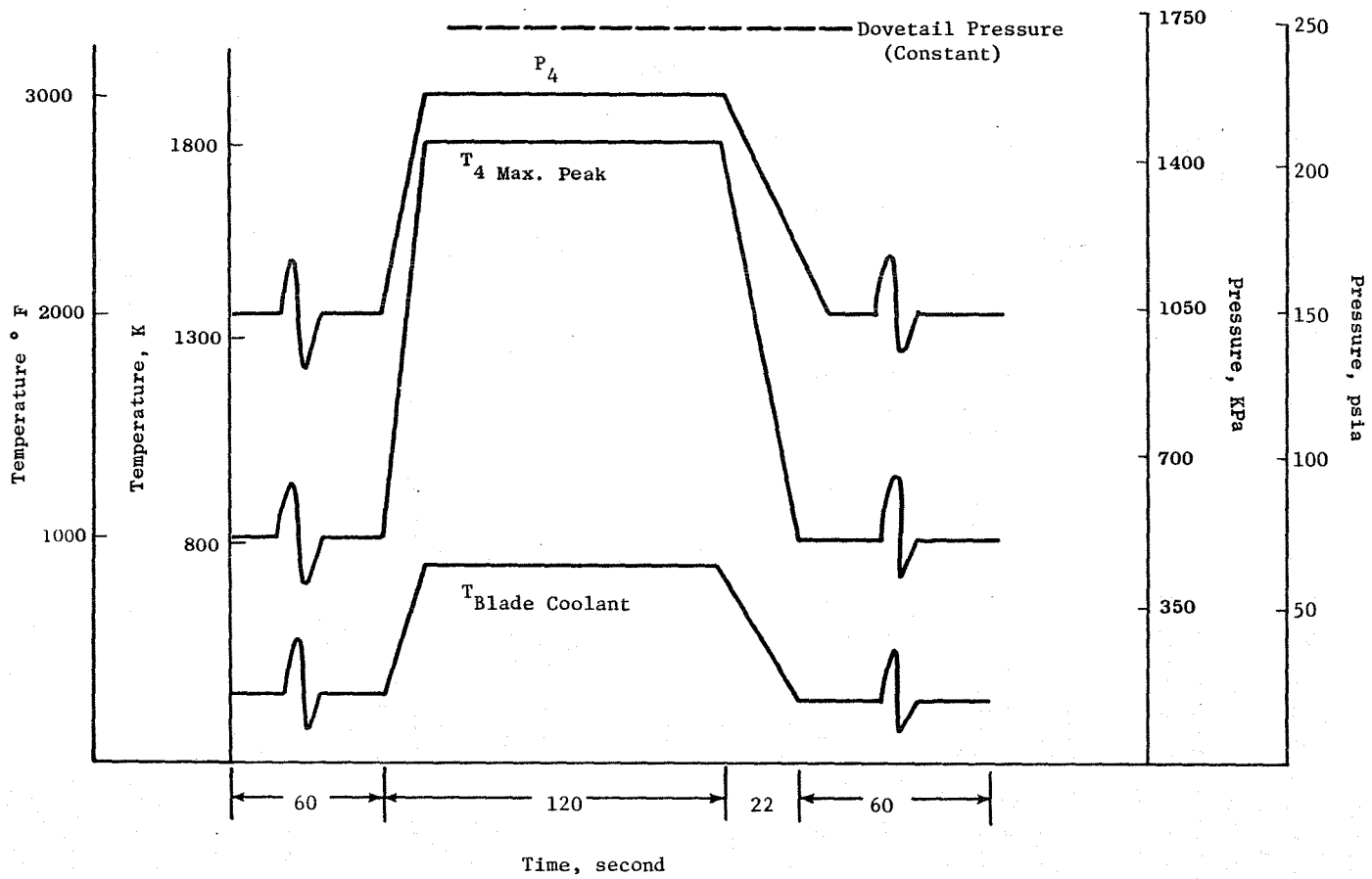


Figure 35. Planned Cyclic Conditions for Cascade Rig Test of Thermal-Barrier-Coated Blades.

erosion. However, the coating had changed to a brown color on the suction side of the blades, presumably due to deposition of a thin iron oxide layer which is normal under the test conditions. The pressure side of the airfoils had a black coating.

During the first 200 cycles, the measured blade temperature was about 220 K (400° F) lower than predicted. For subsequent test cycles, the hot gas temperature and the cooling air inlet temperature were increased to obtain a higher blade metal temperature. After a total of 390 test cycles, failure of a cooling air supply tube resulted in overheating of the blades and leading edge burnout and melting of some blades, as shown in Figure 36.

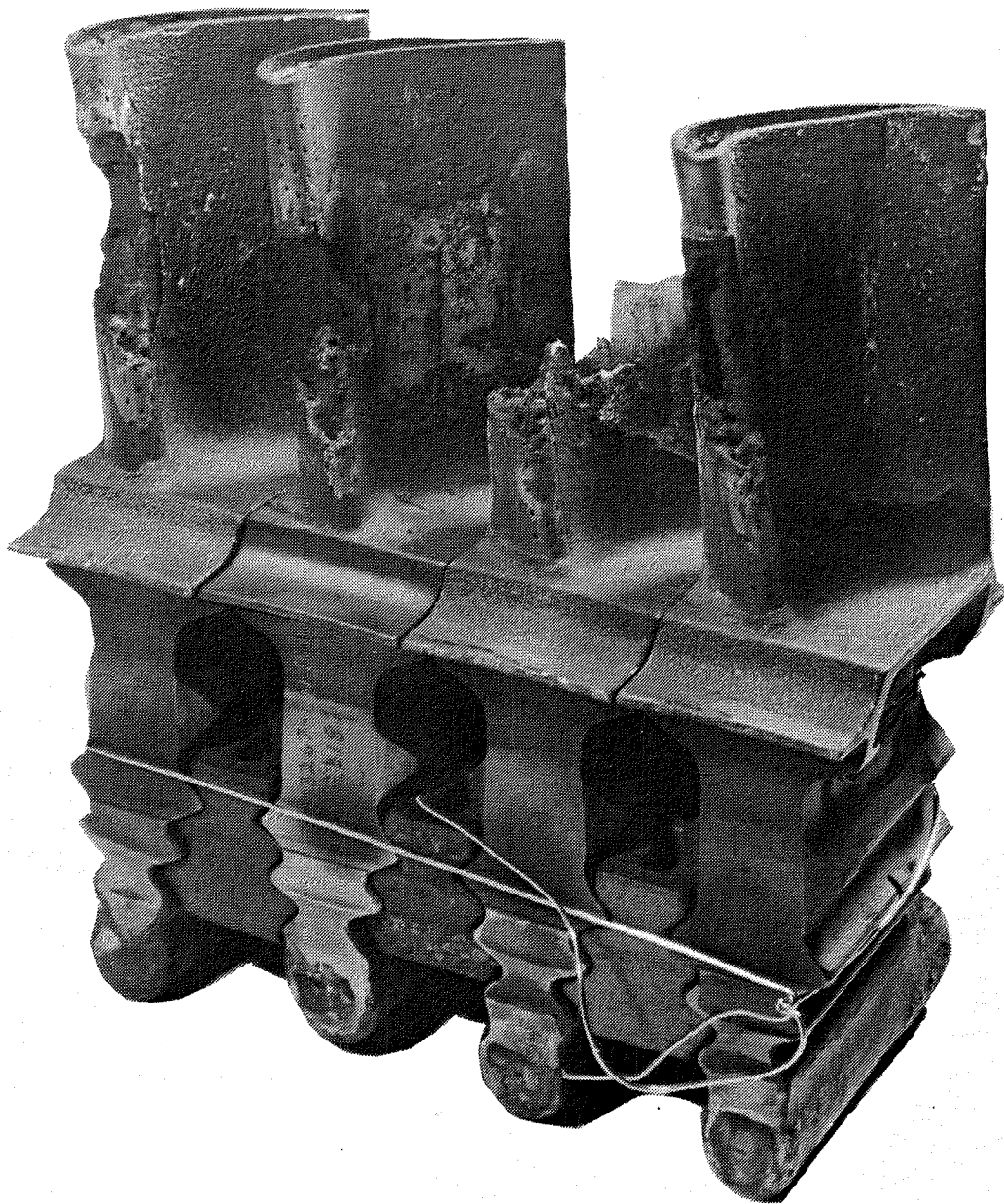
Four blades, including one with only EA Ni-Cr-Al-Hf coating, sustained severe damage and leading edge burnout and melting. The other two thermal-barrier-coated blades did not suffer any burnout and appeared to have most of the thermal barrier coating still well adhered to the substrate. These two blades were used for further cascade rig testing.

The three thermal-barrier-coated blades which had sustained damage still showed the TBC to be intact and adherent in most of the remaining areas, even adjacent to the regions where melting had occurred. One of these blades was used for metallographic evaluations.

The four badly damaged blades were replaced and the test restarted. It was terminated after 605 cycles due to leading edge burnout of two blades caused by negative backflow margin. Figure 37 shows the blades after 605 cycles of cascade rig testing.

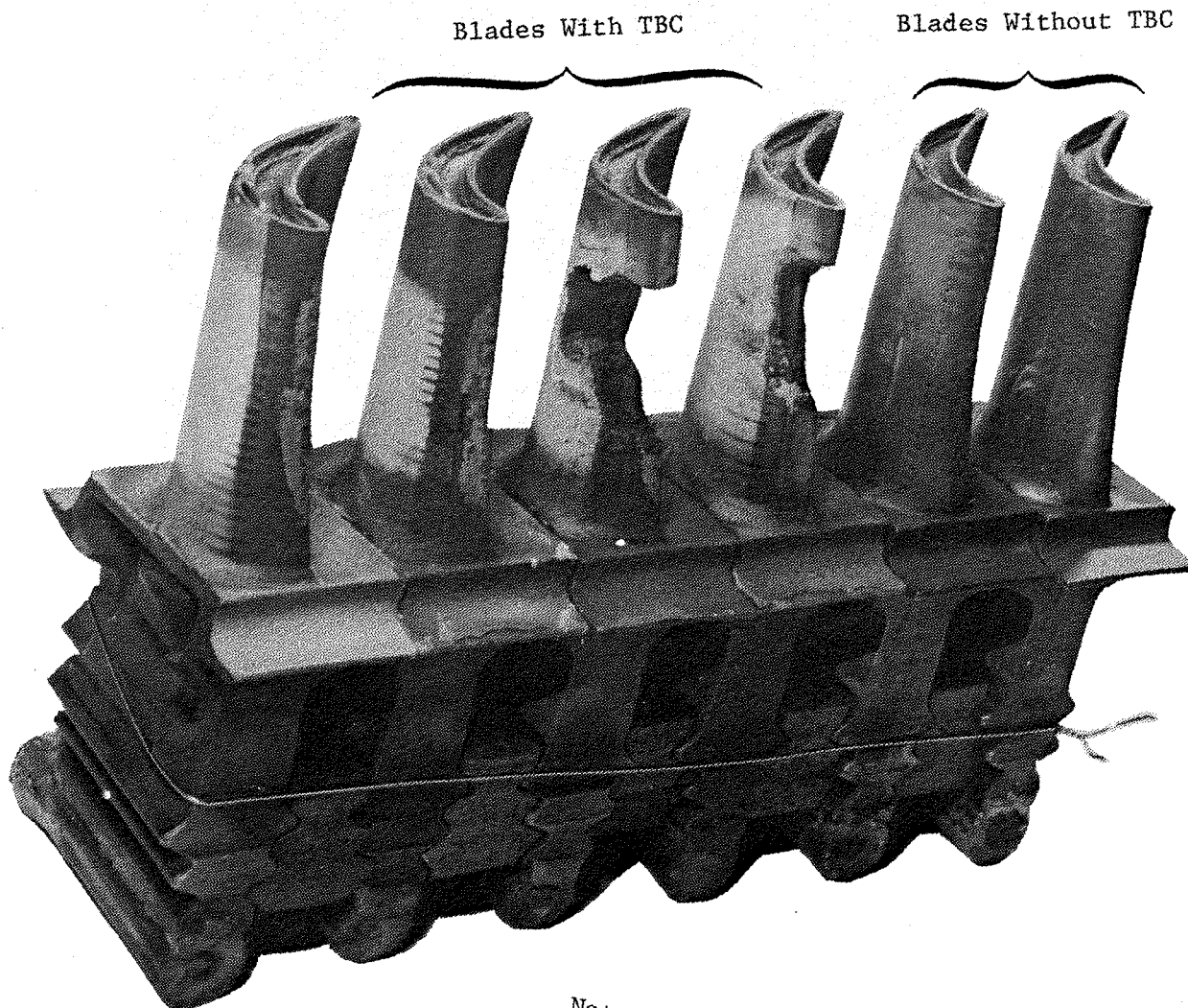
Thermal-barrier-coated blades which had sustained damage in the cascade rig test were evaluated by metallographic and microprobe examinations. Metallographic examination showed the coating to be intact and adherent to the substrate in areas where the blade metal had not been damaged. Figure 38 shows optical micrographs of several regions of the left-most blade in Figure 36. In the region adjacent to the leading edge where the blade metal had melted, the EA Ni-Cr-Al-Hf coating was found to be missing due to either melting or interdiffusion in the substrate and/or bond coat. Despite the loss of the EA Ni-Cr-Al-Hf coating, the bond coat layer and top coat of the TBC system were still present and adhered together. The thermal barrier coating and EA Ni-Cr-Al-Hf coating on other regions of the blade, such as the suction side, near the trailing edge and platform, appeared intact and in good condition.

Microprobe examination showed strong aluminum depletion from the bond coat and from the EA Ni-Cr-Al-Hf environmental coating in the region near the leading edge where local melting had occurred. Also noted in this region was the homogenization of the nickel content in the bond coat, environmental coating, and the DS René 150 substrate. Figure 39 shows the secondary electron image and the elemental X-ray density maps in this region. In a region which had experienced lower temperatures during the test (trailing edge and suction side), the above-mentioned changes did not take place. Coatings retained their original or close to original chemical compositions as shown in Figure 40.



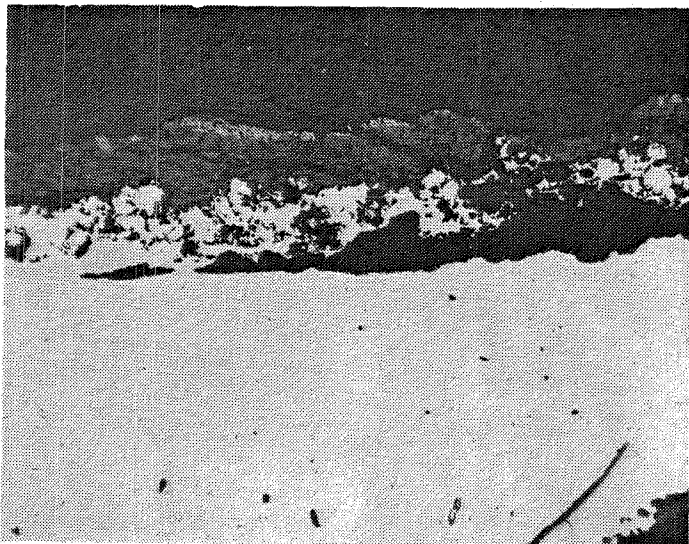
NOTE: The cooling air supply line to the third blade from the left failed after 390 cycles.

Figure 36. Failed Blades After 390 Cycles of Cascade Rig Testing.



Note: The leading edge burnout was caused by a negative backflow margin.

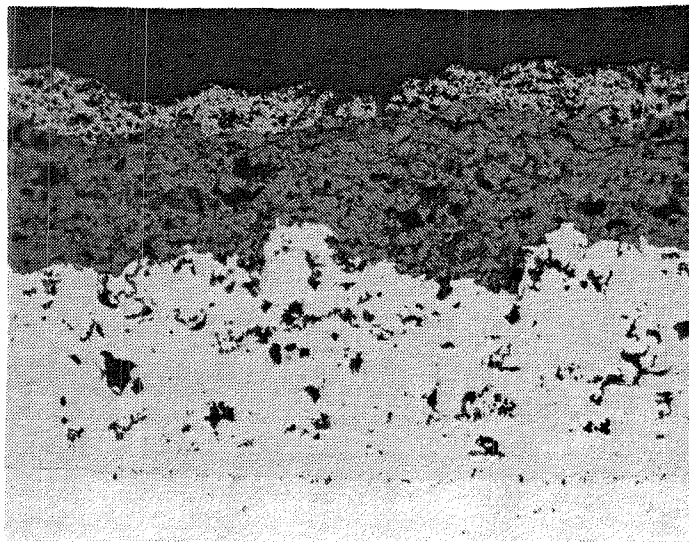
Figure 37. Cascade Rig Test Blades After Termination of Test (605 Cycles).



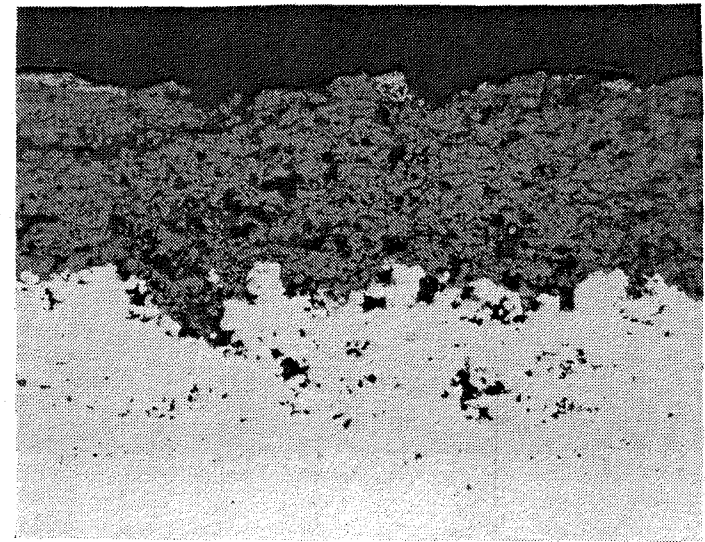
(a) Near Leading Edge in the Damaged Region 200μ



(b) Near Leading Edge in the Damaged Region 100μ

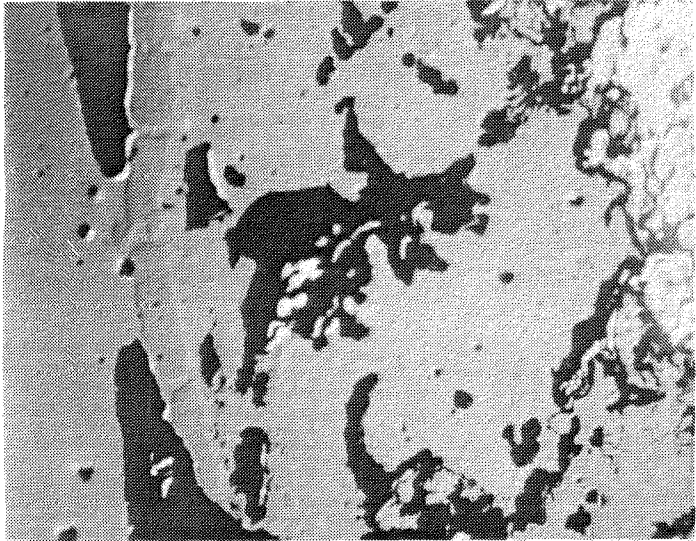


(c) Tip Region, Pressure Side 100μ



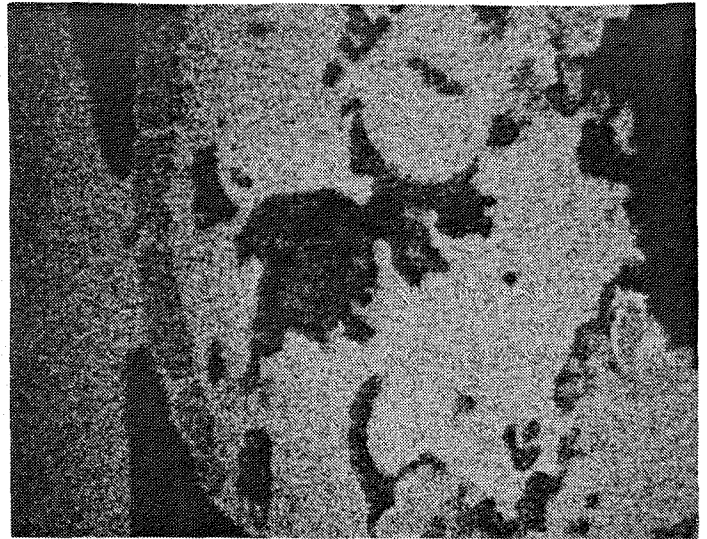
(d) Near Trailing Edge, Pressure Side 100μ

Figure 38. Photomicrographs of Thermal-Barrier-Coated, René 150, CF6-50, Stage 1 HPT Blade (No. 0395) After 390 Cycles of Cascade Rig Testing.

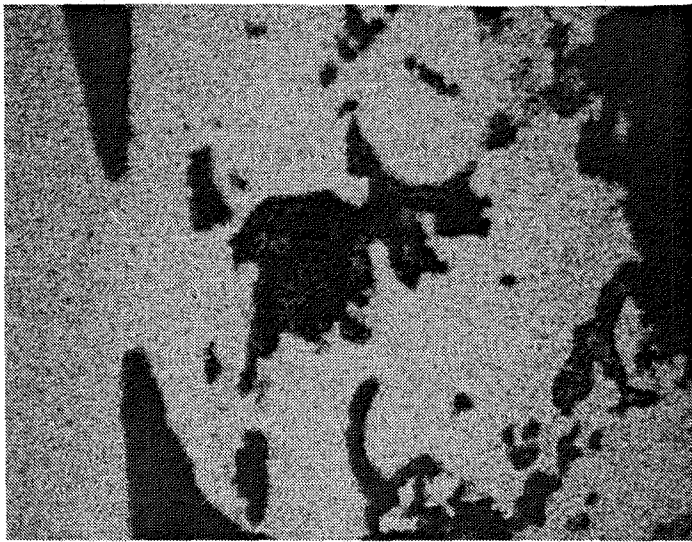


(a) Secondary Electron Image

20 μ

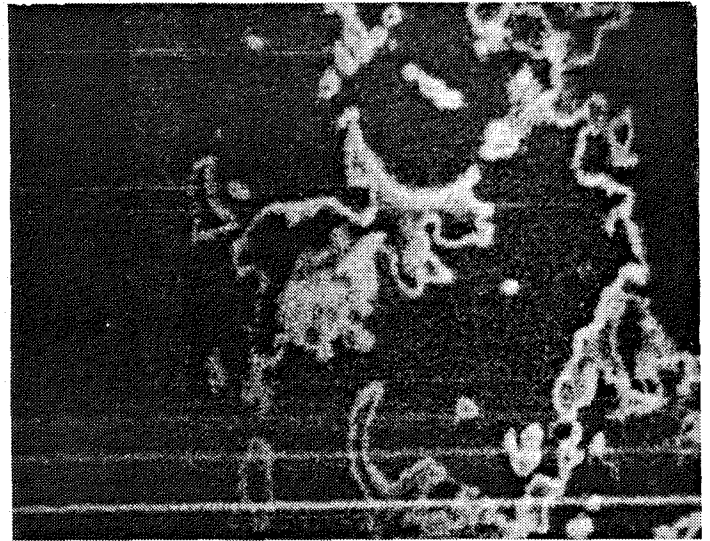


(b) Cr



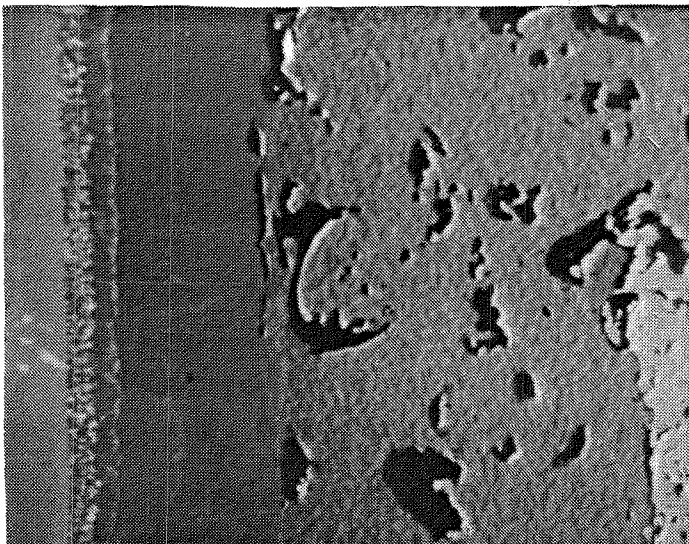
(c) Ni

20 μ

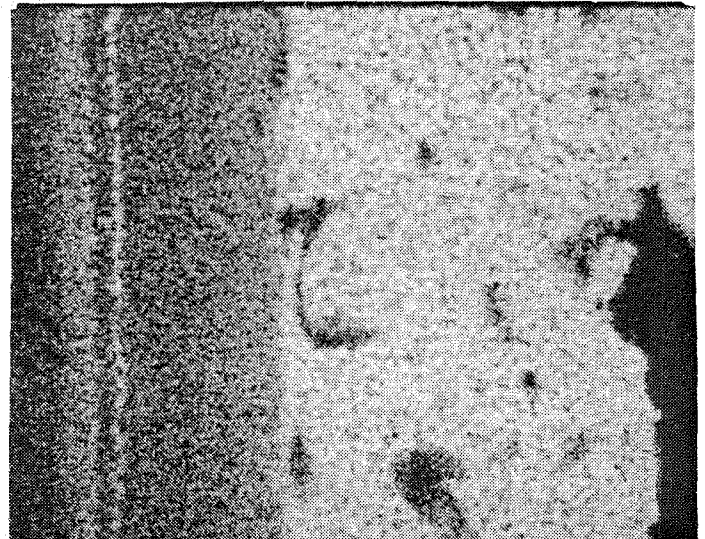


(d) Al

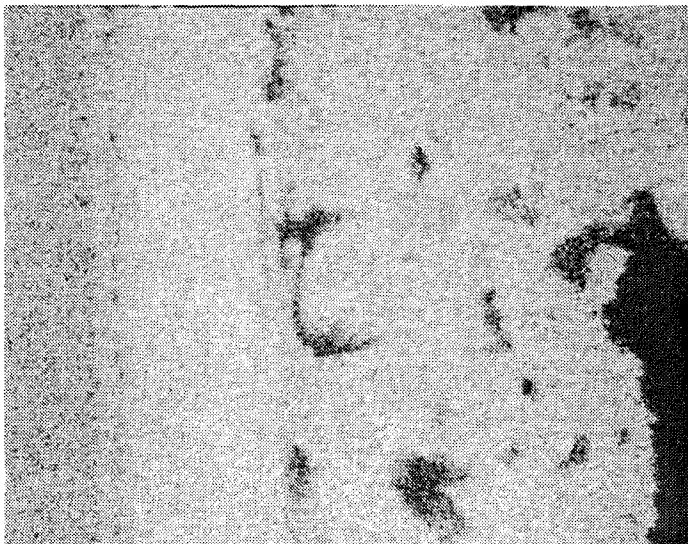
Figure 39. Secondary Electron Image and Elemental X-ray Density Maps of Thermal-Barrier-Coated, CF6-50, Stage 1 HPT Blade (No. 0395) Near the Damaged Region After 390 Cycles of Cascade Rig Testing.



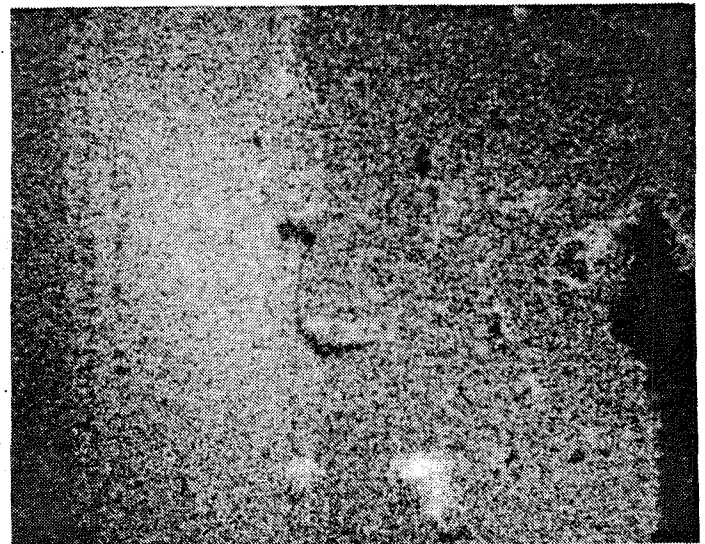
(a) Secondary Electron Image 20 μ



(b) Cr



(c) Ni 20 μ



(d) Al

Figure 40. Secondary Electron Image and Elemental X-ray Density Maps of Thermal-Barrier-Coated, CF6-50, Stage 1 HPT Blade (No. 0395) Near Trailing Edge After 390 Cycles of Cascade Rig Testing.

The black deposit which was observed on the pressure side of the blade was well bonded to the ceramic layer. This deposit was found to contain Fe, Ni, Cr, Co, Cu, and Al. The source of this deposit is believed to be contaminants in the air supply lines to the test cell and surface material losses from the transition components carrying the hot gases from the combustor to the airfoils.

Although the thermal-barrier-coated blades were subjected to much more severe conditions than planned, the durability of the TBC under these severe conditions as exemplified by the presence of the TBC on the blade surface just adjacent to regions that underwent local melting was encouraging.

6.2 COMPONENT HIGH CYCLE FATIGUE TESTS

Several CF6-50 Stage 2 HPT blades coated with nominal thicknesses of 0.13 mm (0.005 in.) Ni-Cr-Al-Y bond coat applied by the VPS process and 0.25 mm (0.010 in.) of ZrO_2 - Y_2O_3 top coat underwent component high cycle fatigue testing. This was done in order to determine whether the presence of the TBC on the blades affects the high cycle fatigue behavior of the blades compared to the behavior of uncoated blades. The assessment was one of the requirements for qualifying the thermal-barrier-coated blades for evaluation in factory engine tests.

The airfoils were heated to test temperature of 1200 K (1700° F) by an induction coil with a suscepter. Temperature was measured using thermocouples; on each blade, one thermocouple was attached to the underside of the platform on the pressure side of the blade and a second thermocouple was inserted into the internal air passages of the blade through one of the cooling inlet holes in the dovetail. This second thermocouple was removed once thermal equilibrium had been reached and before high cycle fatigue testing was begun. The relationship of temperatures at these locations to temperatures at other regions of the blade was determined in a preliminary test of a thermal-barrier-coated blade with thermocouples attached to the airfoil in several areas where the coating had been removed locally.

A total of 11 thermal-barrier-coated, Stage 2 blades were high cycle fatigue tested. Eight of these were coated as part of another research program (Contract NAS3-21727) and tested immediately prior to the testing of the blades coated under this project. The test results of the blades for the two projects were quite similar, permitting acceptance of the blades from this project with a minimum of testing.

High cycle fatigue testing of the blades (coated under Contract NAS3-21727) was begun with a blade tip deflection of 2 mm (0.080 in.). A staircase method was used to determine the tip deflection to be used on subsequent blades. If failure occurred at a given tip deflection, the next blade was tested with 0.25 mm (0.010 in.) less deflection; if failure did not occur (runout was 10^7 cycles), the next blade was run with 0.25 mm (0.010 in.) greater deflection. The test results are shown along with the results from

the other coated blades in Figure 41. The average HCF strength of the thermal-barrier-coated blades compared favorably to the strength of uncoated blades, and the thermal-barrier-coated blades were qualified to be run in engine evaluation.

6.3 ENGINE TESTS

Several thermal-barrier-coated, CF6-50, high pressure turbine components were tested in each of two factory engine tests. Twelve fully coated Stage 2 blades were run in the first of these tests. Ten fully coated Stage 2 blades were run in the second engine test along with four partially coated Stage 1 vane pairs and seven partially coated Stage 2 vane pairs. These engine tests and the behavior of the thermal-barrier-coated components are described below.

Heat transfer and mechanical analyses were performed to predict temperatures and stresses in Stage 2 blades and thermal barrier coating layers under steady-state and transient conditions. The results of these analyses are reported elsewhere (Reference 7). The lack of well-established TBC failure criteria precluded the reliable prediction of coating behavior, but the absence of large compressive stresses or strains in the ceramic layer suggested that the coating should survive the cyclic engine testing. Analysis indicated that if spalling were to occur, the calculated blade life would exceed that required to survive the planned endurance cycle tests.

6.3.1 First Engine Test

Twelve thermal-barrier-coated, CF6-50, Stage 2 blades were run in this engine test (Engine S/N 455-508/20). The blades were fully coated on the airfoils and platforms as shown in Figure 42. Six of the blades were coated at GE-CRD under NASA Contract NAS3-21727 (Reference 7).

The thermal barrier coating consisted of a 0.13 mm (0.005 in.) thick bond coat layer of Ni-22Cr-10Al-1Y applied by vacuum plasma spray and a 0.25 mm (0.010 in.) thick top coat layer of ZrO_2 -Y₂O₃ applied by the conventional arc plasma spray process. The zirconia layer applied to the blades at GE-AEBG had a composition of ZrO_2 -20%Y₂O₃ and was applied using programmed mechanical manipulation of the plasma torch as described in Section 5.1. The blades coated at GE-CRD had a top coat composition of ZrO_2 -8%Y₂O₃ applied with manual manipulation of the plasma torch. The coating of these latter blades is described elsewhere (Reference 7).

The 12 thermal-barrier-coated blades were assembled in a rotor along with 62 standard aluminide coated blades, balanced and tip ground. No damage was observed on the thermal-barrier-coated blades after the tip grinding operation. The rotor was then assembled in the engine which was scheduled to run for 1500 "C" cycles. A typical "C" cycle is shown in Figure 43.

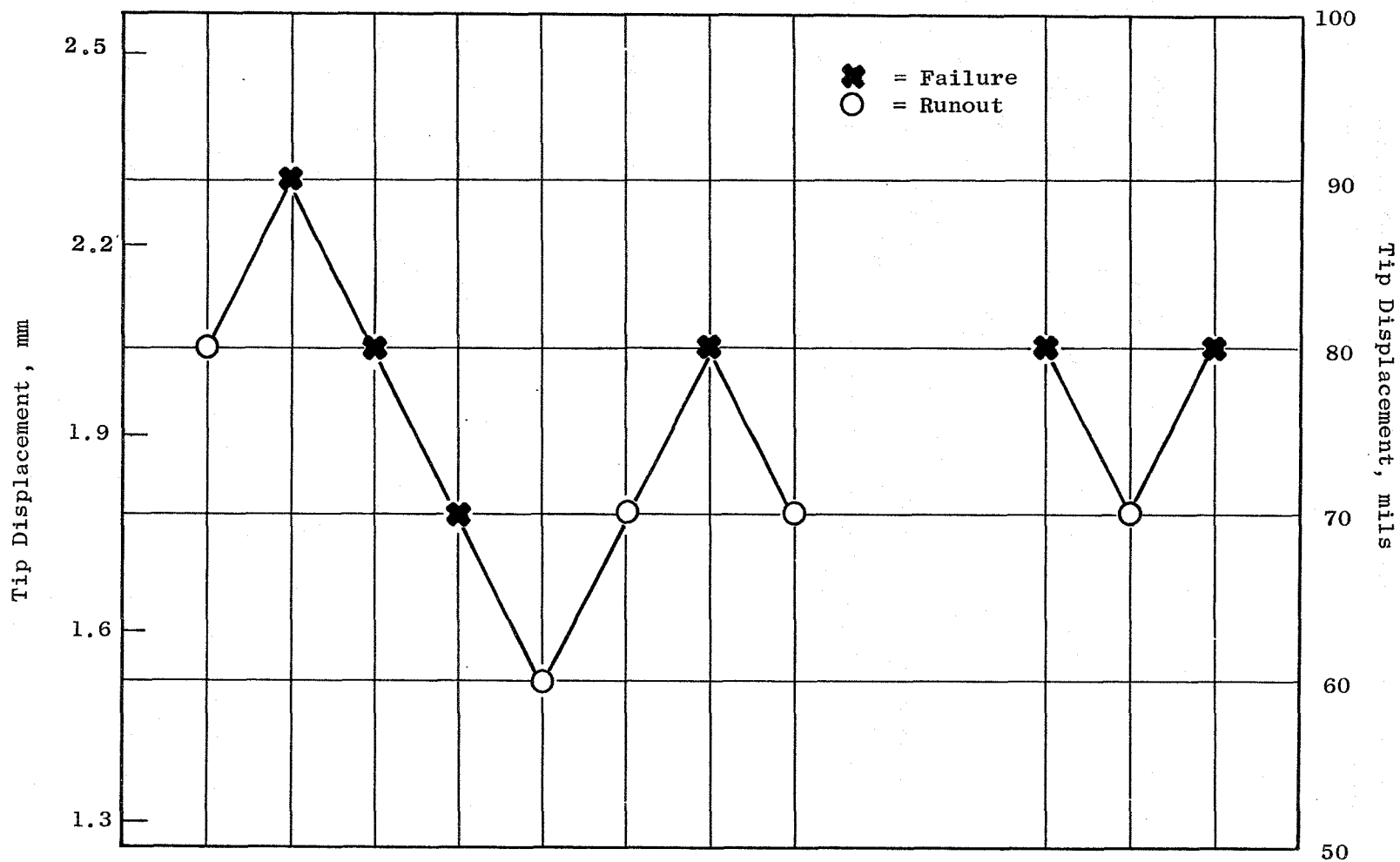


Figure 41. Component High Cycle Fatigue Test Results of Thermal-Barrier-Coated Blades at 1200 K (1700° F).

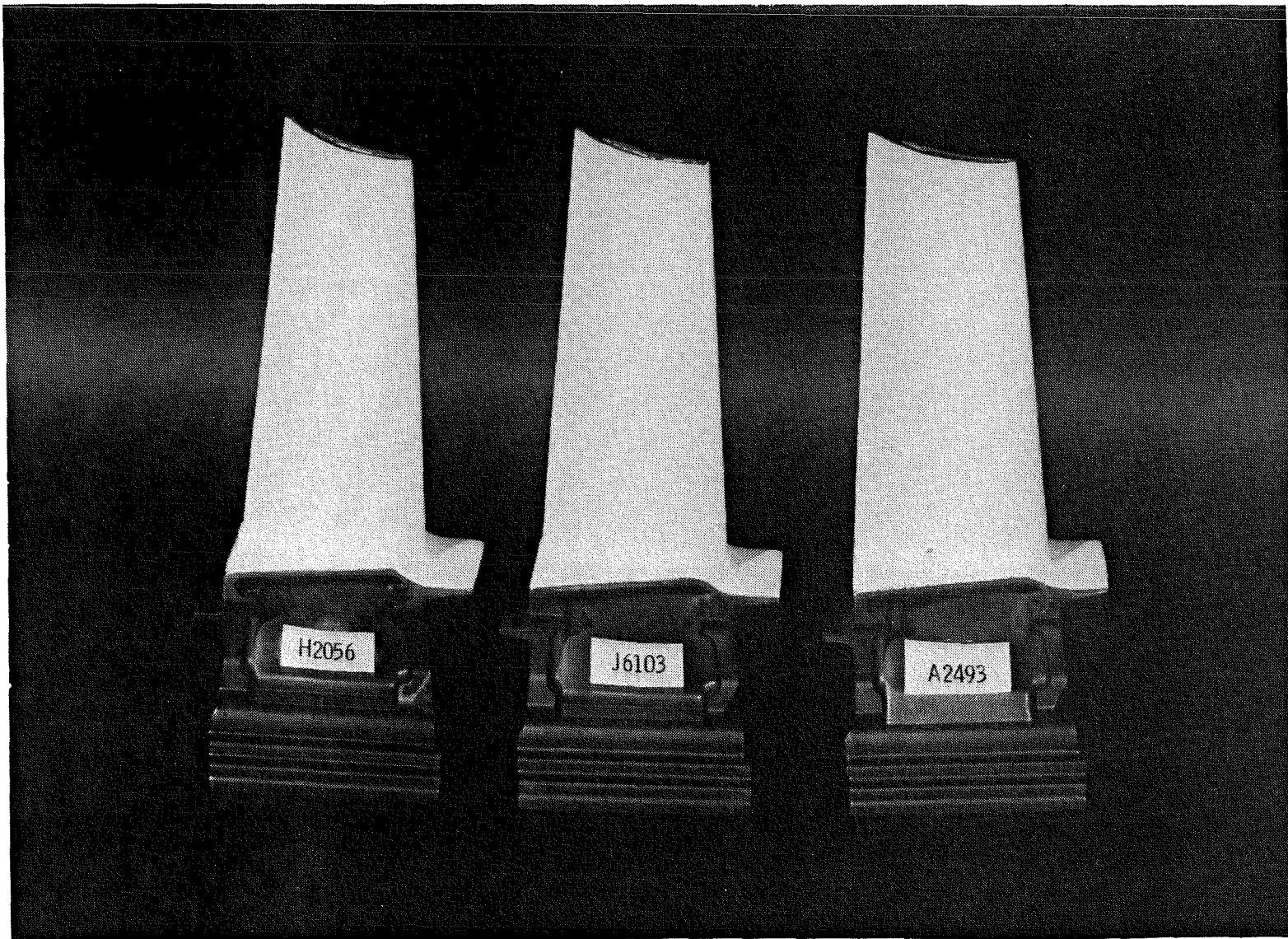


Figure 42. Thermal-Barrier-Coated, CF6-50, Stage 2 Blades.

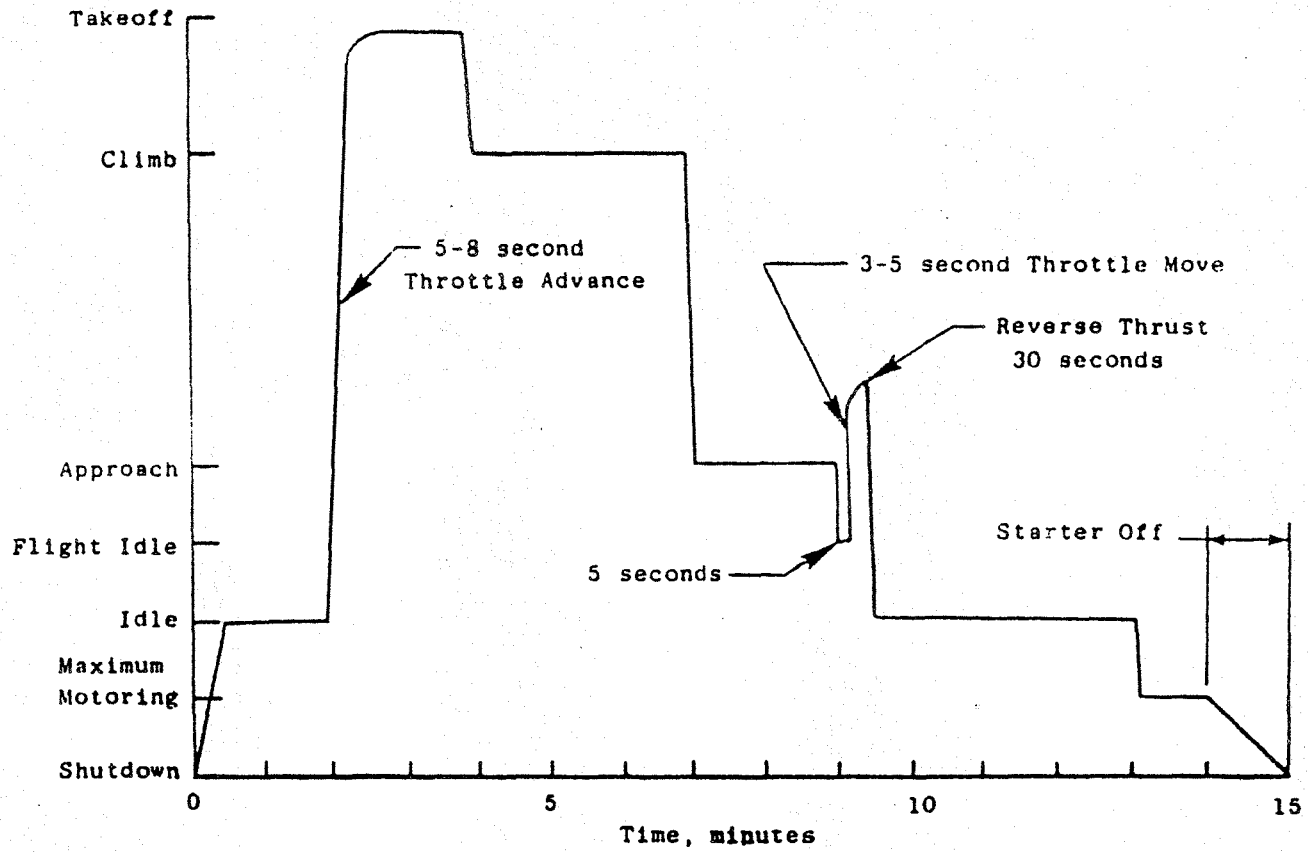


Figure 43. CF6-50 Engine Output Versus Time for Endurance Testing "C" Cycle.

Examination of the blades after 16 hours of engine checkout revealed coating damage on all of the thermal-barrier-coated blades. The damage was restricted to the upper 1/3 of the leading edge on the airfoils and appeared to be small pock marks in the ceramic layer. A photograph of the damage, taken through a borescope, is shown in Figure 44. The damage is believed to be due to impact of material lost by some developmental shrouds in the first stage of the high pressure turbine. Subsequent borescope examination of the blades during the test showed no observable progression of the damage to the leading edge after 316 "C" cycles. However, examination after 467 "C" cycles showed additional ceramic coating loss at the leading edge as shown in Figure 45. No coating loss was observed at any other location on the blades. The test was terminated after 626 "C" cycles due to an engine failure unrelated to the second stage blades.

All of the second stage blades (those with and without TBC) were severely damaged when the engine failed. Extensive loss of blade material occurred at the leading edge and blade tip. In addition, considerable impact damage was noted on the suction side of the airfoils near the leading and trailing edges. Evaluation of the engine-run blades was limited because of the extensive damage. However, despite the abnormally severe conditions, the TBC remained adherent over most of the airfoil and platform except in areas where severe impact had occurred.

6.3.2 Second Engine Test

A number of thermal-barrier-coated, high pressure turbine components were run in a second CF6-50 factory engine test for 1000 "C" cycles (engine S/N 455-508/21). Included were four Stage 1 vane pairs, seven Stage 2 vane pairs, and 10 Stage 2 blades. The vanes were coated in selected areas of the airfoils and bands with a TBC comprising 0.13 mm (0.005 in.) of Ni-Cr-Al-Y bond coat and 0.30 mm (0.012 in.) of $ZrO_2-20\%Y_2O_3$ top coat. Both coating layers were manually sprayed in air. The areas which were coated on the Stage 1 vanes are shown in Figure 30, and Figure 31 shows the coated areas of Stage 2 vanes.

The 10 Stage 2 blades were coated with a nominal thickness of 0.13 mm (0.005 in.) of Ni-Cr-Al-Y bond coat and 0.25 mm (0.010 in.) of $ZrO_2-Y_2O_3$ top coat. The Ni-Cr-Al-Y bond coat was applied in a low pressure, inert gas environment using automated manipulation. Five of the blades had a top coat of $ZrO_2-20\%Y_2O_3$, whereas the other five had a top coat of $ZrO_2-8\%Y_2O_3$. Three of the blades with $ZrO_2-8\%Y_2O_3$ were coated at GE-CRD under NASA Contract NAS3-21727 (Reference 7). Three coated Stage 2 blades are shown in Figure 42. The results of the engine tested, thermal-barrier-coated, high pressure turbine components are described below.

Some minor coating damage consisting of small chips from the edge of the coating at the tip on the pressure side of the airfoils occurred during tip grinding of the blades prior to engine assembly. The next examination of the blades took place after 27 hours of engine checkout. A borescope examination revealed some coating damage on the leading edge near the tips of the thermal-barrier-coated blades, as shown in Figure 46. Some of the ceramic layer was

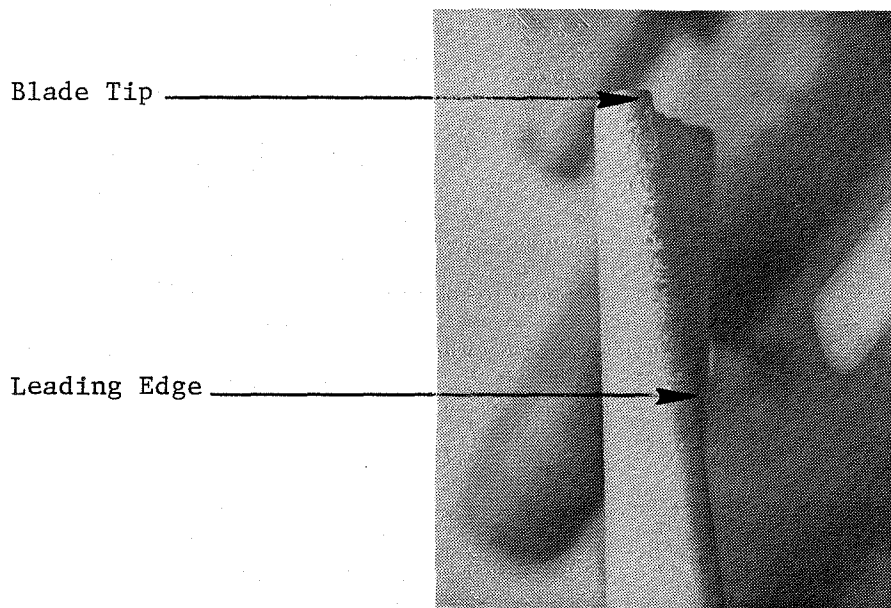


Figure 44. Photograph Showing Damage to Leading Edge of Thermal-Barrier-Coated Blade After 16 Hours of Engine Checkout.

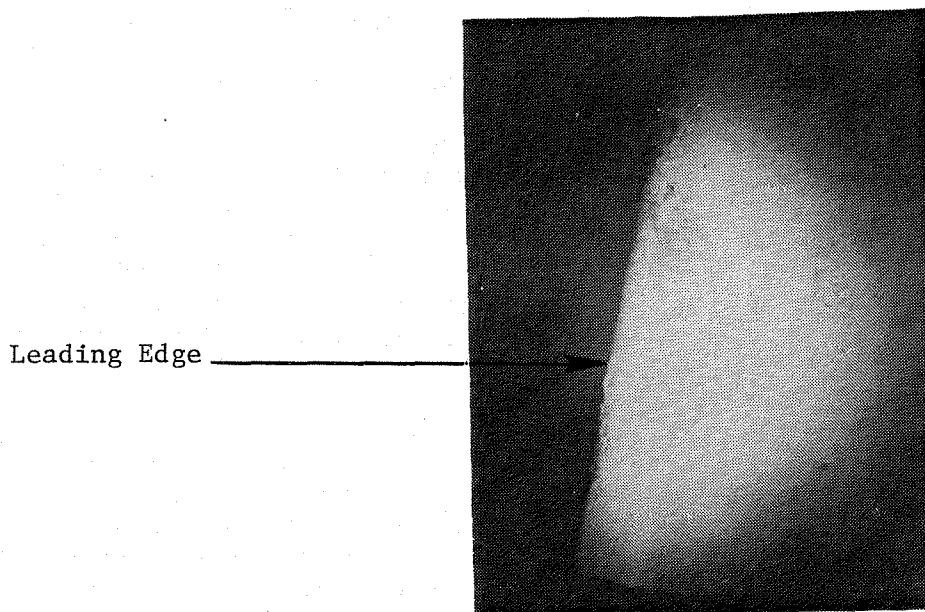


Figure 45. Borescope Photograph Showing Extent of Damage to Leading Edge of Thermal-Barrier-Coated Blade After 476 "C" Cycles.

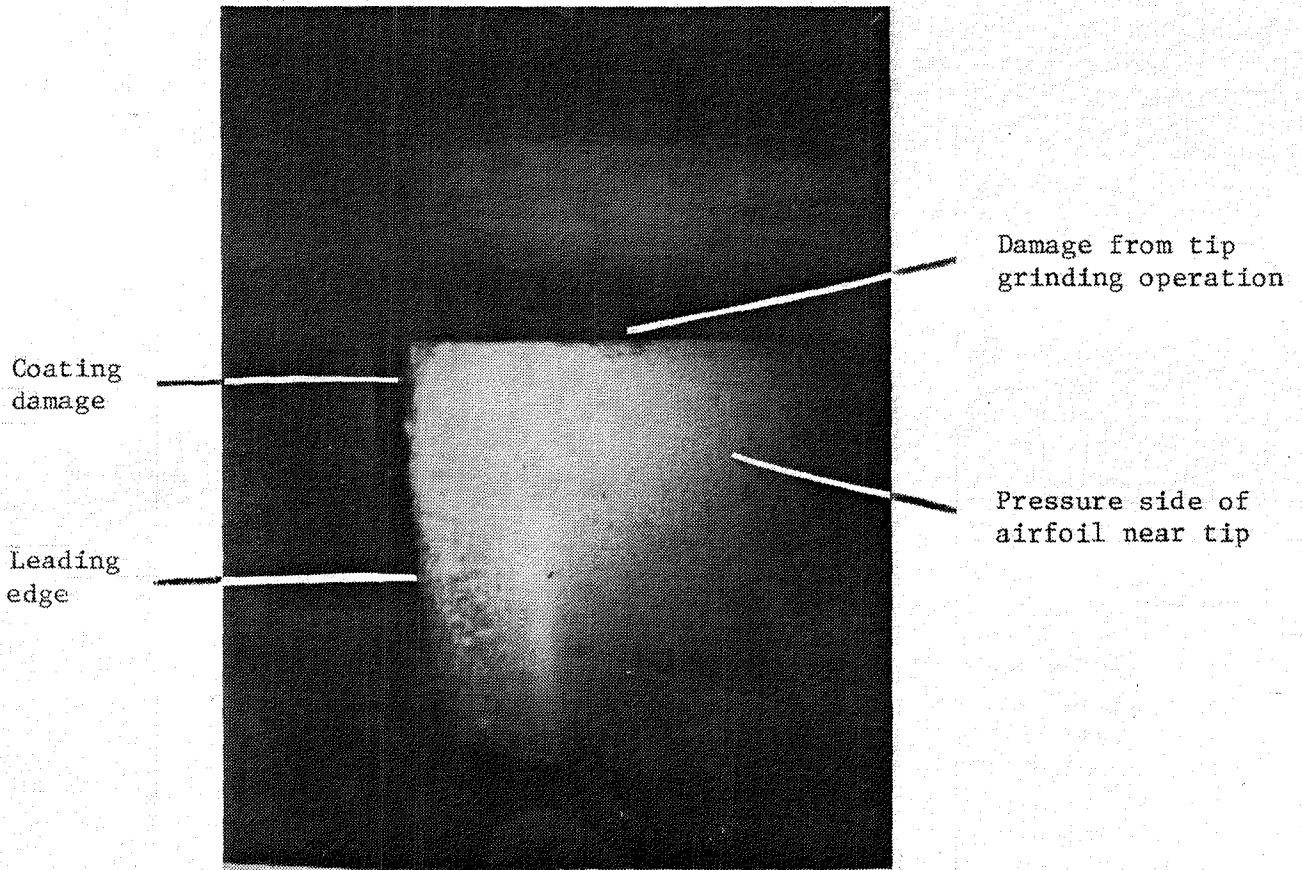


Figure 46. Borescope Photograph of Coating Damage After 27 Hours of Engine Checkout (Blade A2139).

missing, but it was not apparent through the borescope whether the loss occurred as a result of thermal cycling or as the result of impact damage. Bore-scope inspections after 225, 450, and 663 cycles of testing showed the damage still to be limited to the area from about 75% span to the tip, but the damage appeared to progress somewhat during the course of the testing. The vanes were not readily accessible to borescope inspection. At the conclusion of the 1000 "C" cycle test, the Stage 2 blades and vanes were removed from the engine and examined. The Stage 1 vanes remained in the engine for use in a subsequent build.

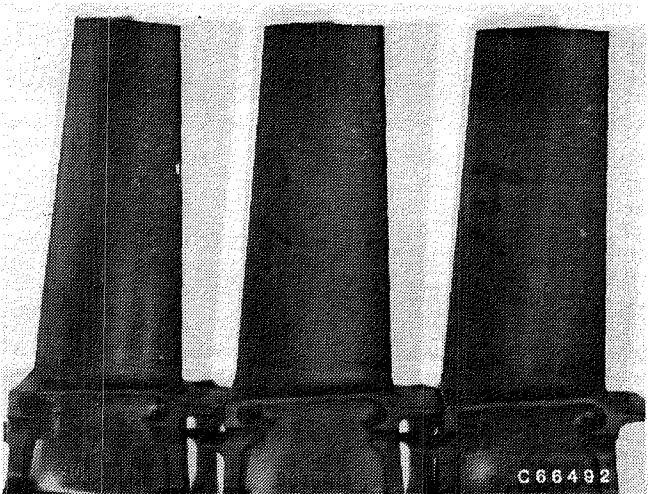
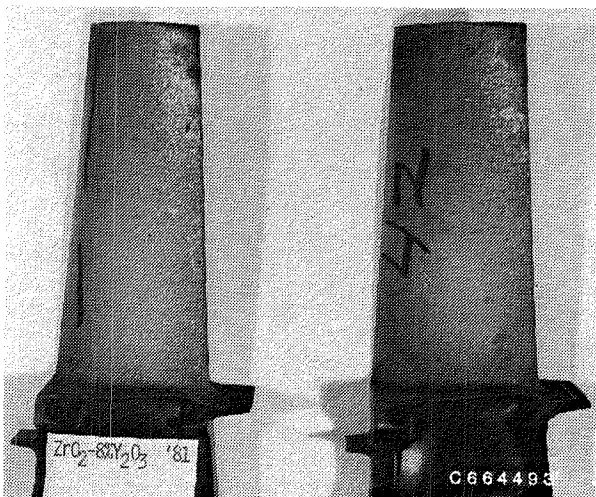
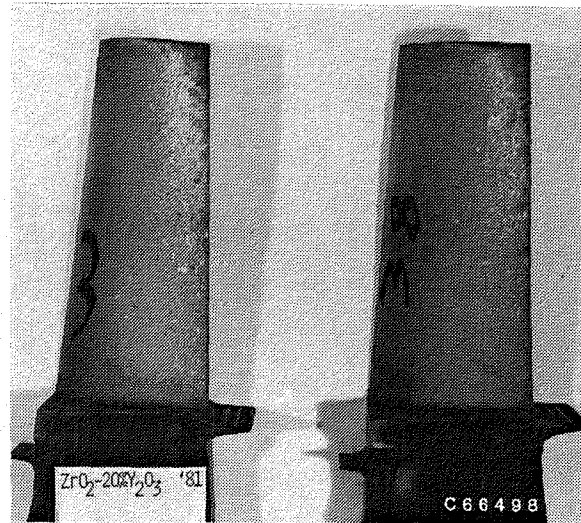
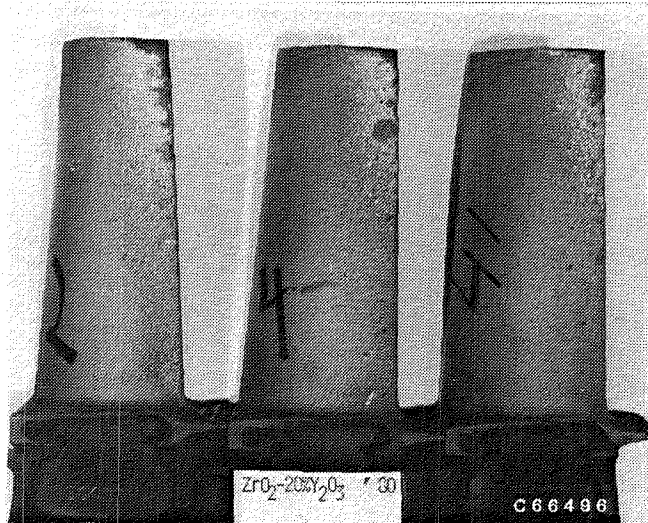
6.3.3 Posttest Analyses

Blades

Visual examination of the thermal-barrier-coated blades after removal from the engine showed the TBC to be in excellent condition, except at the leading edge on the suction side, as shown in Figure 47a. Figure 47b shows the pressure side of the engine-tested blades. It was observed that there was no loss of coating on the platforms except for one spalled area (approximately 7.5 by 5 mm) on one blade. The coating on the forward extension of the platform (angel wing) of several of the blades contained deep grooves caused by radial rubs against stationary parts; however, the TBC adjacent to the grooves remained intact. There was no loss of coating from the pressure side of the airfoils or from the greater part of the suction side of the airfoils.

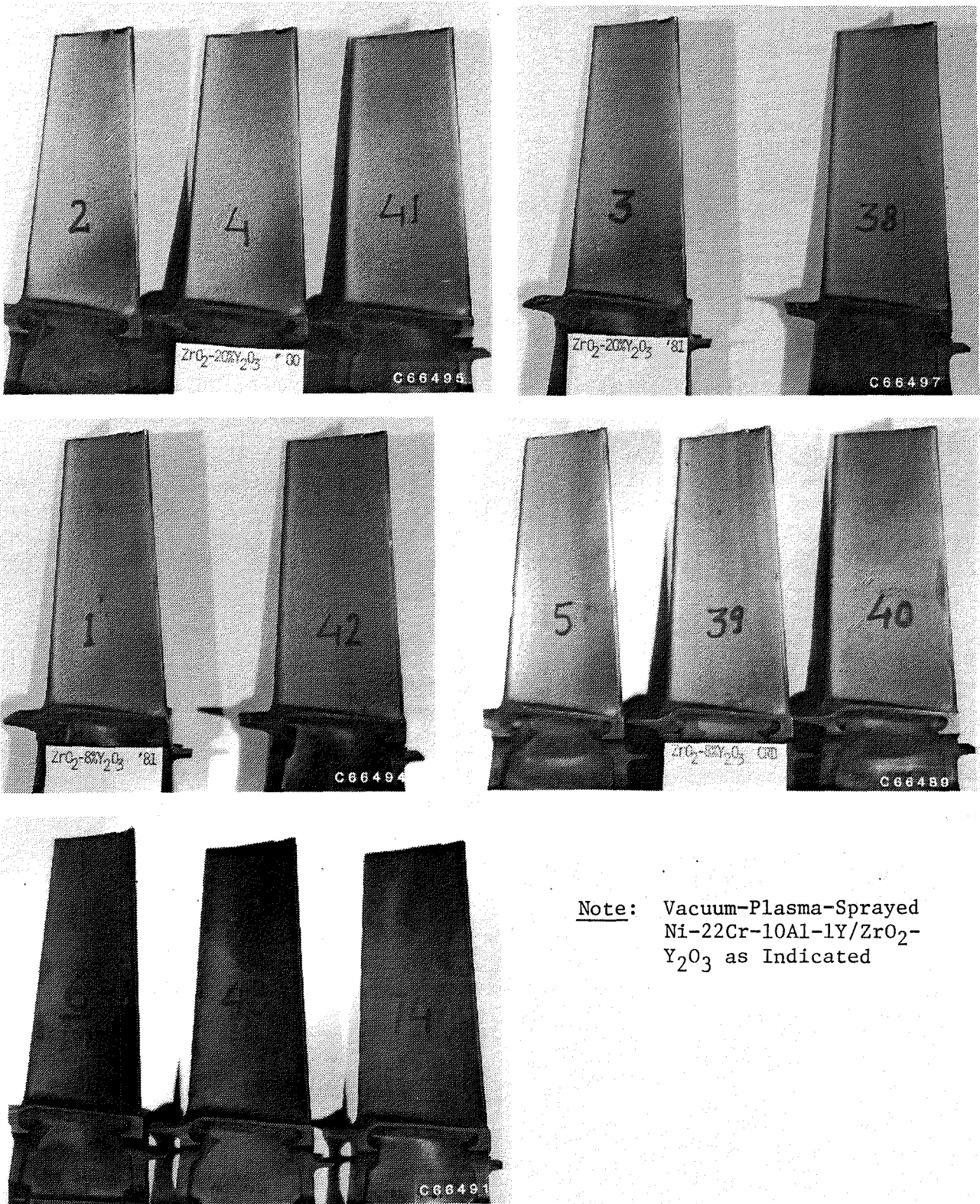
All of the blades had a similar pattern of coating damage confined to the leading edge on the suction side, although the extent of damage varied from blade-to-blade, as can be observed in Figure 47a. In small areas of the leading edge at the blade tip, ranging in size from 20 mm² (0.03 in.²) to 100 mm² (0.16 in.²) and averaging 65 mm² (0.1 in.²), the entire thickness of the ceramic layer was missing. The loss of ceramic layer in these areas may be related to a number of factors, such as development of cracks in the ceramic layer during tip grinding, spallation of the ceramic layer due to thermal cycling and geometry effects, and loss due to erosion and impact damage.

In other areas of the forward part on the suction side, the damage was characterized by a roughened coating surface, the presence of pockmarks and small craters, and isolated loss of ceramic coating. In these areas, a thin layer of the ceramic coating was still present. This damage appeared to be impact and erosion damage caused by particulate impingement. A tabulation listing the areas of the two extents of damage for each blade is given in Table XV. As noted in the table, the average size of the damaged area was 112 mm² (0.174 in.²) which is only 1.2% coated area. The average size area where all of the ceramic layer was missing was only 0.6% of the coated area. Blades without a thermal barrier coating (Codep only) also showed signs of particulate impingement at the leading edge on the suction side, as shown in Figure 47a. This area appeared rougher than the rest of the airfoil and had a greenish foreign material adhering to the surface at the leading edge. An attempt was made to identify the source of this material by chemical analysis.



Note: Vacuum-Plasma-Sprayed
 Ni-22Cr-10Al-1Y/ZrO₂-
 Y₂O₃ as Indicated

Figure 47a. Photos of Engine-Tested (1000 "C" Cycles) CF6-50 Stage 2 Blades (René 80) With and Without TBC, Suction Side.



Note: Vacuum-Plasma-Sprayed
 Ni-22Cr-10Al-1Y/ZrO₂-
 Y₂O₃ as Indicated

Figure 47b. Photos of Engine-Tested (1000 "C" Cycles) CF6-50 Stage 2 Blades (René 80) With and Without TBC, Pressure Side.

EDAX results, Figure 48, showed the deposits to be mostly Ni-Al with the amount of aluminum varying from 5% to 40%. Other minor elements detected were Co, Fe, Cr, and Ca. Although the exact source of the material in the observed deposits is not known because of the many possible sources of Ni and Al in the engine, it is known that some nickel-aluminum material was lost from the Stage 1 shrouds during the engine test and possibly was the particulate matter that damaged the TBC. The presence of particulate matter in the gas stream is not uncommon and should be taken into consideration in the design and application of thermal-barrier-coatings on HPT components.

Table XV. Summary of Damage to Thermal-Barrier-Coated, CF6-50, Stage 2 HPT Blades, 1000 "C" Cycle Engine Test.

Blade No.	Top Coat Composition	Area of Damage, mm ² (in. ²)		
		Top Coat Missing	Some Top Coat Remaining	Total
2	ZrO ₂ -20%Y ₂ O ₃	39 (0.06)	71 (0.11)	110 (0.17)
3	"	58 (0.09)	129 (0.20)	187 (0.29)
4	"	52 (0.08)	13 (0.02)	65 (0.10)
38	"	90 (0.14)	84 (0.13)	174 (0.27)
41	"	65 (0.10)	32 (0.05)	97 (0.15)
1	ZrO ₂ -8%Y ₂ O ₃	58 (0.09)	52 (0.08)	110 (0.17)
42	"	77 (0.12)	90 (0.14)	167 (0.26)
5	ZrO ₂ -8%Y ₂ O ₃ (NAS3-21727)	19 (0.03)	26 (0.04)	45 (0.07)
39	"	103 (0.16)	39 (0.06)	142 (0.22)
40	"	26 (0.04)	0	26 (0.04)

Note: Total coated area was 9400 mm² (14.6 in.²). Average area of damage [112 mm² (0.174 in.²)] was 1.2% of the coated area.

Three of the engine-tested thermal-barrier-coated blades, one with each type of ceramic layer and one blade without TBC (Codep only), were sectioned at 40%, 70%, and 90% span and in the platform region and prepared for metallographic examination. Microstructural examination showed the thermal barrier coatings on all three blades to be in excellent condition in all areas except at the leading edge of the suction side where the ceramic layer had been damaged. The blade with Codep coating only showed normal microstructure without any damage.

Figures 49 through 51 show the optical photomicrographs of the thermal-barrier-coated blade cross sections at the three span heights and at the platform. Photomicrographs show the blade material (René 80) with Codep coating

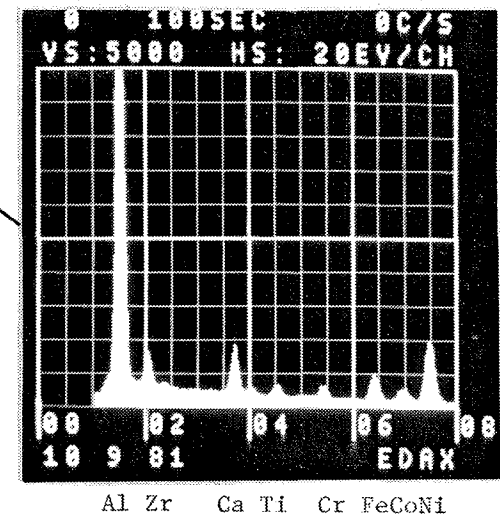
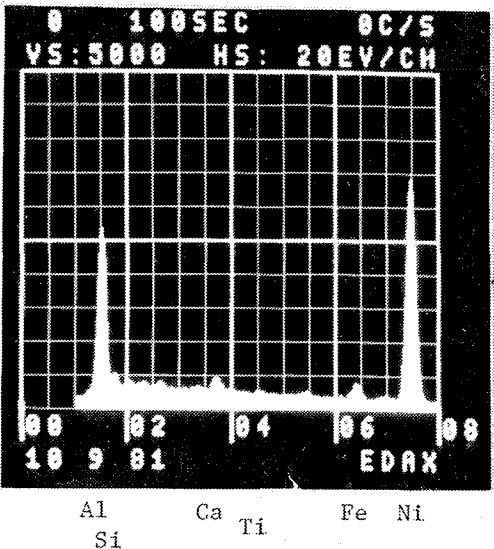
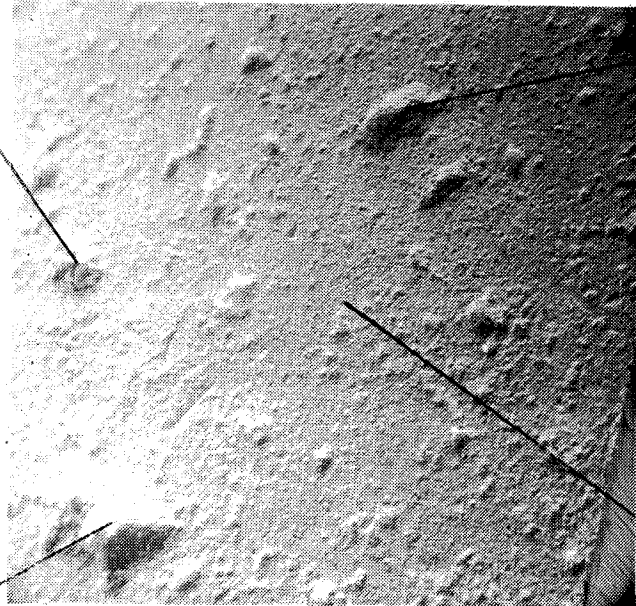
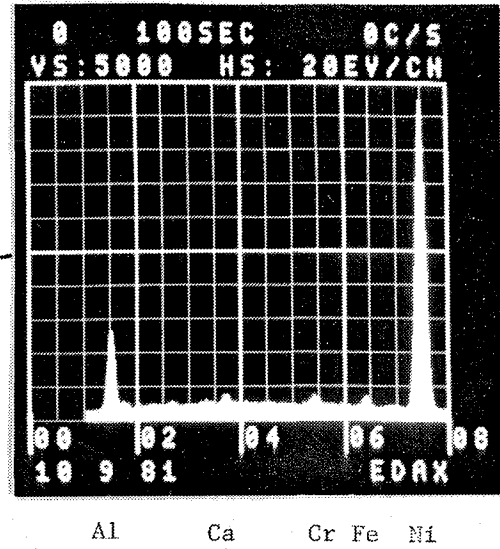
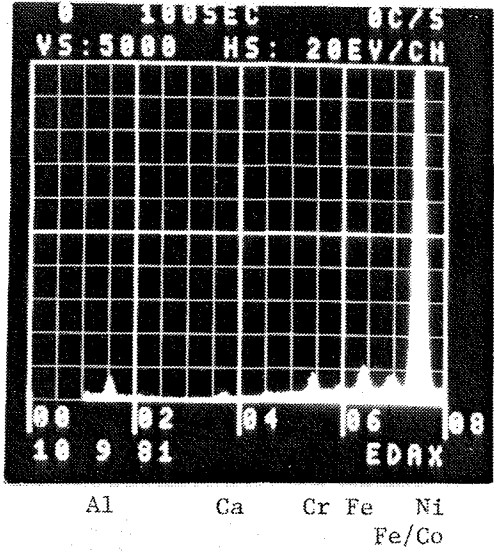


Figure 48. Chemical Analysis by EDAX of the Greenish Deposits on the Leading Edge, Suction Side of an Engine-Tested, Stage 2 Blade.

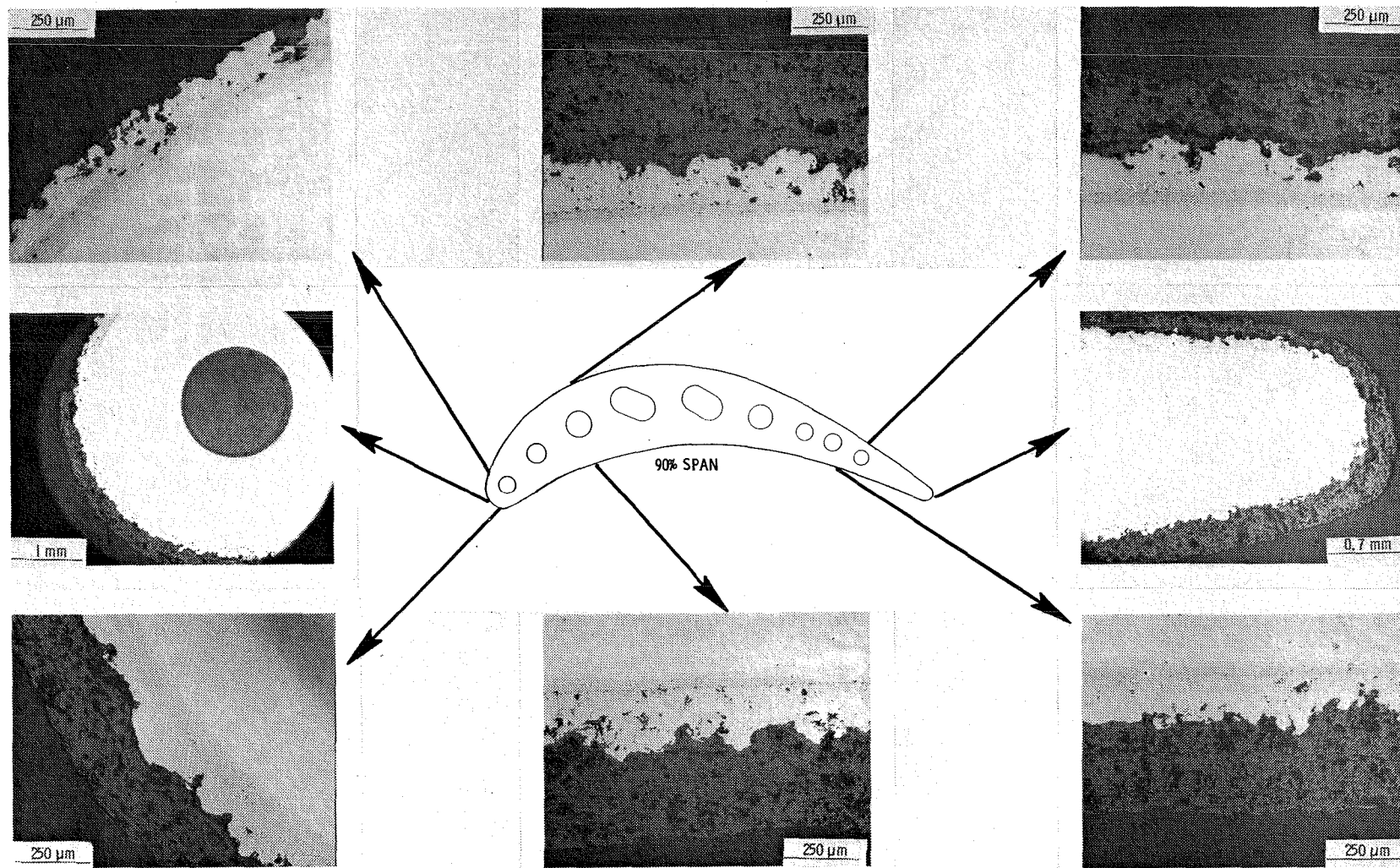


Figure 49a. Photomicrographs of Engine-Tested (1000 "C" Cycles) CF6-50 Stage 2 Blade With TBC (Ni-22Cr-10Al-1Y/ZrO₂-20%Y₂O₃ Duplex), 90% Span (Blade No. 41, Table XV).

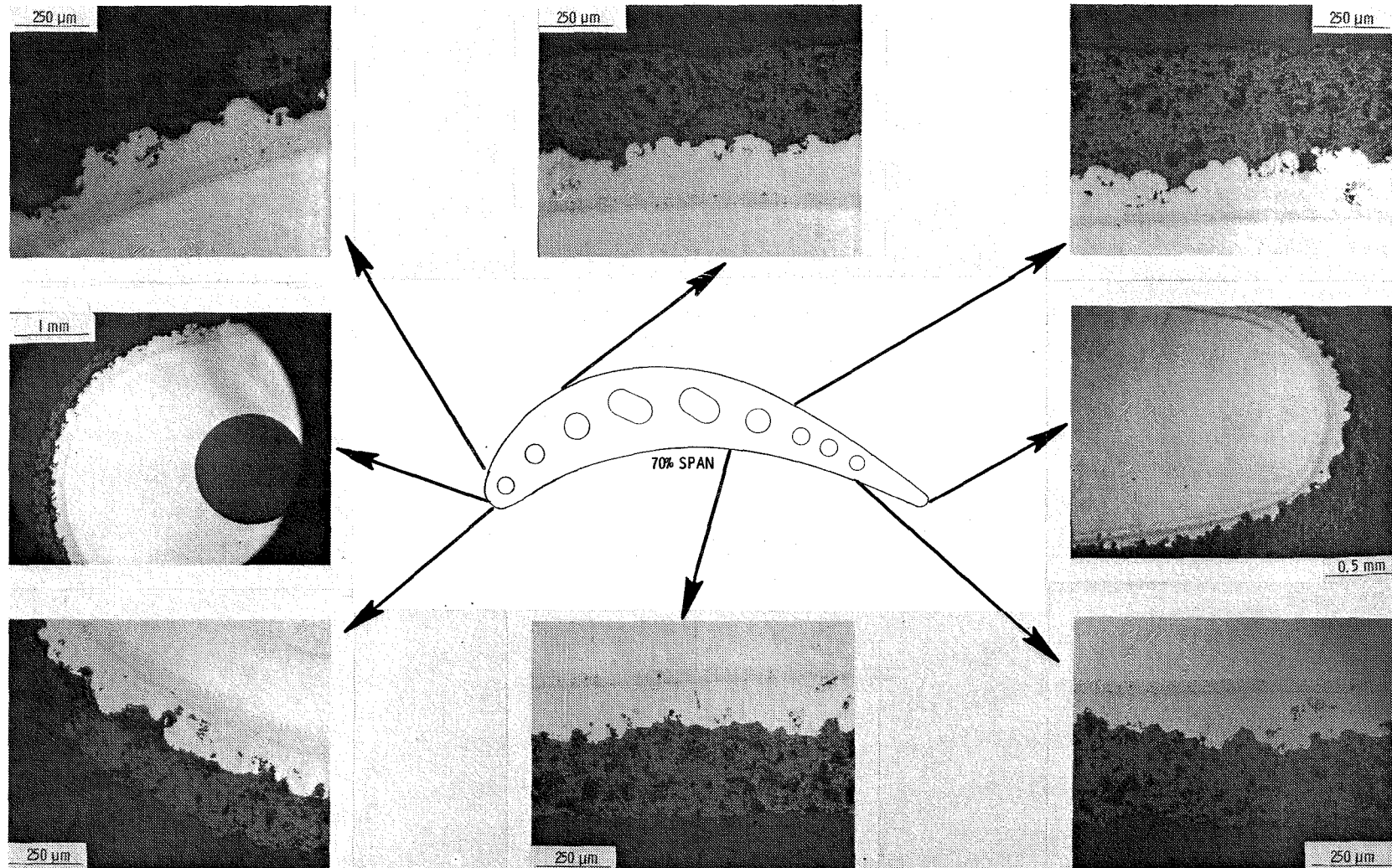


Figure 49b. Photomicrographs of Engine-Tested (1000 "C" Cycles) CF6-50 Stage 2 Blade With TBC (Ni-22Cr-10Al-1Y/ZrO₂-20%Y₂O₃ Duplex), 70% Span (Blade No. 41, Table XV).

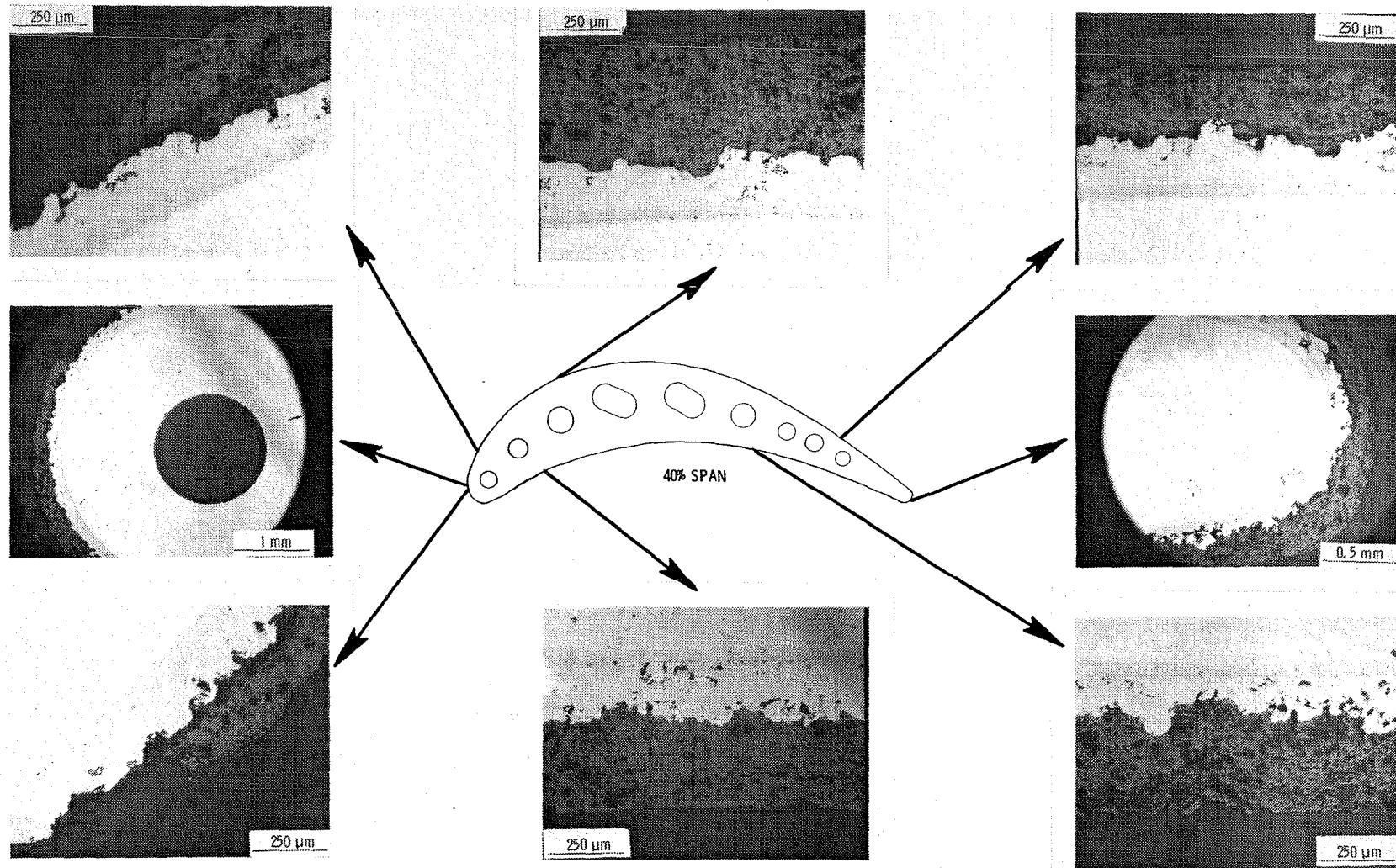


Figure 49c. Photomicrographs of Engine-Tested (1000 "C" Cycles) CF6-50 Stage 2 Blade With TBC (Ni-22Cr-10Al-1Y/ZrO₂-20%Y₂O₃ Duplex), 40% Span (Blade No. 41, Table XV).

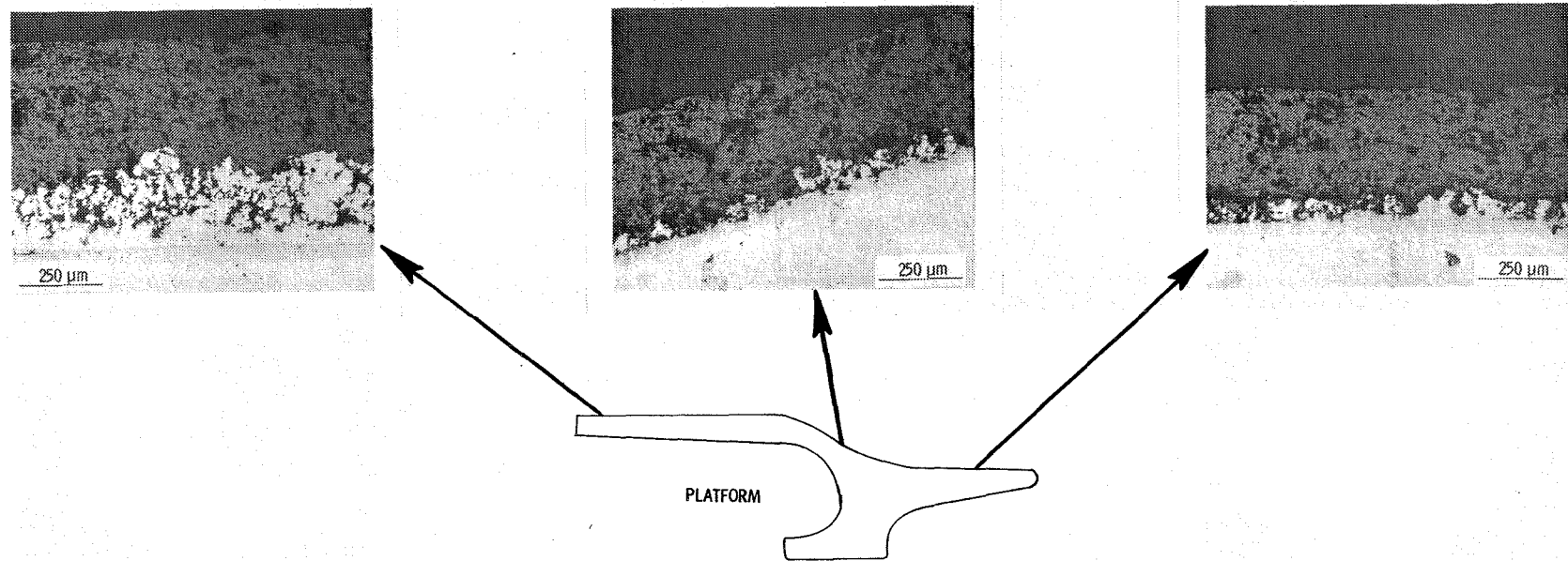


Figure 49d. Photomicrographs of Engine-Tested (1000 "C" Cycles) CF6-50 Stage 2 Blade With TBC (Ni-22Cr-10Al-1Y/ZrO₂-20%Y₂O₃ Duplex), Platform (Blade No. 41, Table XV).

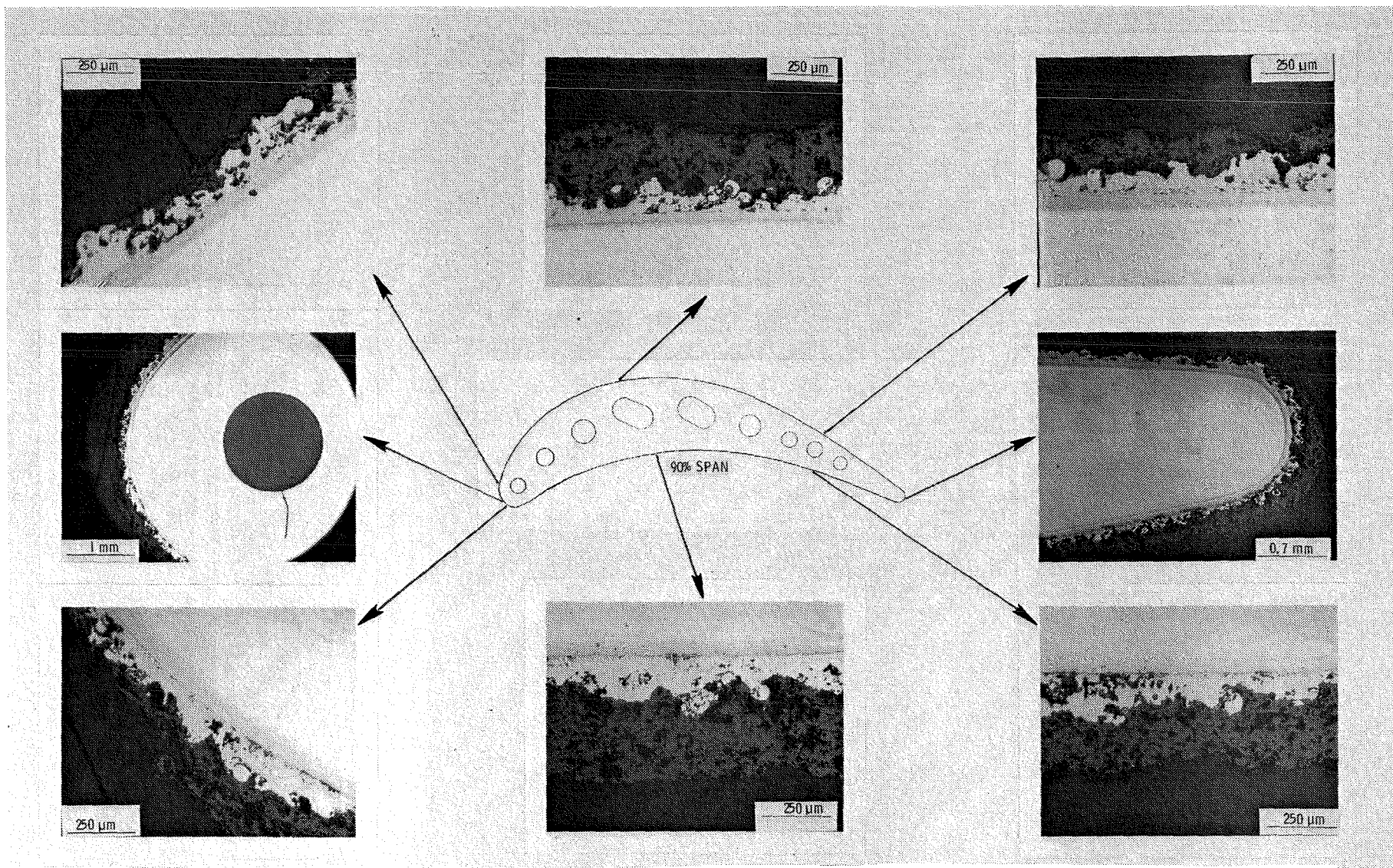


Figure 50a. Photomicrographs of Engine-Tested (1000 "C" Cycles) CF6-50 Stage 2 Blade With TBC (Ni-22Cr-10Al-1Y/ZrO₂-8%Y₂O₃ Duplex), 90% Span (Blade No. 42, Table XV).

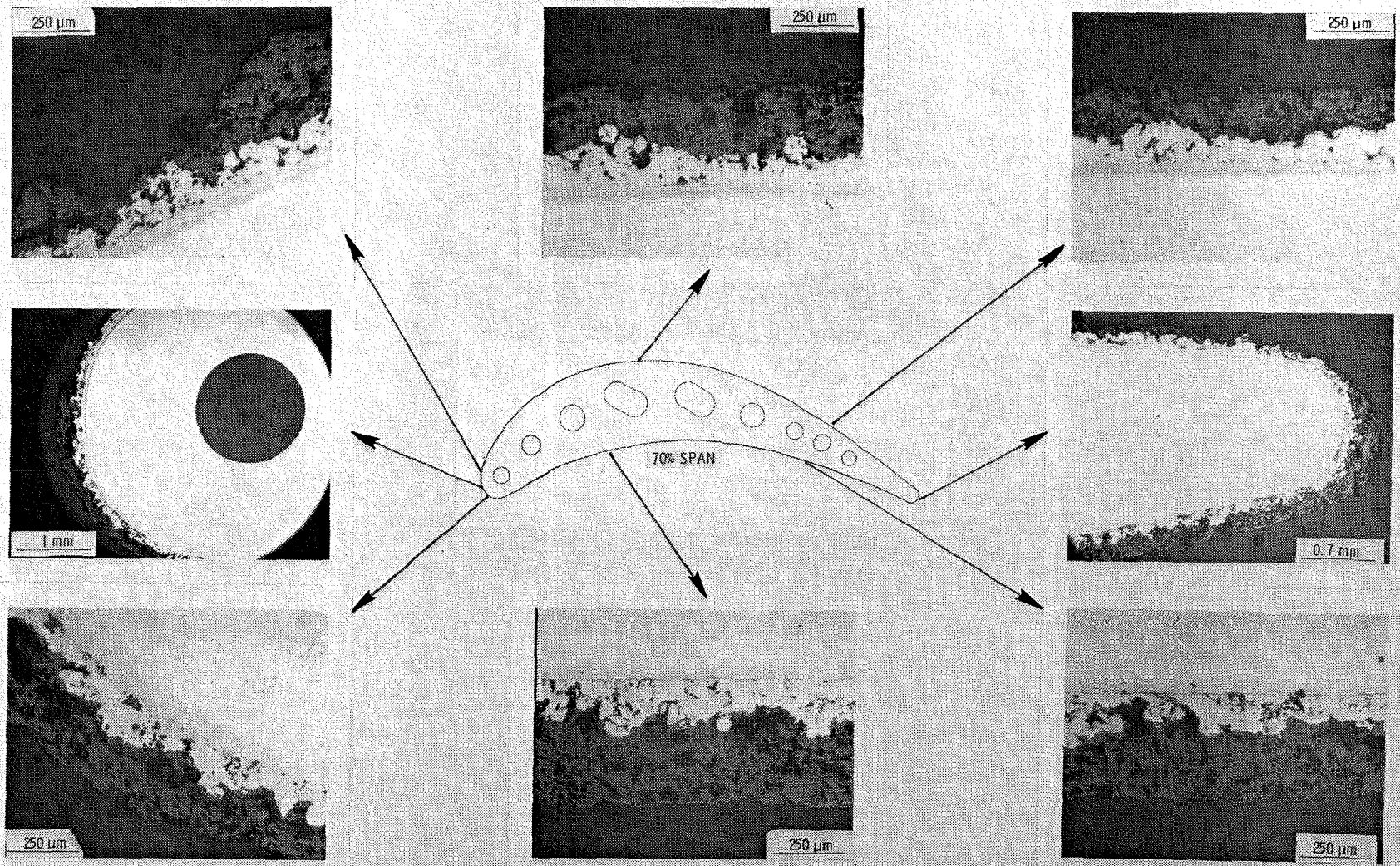


Figure 50b. Photomicrographs of Engine-Tested (1000 "C" Cycles) CF6-50 Stage 2 Blade With TBC (Ni-22Cr-10Al-1Y/ZrO₂-8%Y₂O₃ Duplex), 70% Span (Blade No. 42, Table XV).

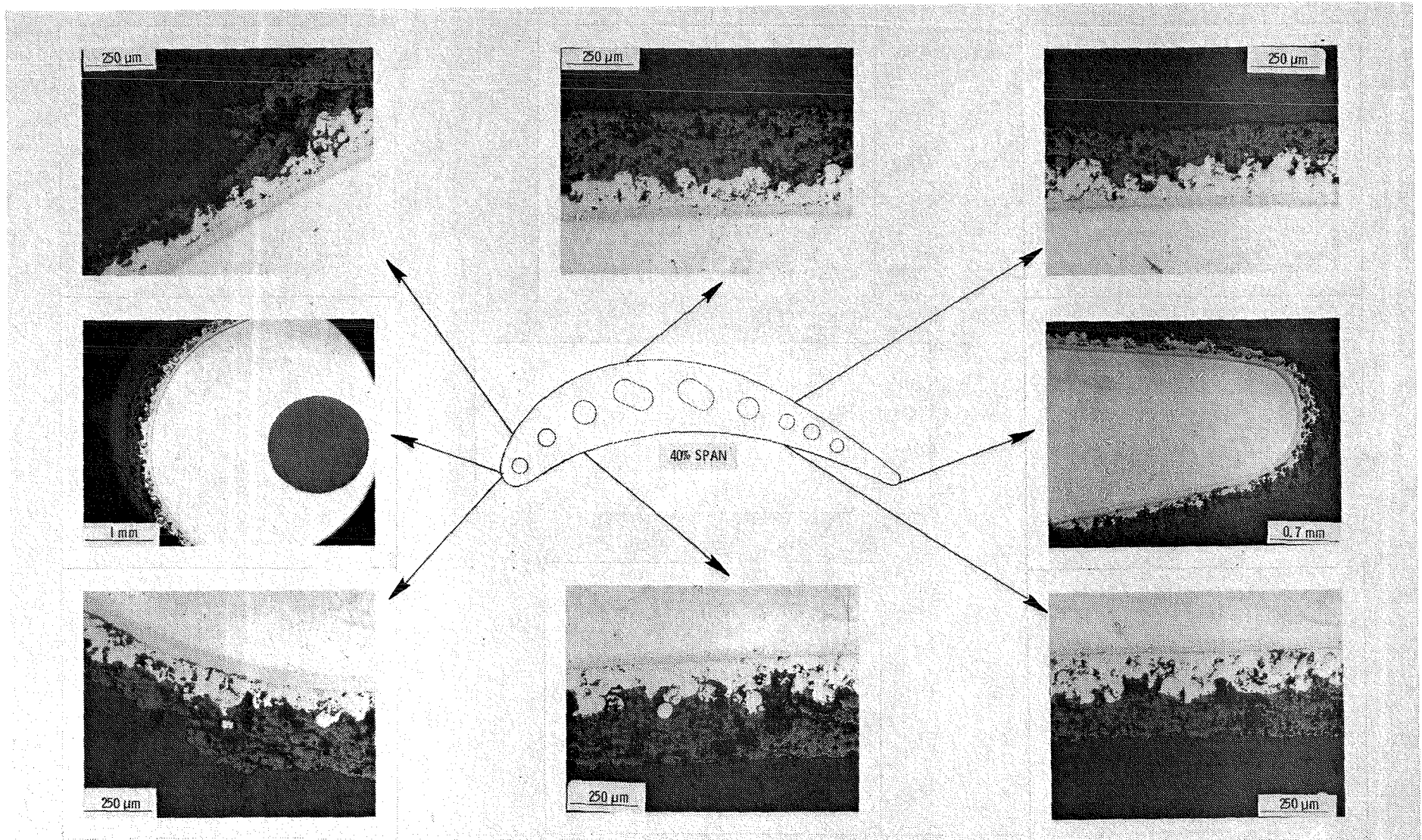


Figure 50c. Photomicrographs of Engine-Tested (1000 "C" Cycles) CF6-50 Stage 2 Blade With TBC (Ni-22Cr-10Al-1Y/ZrO₂-8%Y₂O₃ Duplex), 40% Span (Blade No. 42, Table XV).

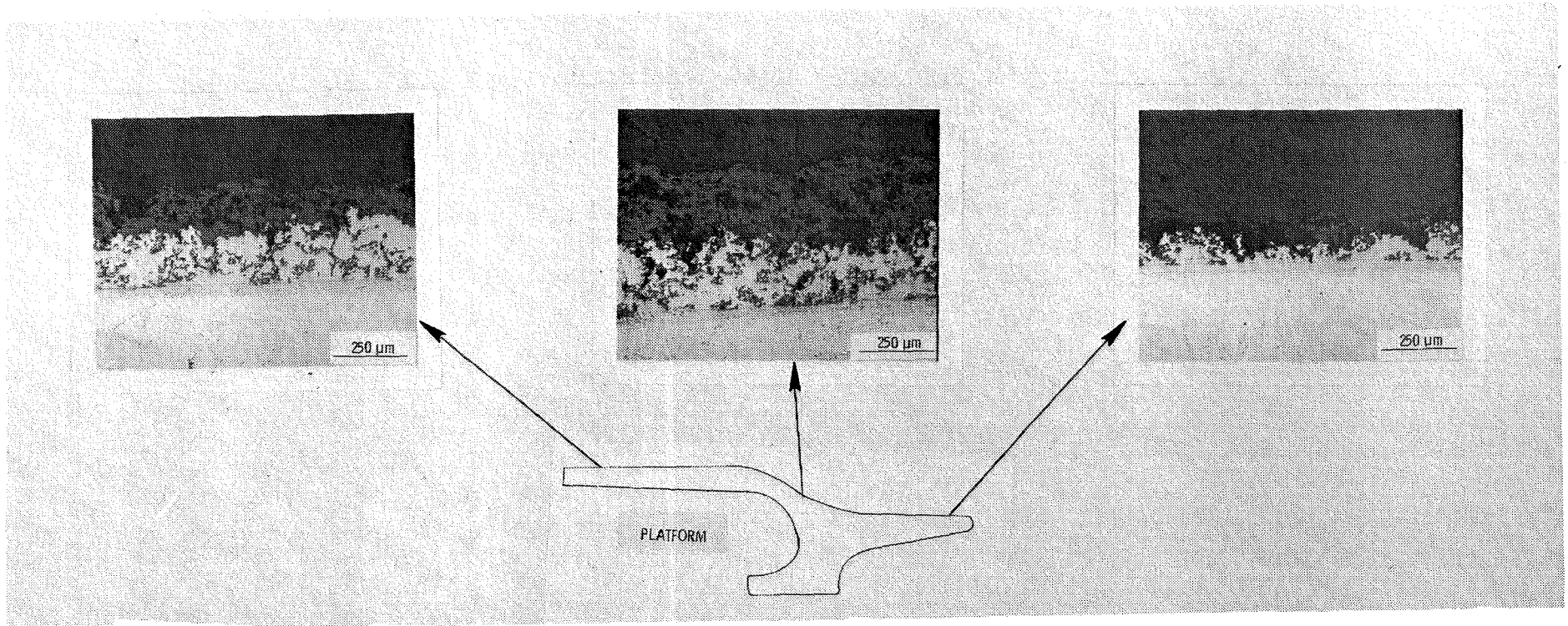


Figure 50d. Photomicrographs of Engine-Tested (1000 "C" Cycles) CF6-50 Stage 2 Blade With TBC (Ni-22Cr-10Al-1Y/ZrO₂-8%Y₂O₃ Duplex), Platform (Blade No. 42, Table XV).

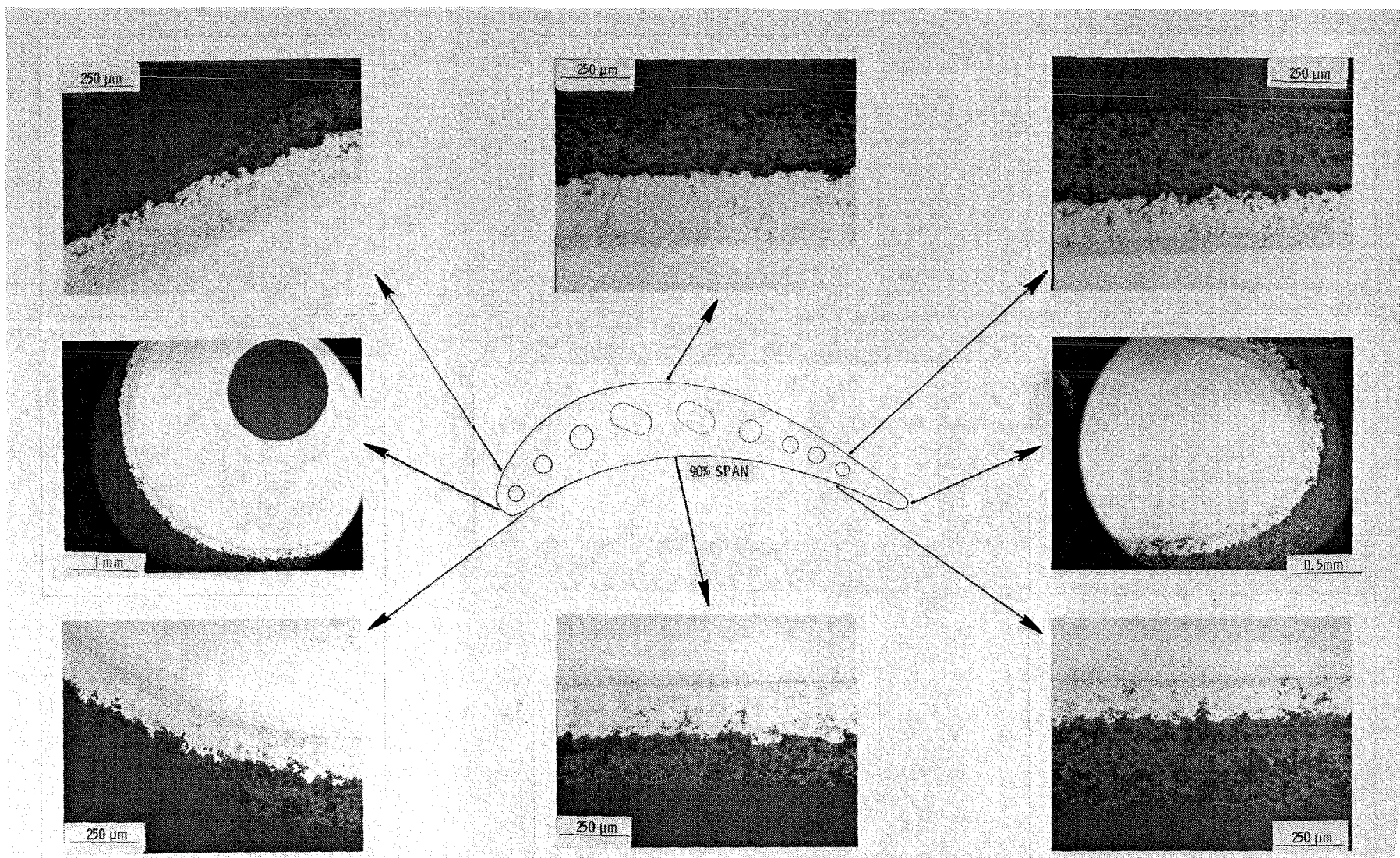


Figure 51a. Photomicrographs of Engine-Tested (1000 "C" Cycles) CF6-50 Stage 2 Blade With TBC (Ni-22Cr-10Al-1Y/ZrO₂-8%Y₂O₃ Duplex), 90% Span (Blade No. 39, Table XV).

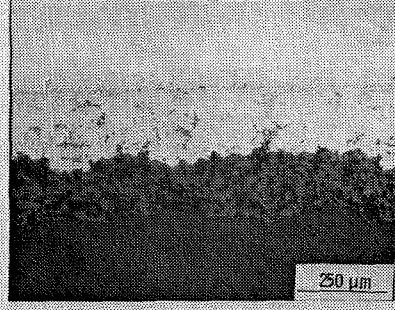
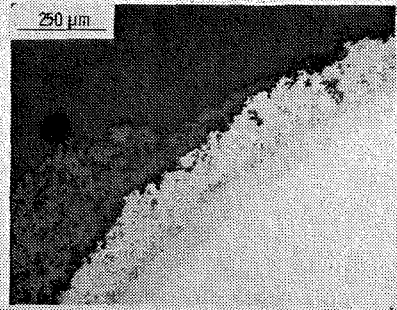
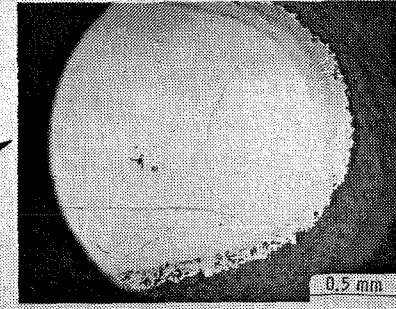
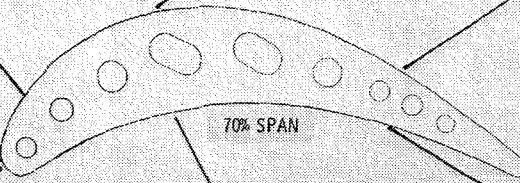
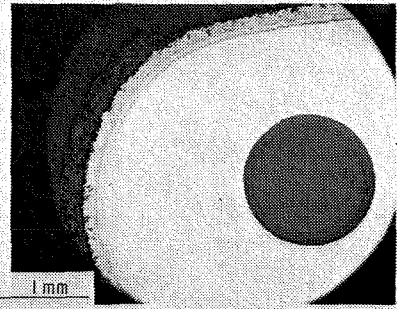
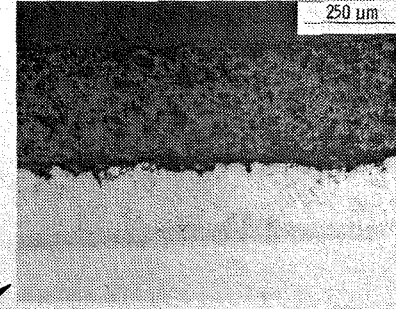
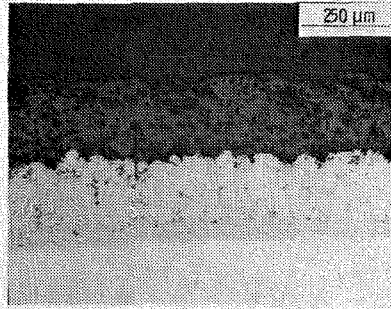
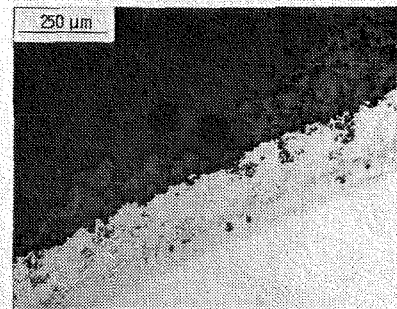


Figure 51b. Photomicrographs of Engine-Tested (1000 "C" Cycles) CF6-50 Stage 2 Blade With TBC (Ni-22Cr-10Al-1Y/ZrO₂-8%Y₂O₃ Duplex), 70% Span (Blade No. 39, Table XV).

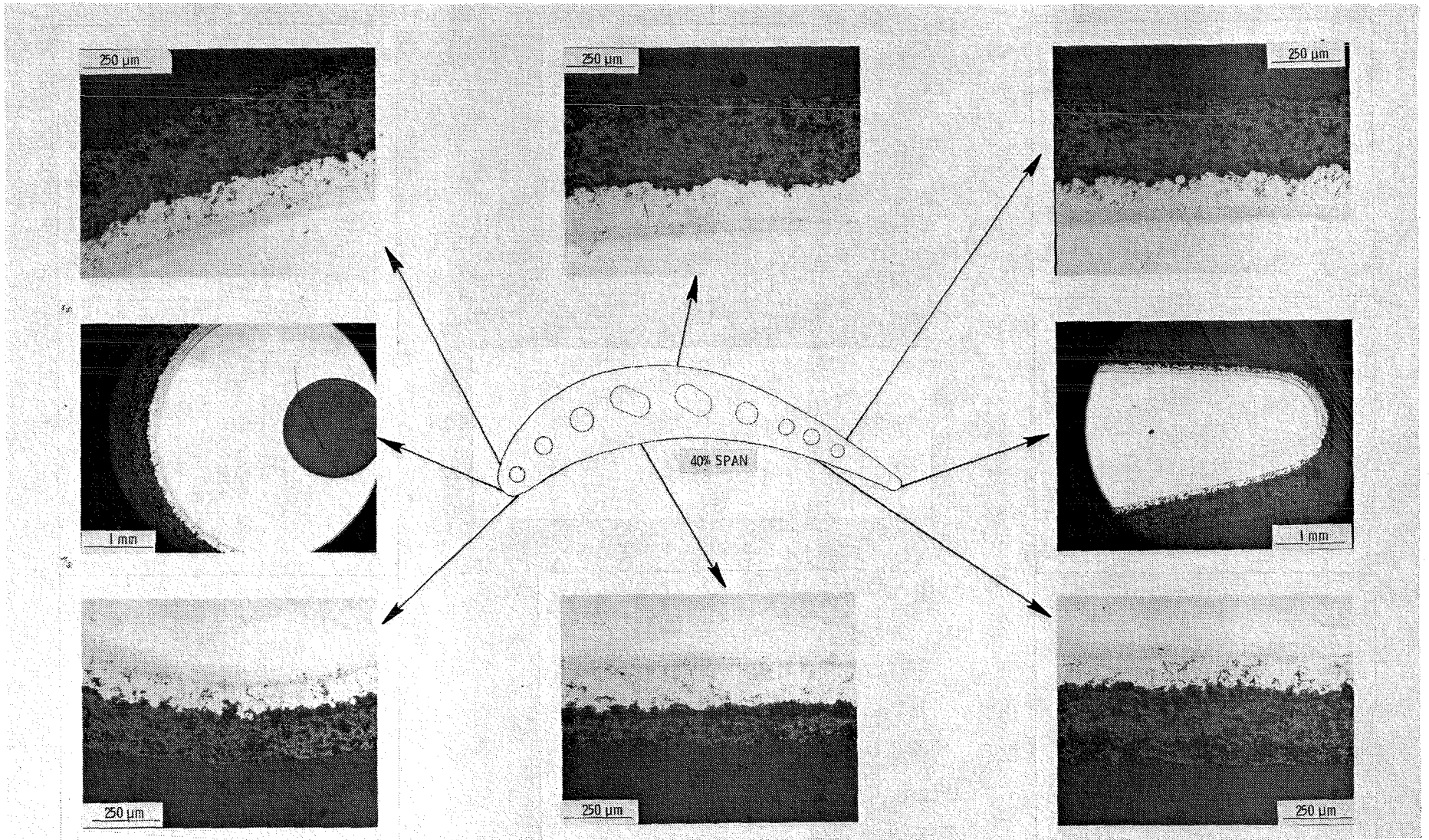


Figure 51c. Photomicrographs of Engine-Tested (1000 "C" Cycles) CF6-50 Stage 2 Blade With TBC (Ni-22Cr-10Al-1Y/ZrO₂-8%Y₂O₃ Duplex), 40% Span (Blade No. 39, Table XV).

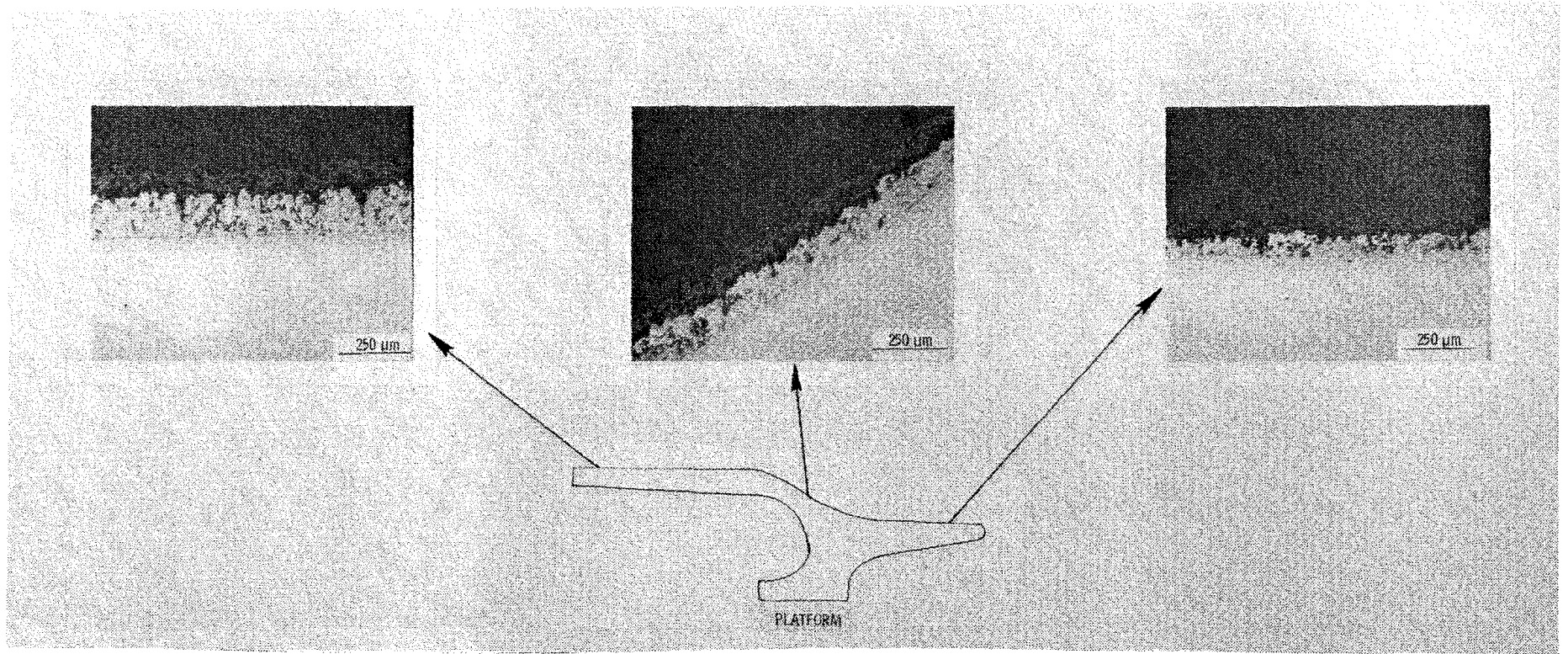


Figure 5ld. Photomicrographs of Engine-Tested (1000 "C" Cycles) CF6-50 Stage 2 Blade With TBC (Ni-22Cr-10Al-1Y/ZrO₂-8%Y₂O₃ Duplex), Platform (Blade No. 39, Table XV).

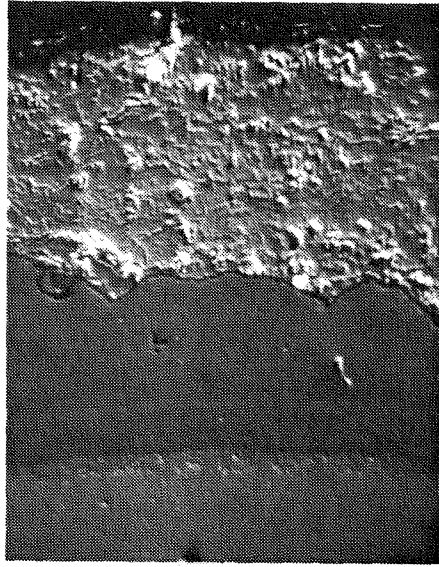
followed by the Ni-Cr-Al-Y bond coat and the ZrO_2 - Y_2O_3 ceramic top coat. The bond coat is intimately bonded to the Codep layer. The microstructure, porosity, and thickness uniformity are typical of VPS applied bond coats on Blades 39 and 41, but the structure of the coating on Blade 42 is, for some reason, unusually porous and nonuniform for low pressure, plasma-sprayed bond coats. There was no loss or separation of the bond coat from the airfoil surface, including areas where the ceramic layer was damaged. Very little, if any, bond coat oxidation was observed on any of the blades. The ceramic layer on all three blades also appeared to be in excellent condition over most of the airfoil surface with the exception of the leading edge on the suction side where impact damage had occurred. The ceramic layer is adherent to the bond coat and shows no evidence of cracking or separation. Its microstructure is typical of conventionally plasma-sprayed ceramic coatings. Overall, the thermal barrier coatings on all three blades appear in sound condition microstructurally.

Electron microprobe analysis was performed at the 80% span to examine for interaction and interdiffusion between the TBC and the substrate. Figures 52 through 54 show the secondary electron images and X-ray density maps of Ni, Cr, Al, Zr, and Y for the three blades. It can be observed that no interaction or extensive interdiffusion occurred between the ceramic layer and the metallic bond coat layer. A thin scale (4-5 μm) of Al_2O_3 is present at the top coat/bond coat interface, which is normal, but there was no further oxidation of the bond coat. Interdiffusion between the bond coat and Codep layer and the Codep layer and René 80 substrate was minimal as indicated by the uniform distribution of the bond coat elements Ni, Cr, and Al. This may be attributed to the presence of the Codep layer between the bond coat and René 80 and to bond coat temperatures not exceeding 1255 K (1800° F) in most areas of the blade.

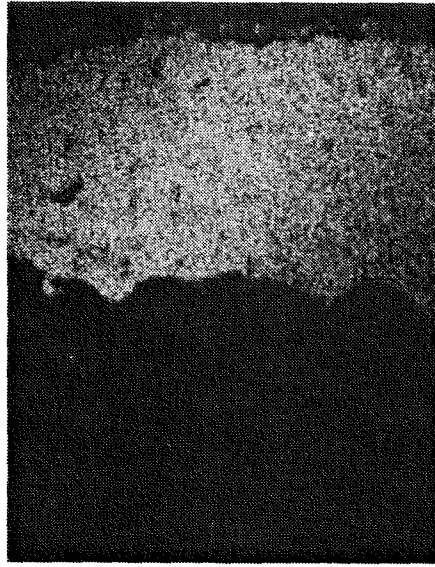
X-ray diffraction analysis was performed on the ceramic layer samples taken from the three blades to observe any phase changes which may have occurred during the engine test. The results showed the ZrO_2 -20% Y_2O_3 coating to be mostly cubic phase, with a small percentage of monoclinic phase, whereas the ZrO_2 -8% Y_2O_3 coating consisted of a mixture of cubic/tetragonal phases with a small percentage of the monoclinic phase. Before test, the ZrO_2 -20% Y_2O_3 coating is essentially all cubic and the ZrO_2 -8% Y_2O_3 coating is mostly cubic with small amounts of tetragonal and monoclinic phases. The presence of a small amount of the monoclinic phase in the ZrO_2 -20% Y_2O_3 coating after the engine test indicates that some phase transformation had taken place. This is consistent with observations from the previous engine test and laboratory cyclic thermal exposure testing. There was an increase in the amount of tetragonal phase in the ZrO_2 -8% Y_2O_3 during the engine test; this is also consistent with previous observations. The surface roughness of the engine-tested, thermal-barrier-coated blades was similar to that of untested blades except on leading edges where impact damage had occurred.

Vanes

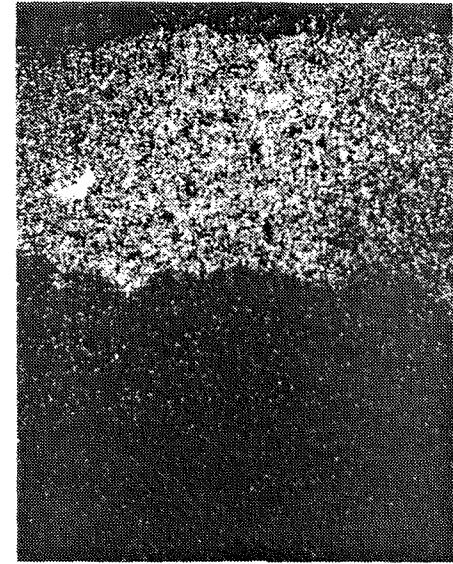
Figure 55 shows the leading edge and trailing edge views of the engine-tested, thermal-barrier-coated, Stage 2 vanes, and Figure 56 shows a closeup



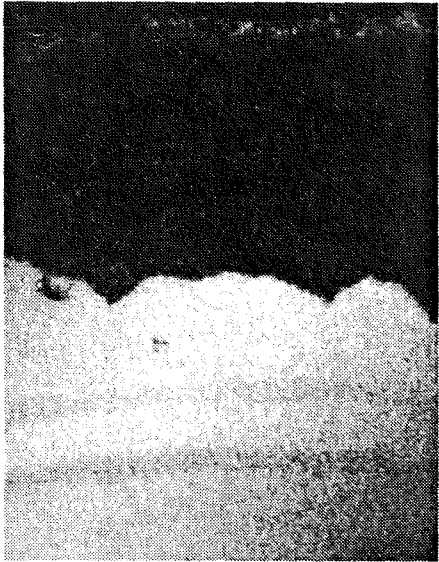
(a) Secondary Electron Image



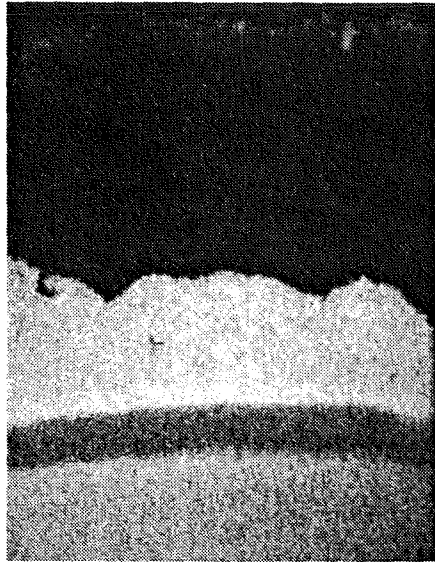
(b) Zr



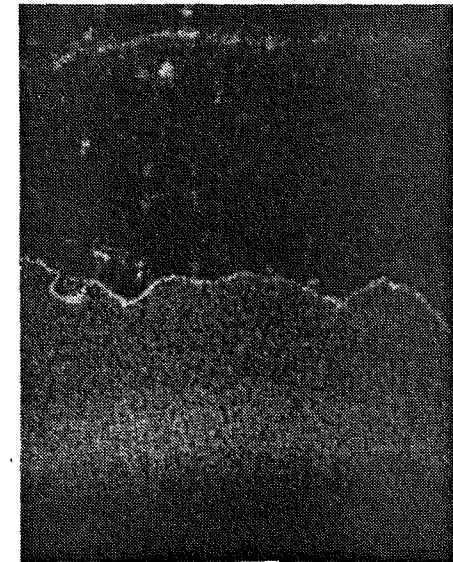
(c) Y



(d) Ni



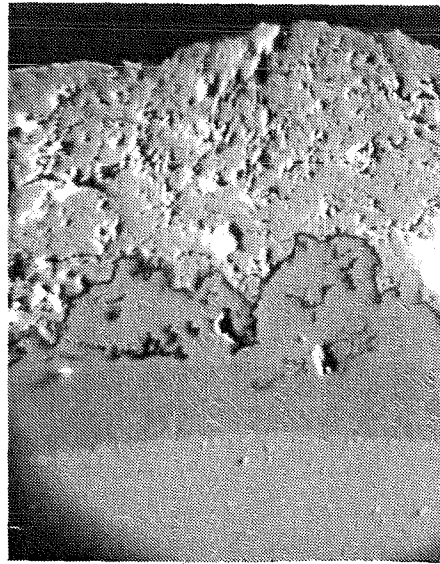
(e) Cr



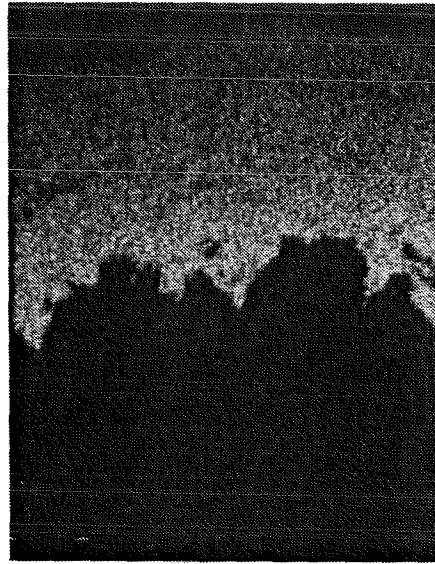
(f) Al

100 μ m

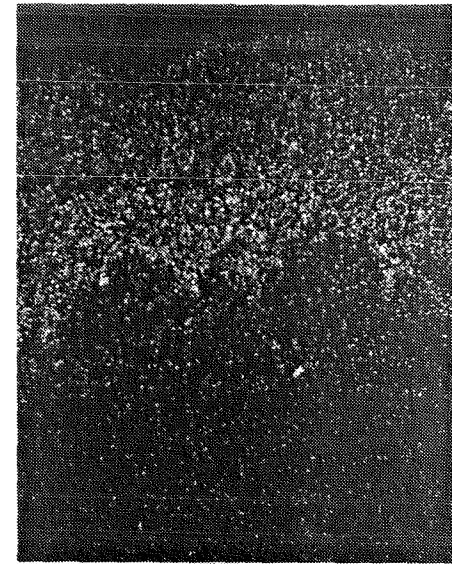
Figure 52. Secondary Electron Image and Elemental X-Ray Density Maps of Engine-Tested Stage 2 Blade (René 80) With Codep, Vacuum Plasma Sprayed Ni-22Cr-10Al-1Y and ZrO_2 -20% Y_2O_3 Coatings - Leading Edge, Suction Side at 80% Span (Blade No. 41, Table XV).



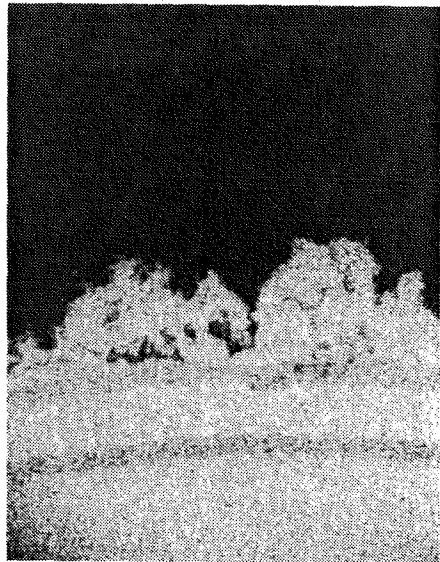
(a) Secondary Electron Image



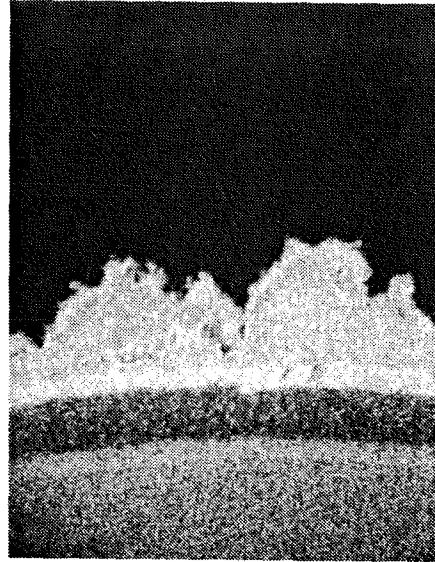
(b) Zr



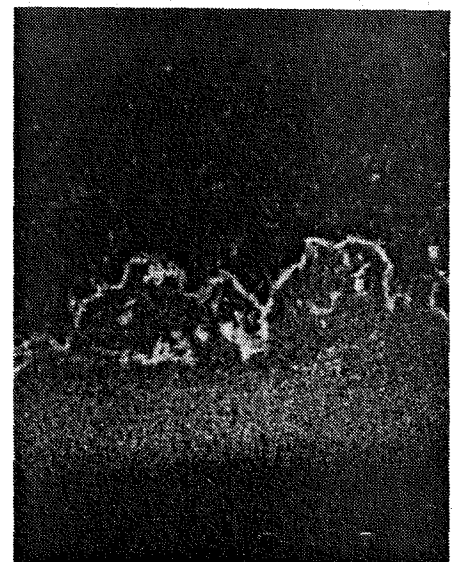
(c) Y



(d) Ni



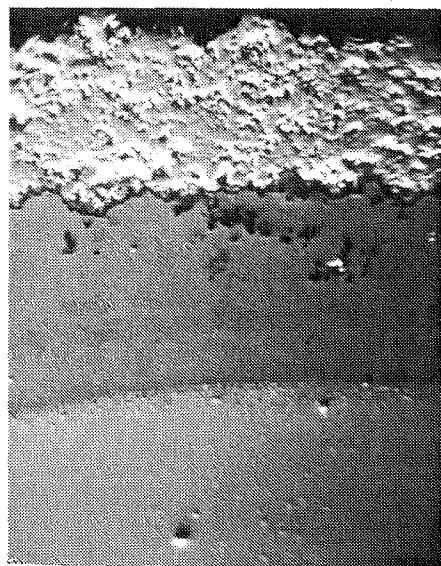
(e) Cr



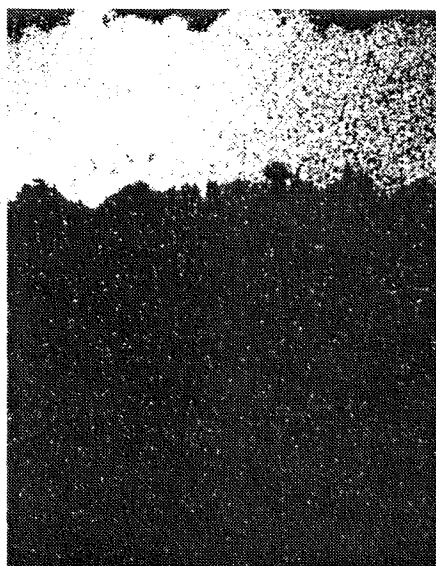
(f) Al

100 μm

Figure 53. Secondary Electron Image and Elemental X-Ray Density Maps of Engine-Tested Stage 2 Blade (René 80) With Codep, Vacuum Plasma Sprayed Ni-22Cr-10Al-1Y and ZrO_2 -8% Without Y_2O_3 Coatings - Leading Edge, Suction Side at 80% Span (Blade No. 42, Table XV).



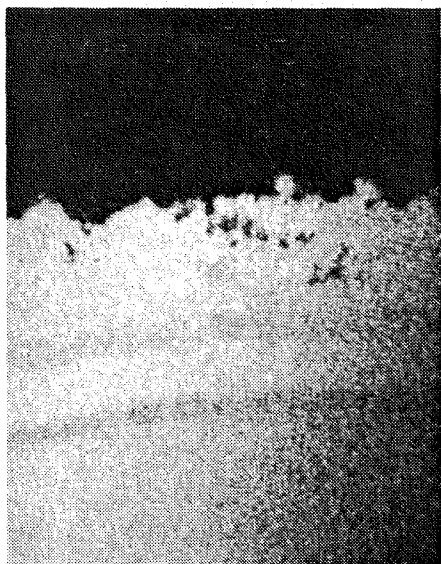
(a) Secondary Electron Image



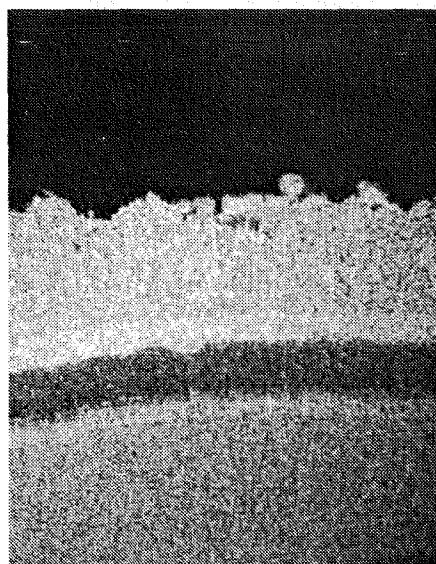
(b) Zr



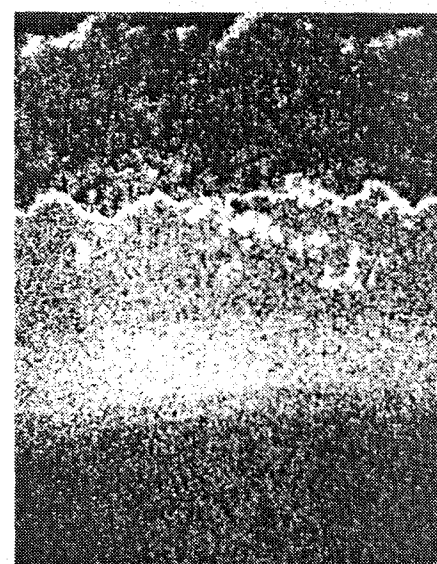
(c) Y



(d) Ni



(e) Cr



(f) Al

100 μm

Figure 54. Secondary Electron Image and Elemental X-Ray Density Maps of Engine-Tested Stage 2 Blade (René 80) With Codep, Vacuum Plasma Sprayed Ni-22Cr-10Al-1Y and ZrO₂-8% Without Y₂O₃ Coatings - Leading Edge, Suction Side at 80% Span (Blade No. 39, Table XV).

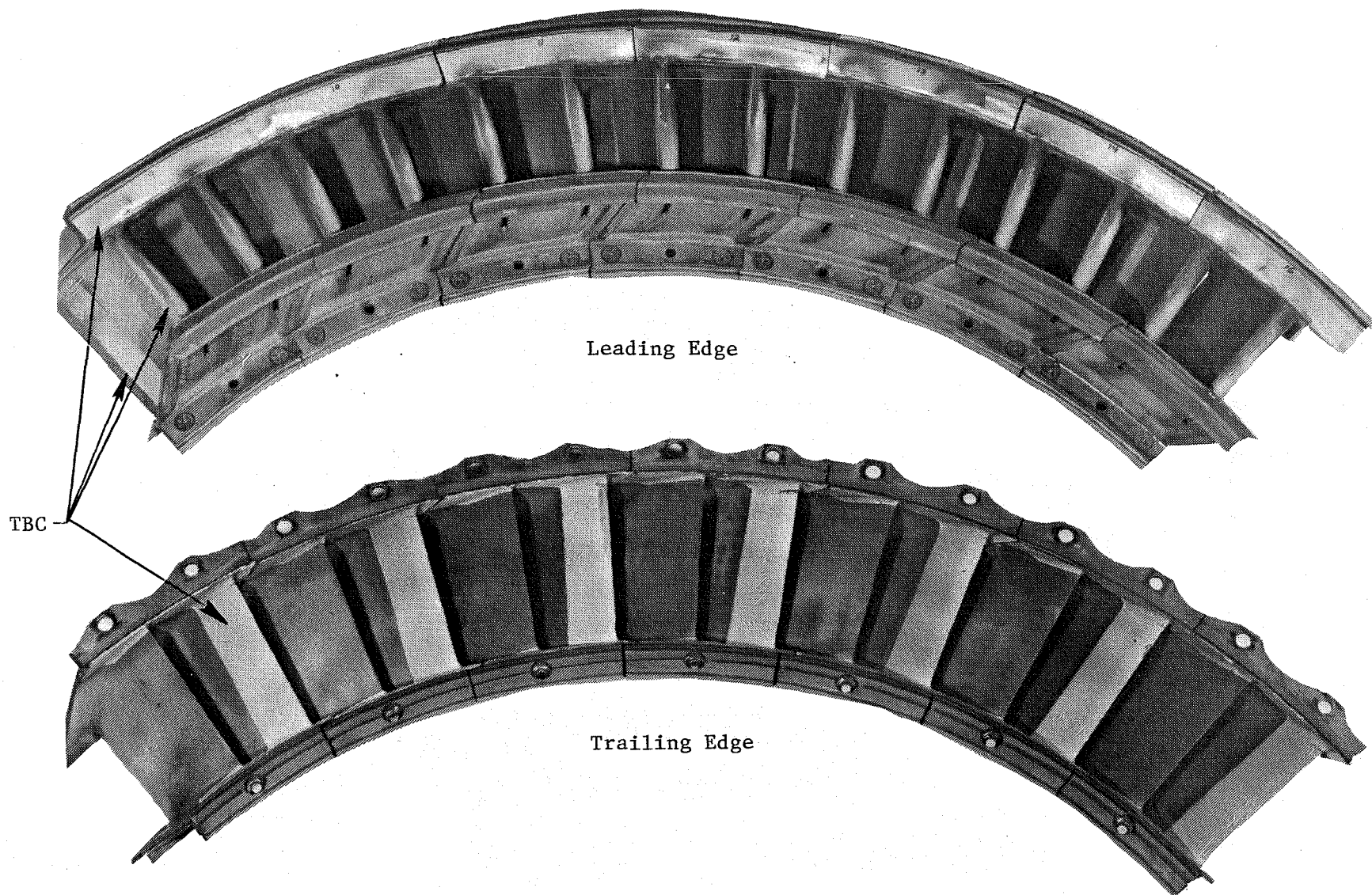


Figure 55. Thermal-Barrier-Coated, CF6-50, Stage 2 Vanes After Factory Engine Test of 1000 "C" Cycles.

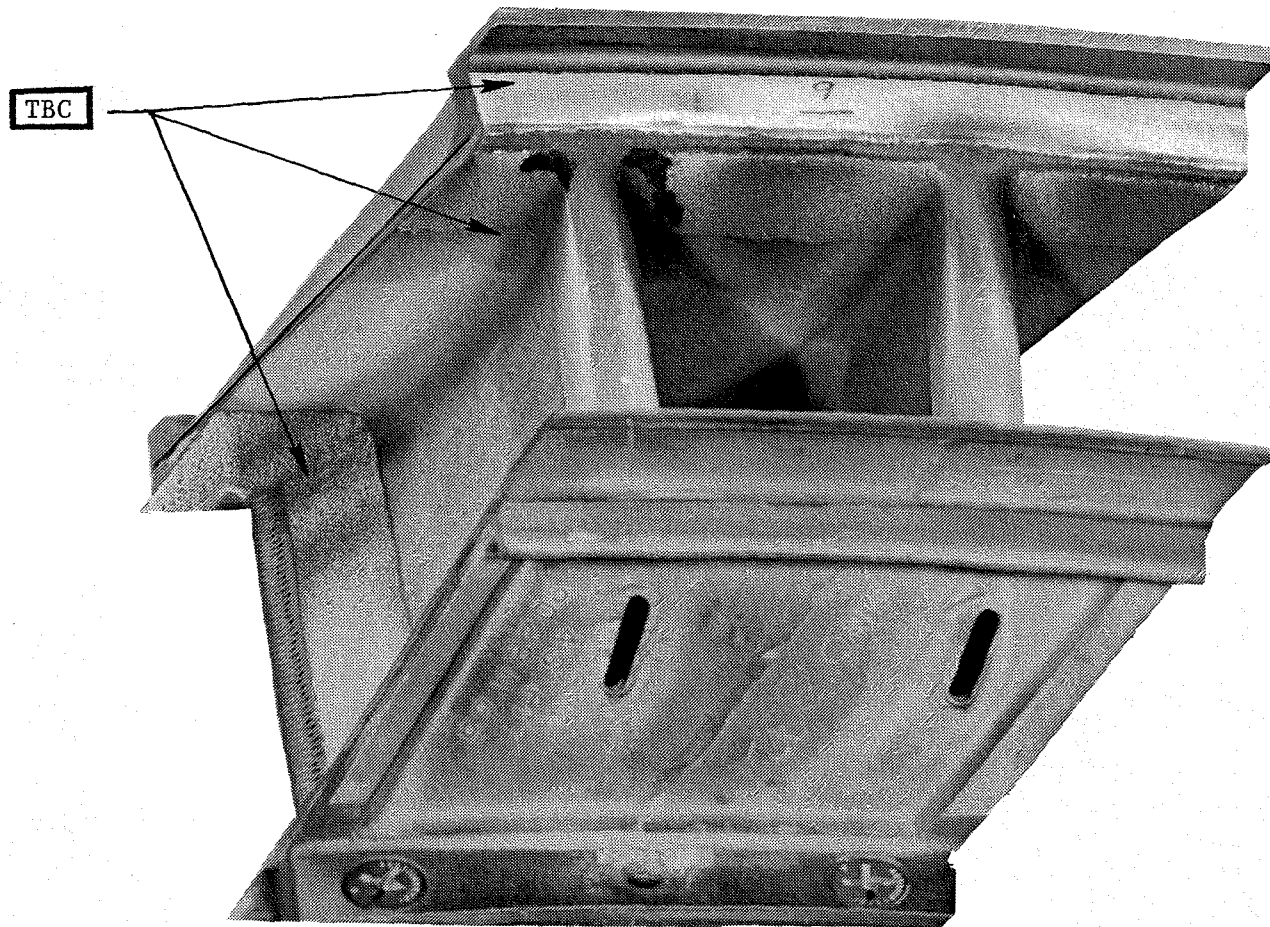


Figure 56. Thermal-Barrier-Coated, CF6-50 Stage 2 Vane After 1000 "C" Cycle Factory Engine Test.

view of one of the vanes. It can be observed that the TBC was damaged rather extensively on the outer one-third to two-thirds of the airfoil leading edges. Some pretest damage to the TBC on the leading edges of the airfoils had occurred during shroud grinding and may have contributed to the extent of damage observed after the test. All of the ceramic layer of the TBC was missing from localized areas of the outer band near the leading edge of some of the airfoils (Figure 56). The appearance of these areas suggests that the coating was eroded away by impingement of particulate matter. Local penetration of the bond coat occurred in some of these areas. The TBC was in good condition on the trailing edges of the airfoils and on the aft edges of the inner and outer bands. Minor loss near the trailing edge on the suction side of some of the airfoils had taken place during the engine test. The thermal barrier coating on the pressure side appeared generally to be in good condition, although some thinning of the coating had occurred near the outer band.

Two engine-tested Stage 2 vanes (paired), one with TBC and one without (Codep only), were sectioned at 15%, 50%, and 95% spans and in the outer and inner band regions for metallographic examination. Microstructural examination showed the Codep coating to be in good condition, whereas the thermal barrier coating was extensively damaged. It also showed that the Codep layer had been completely removed as planned by grit blasting in areas where the bond coat and ceramic top coat were applied by conventional plasma spraying. Figures 57a and 57b show the optical photomicrographs of a thermal-barrier-coated airfoil at 95% and 15% span cross sections, respectively. It can be observed that at 95% span, near the outer band, the TBC was severely damaged. The ceramic layer had spalled and local oxidation of the René 80 substrate had taken place at the leading edge; maximum penetration of René 80 in localized regions was 0.13 mm (0.005 in.). The TBC appeared to be in better condition at the trailing edge, but thinning of the ceramic layer was observed. It should be noted that the bond coat, wherever remaining on the airfoil surface, had provided adequate oxidation protection to the underlying substrate. The TBC appeared to be in much better condition at the 15% span, although thinning of the ceramic layer was observed on the suction as well as pressure side of the airfoil. The bond coat and top coat layers were not nearly as uniform in thickness on the Stage 2 vanes as they were on the blades. This is due to the difficulty in manually coating a complex shape such as a Stage 2 vane. Further improvements in the application of the coating, preferably by an automatic process, are needed to apply a quality coating. Improvement is also needed in the erosion resistance of the ceramic layer.

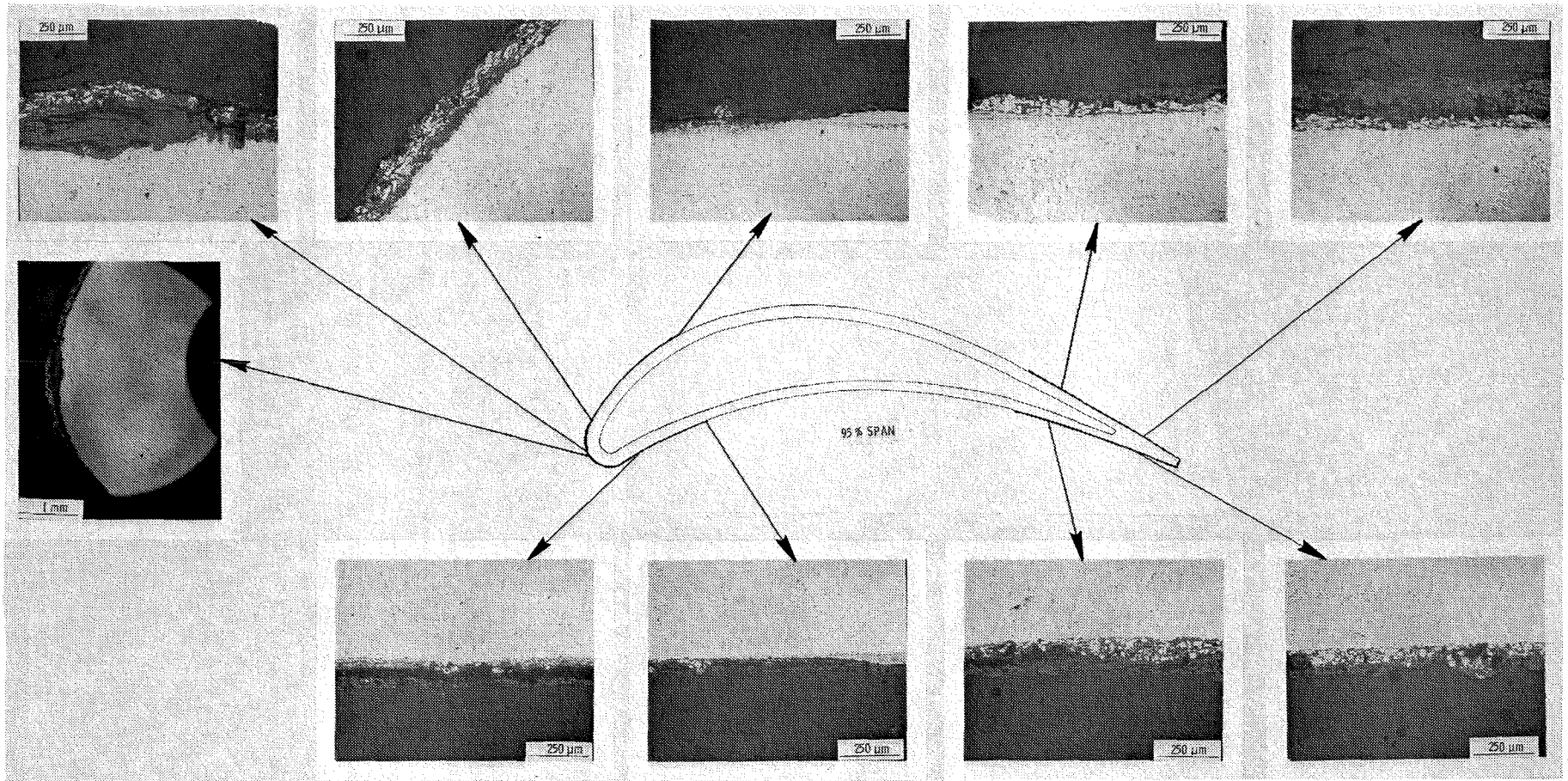


Figure 57a. Photomicrographs of Engine-Tested (1000 "C" Cycles), CF6-50, Stage 2 Vane With TBC (Ni-22Cr-10Al-1Y/ZrO₂-20%Y₂O₃ Duplex); 95% Span.

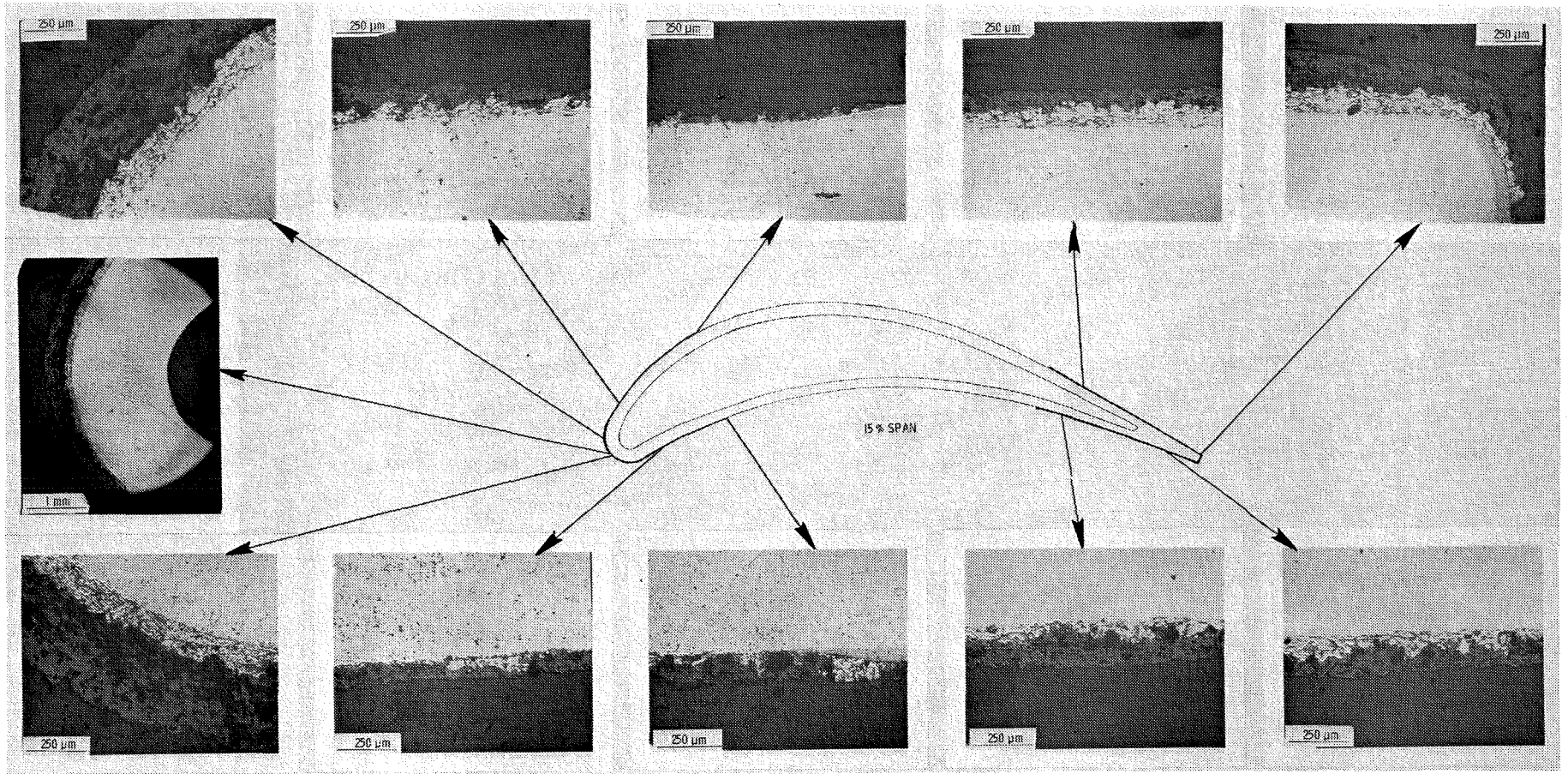


Figure 57b. Photomicrographs of Engine-Tested (1000 "C" Cycles), CF6-50, Stage 2 Vane With TBC (Ni-22Cr-10Al-1Y/ZrO₂-20%Y₂O₃ Duplex); 15% Span.

7.0 CONCLUSIONS

1. Thermal barrier coatings with a ZrO_2 - Y_2O_3 (8% or 20% Y_2O_3) ceramic layer were the most durable coatings of those tested, followed by coatings with ceramic layers of ZrO_2 -24%MgO and HfO_2 . Al_2O_3 coatings suffered the most loss of ceramic in the tests performed.
2. Two-layer (duplex) thermal-barrier-coatings with Ni-Cr-Al-Y bond coat layers and ZrO_2 -20% Y_2O_3 and ZrO_2 -8% Y_2O_3 top coat layers had equivalent lives on flat specimens in thermal cycle tests [533 to 1310 K (500° to 1900° F)]. [Recent data from other programs on specimens tested at 1366 K (2000° F) show ZrO_2 -8% Y_2O_3 to have longer test lives.]
3. Two-layer (duplex) thermal-barrier-coatings were better than three-layer (triplex) coatings. The metal particles in the blend layer of triplex coatings oxidize more rapidly than those in the bond coat layer, leading to an increased blend layer volume and stresses sufficient to cause bending of thin substrates.
4. The presence of an Ni-Cr-Al-Y/ ZrO_2 - Y_2O_3 TBC does not affect the high cycle fatigue or stress rupture strengths at 1255 K (1800° F) of the blade alloys René 80 and DS René 150 or the vane alloy X-40.
5. The TBC surrounding the site of impact damage does not degrade preferentially in thermal cycle tests [533 to 1310 K (500° to 1900° F)].
6. Thermal barrier coatings with the Ni-Cr-Al-Y bond coat layer applied by the vacuum plasma spray process to HPT blades had better durability in laboratory thermal shock tests than thermal-barrier-coatings with the bond coat applied by the conventional plasma spray process.
7. Oxidation of Ni-Cr-Al-Y bond coats applied by the VPS process occurs more slowly than it does for bond coats applied by the conventional plasma spray process. Because of their higher densities, VPS bond coats undergo frontal oxidation, whereas in conventionally plasma-sprayed bond coats, oxidation occurs around each individual particle.
8. VPS applied bond coats adhere satisfactorily to aluminided surfaces.
9. The selected TBC, applied to CF6-50 Stage 2 blades, showed excellent durability after 1000 "C" cycles of testing, except for coating damaged by particle impingement.
10. Some loss of the ceramic layer of the TBC from the leading edge of Stage 2 vane airfoils occurred by spalling and some erosion damage occurred to the TBC on the vane bands. The TBC survived well in other coated areas on the vanes.

8.0 RECOMMENDATIONS

The following recommendations are offered for further studies:

1. Methods for improving the impact resistance and erosion resistance of the ceramic layer should be investigated.
2. Efforts should be continued to improve the spalling resistance of thermal barrier coatings. The effects of process variables and powder characteristics need to be further investigated, particularly for the ceramic layer.
3. The application of thermal barrier coatings to components with complex geometries, such as HPT blades and vanes, should be done with programmed manipulation of the plasma torch and/or part.
4. Attention should be given to the development of technology for coating parts with cooling holes without clogging the holes.
5. Efforts should be undertaken to develop nondestructive evaluation techniques for assessing the quality of thermal barrier coatings.
6. Continued interaction of design and materials technologists in the development and application of thermal barrier coating should be encouraged.

REFERENCES

1. Schafer, L.J., Jr, Stepka, F.S., and Brown, W.B., "Comparison of Theoretically and Experimentally Determined Effects of Oxide Coatings Supplied by Fuel Additives on Uncooled Turbine-Blade Temperature During Transient Turbojet Engine Operation," NACA RM E53A19, 1953.
2. Bartoo, E.R., and Clure, J.L., "Experimental Investigation of Air-Cooled Turbine Blades in Turbojet Engine XIII - Endurance Evaluation of Several Protective Coatings Applied to Turbine Blades of Nonstrategic Steels," NACA RM E53E18, 1953.
3. Liebert, C.H., and Stepka, F.S., "Potential Use of Ceramic Coating as a Thermal Insulation on Cooled Turbine Hardware," NASA TM X-3352, 1976.
4. Liebert, C.H., and Stepka, F.S., "Ceramic Thermal-Barrier Coatings for Cooled Turbines," AIAA Paper 76-729, July 1976.
5. Liebert, C., et al., "Durability of Zirconia Thermal-Barrier Ceramic Coatings on Air-Cooled Turbine Blades in Cyclic Jet Engine Operation," NASA TM X-3410, 1976.
6. Stecura, S., "Two-Layer Thermal-Barrier Coating for Turbine Airfoils - Furnace and Burner Rig Test Results," NASA TM X-3425, 1976.
7. Siemers, P.A. and Hillig, W.B., "Thermal-Barrier-Coated Turbine Blade Study," NASA CR-165351, 1981.
8. Stecura, S., and Liebert, C.H., "Thermal Barrier Coating System," U.S. Patent 4,055,705, 25 October 1977.
9. "Standard Method for Adhesion or Cohesive Strength of Flame Sprayed Coatings," ASTM C633-69, 1969.
10. Levine, S.R., "Adhesive/Cohesive Strength of a $ZrO_2-12\%Y_2O_3/Ni-Cr-Al-Y$ Thermal Barrier Coating," NASA TM-73792, 1978.
11. Stecura, S., "Effects of Compositional Changes on the Performance of a Thermal Barrier Coating System," NASA TM-78976, 1978.

DISTRIBUTION

NASA Headquarters
600 Independence Avenue, SW
Washington, DC 20546
Attention: RTP-6/R.S. Colladay
 RTP-6/C.C. Rosen
 RTP-6/J. Facey
 RTM-6/L. Harris

NASA-Lewis Research Center
21000 Brookpark Road
Cleveland, OH 44135

Attention: D.L. Nored	MS 301-2
C.C. Ciepluch	MS 301-4 (18 copies)
J.W. Schaefer	MS 301-4
P.G. Batterton	MS 301-4
G.K. Sievers	MS 301-2
M.A. Beheim	MS 3-5
M.J. Hartmann	MS 3-7
R.A. Rudey	MS 86-5
W.C. Strack	MS 501-10
T.P. Moffitt	MS 77-2
R.E. Jones	MS 86-6
L.J. Kiraly	MS 23-2
D.C. Mikkelson	MS 86-1
A. Long	MS 500-305
J.F. Groeneweg	MS 54-3
W.M. Braithwaite	MS 500-208
J.C. Williams	MS 500-211
R.L. Davies	MS 106-1
R.H. Johns	MS 49-6
L.J. Kaszubinski	MS 86-2
J.F. Sellers	MS 100-1
J.R. Mihalow	MS 100-1
L. Reid	MS 5-9
D.W. Drier	MS 86-2
R.W. Niedzwiecki	MS 86-6
AFSC Liaison Office	MS 501-3
ARMY R&T Propulsion Lab	MS 302-2

NASA Ames Research Center
Moffett Field, CA 94035
Attention: 202-7/M.H. Waters

NASA Langley Research Center
Langley Field, VA 23365
Attention: R. Leonard
 D. Maiden
 L.J. Williams

NASA Dryden Flight Research Center
P.O. Box 273
Edwards, CA 93523
Attention: J.A. Albers

Department of Defense
Washington, DC 20301
Attention: R. Standahar 3D1089 Pentagon

Wright-Patterson Air Force Base
Dayton, OH 45433
Attention: APL Chief Scientist
E.E. Abell
H.I. Bush
E.E. Bailey (NASA Liaison)
R.P. Carmichael
R. Ellis
W.H. Austin, Jr.

Eustis Directorate
U.S. Army Air Mobility
R&D Laboratory
Fort Eustis, VA 23604
Attention: J. Lane, SAVDL-EU-Tapp

NAVY Department
Naval Air Systems Command
Washington, DC 20361
Attention: W. Koven AIR-03E
J.L. Byers AIR-53602
E.A. Lichtman AIR-330E
G. Derderian AIR-5362C

NAVAL Air Propulsion Test Center
Trenton, NJ 08628
Attention: J.J. Curry
A.A. Martino

U.S. Naval Air Test Center
Code SY-53
Patuxent River, MD 20670
Attention: E.A. Lynch

USAVRAD Command
P.O. Box 209
St. Louis, MO 63166
Attention: Robert M. Titus

Detroit Diesel Allison Div. G.M.C.
333 West First St.
Dayton, OH 45202
Attention: F.H. Walters

AFWAL/PS
ASD/YZE
AFWAL/POT
AFWAL/NASA
ASD/XRHI
ASD/YZN
ASD/ENF

Department of Transportation
NASA/DOT Joint Office of
Noise Abatement
Washington, D.C. 20590
Attention: C. Foster

Federal Aviation Administration
Noise Abatement Division
Washington, DC 20590
Attention: E. Sellman AEE-120

Rohr Corporation
P.O. Box 1516
Chuyla Vista, CA 92012
Attention: James C. Fuscoe

TRW Equipment
TRW Inc.
23555 Euclid Ave.
Cleveland, Ohio 44117
Attention: I. Toth

Federal Aviation Administration
12 New England Executive Park
Burlington, MA 18083
Attention: Jack A. Sain, ANE-200

Curtiss Wright Corporation
Woodridge, NJ 07075
Attention: S. Lombardo
S. Moskowitz

AVCO/Lycoming
550 S. Main Street
Stratford, CN 06497
Attention: H. Moellmann

Williams Research Co.
2280 W. Maple Road
Walled Lake, MI 48088
Attention: R. VanNimwegen
R. Horn

Teledyne CAE, Turbine Engines
1330 Laskey Road
Toledo, OH 43612
Attention: R.H. Gaylord

Pratt & Whitney Aircraft Group/UTC
Government Products Division
P.O. Box 2691
West Palm Beach, FL 33402
Attention: B.A. Jones

Boeing Commercial Airplane Co.
P.O. Box 3707
Seattle, WA 98124
Attention: P.E. Johnson MS 9H-46
D.C. Nordstrom MS-73-01

Brunswick Corporation
2000 Brunswick Lane
Deland, FL 32720
Attention: A. Erickson

Delta Airlines, Inc.
Hartsfield-Atlanta International Airport
Atlanta, GA 30320
Attention: C.C. Davis

FluiDyne Engineering Corp.
5900 Olson Memorial Highway
Minneapolis, MN 55422
Attention: J.S. Holdhusen

Massachusetts Inst. of Technology
Dept. of Astronautics & Aeronautics
Cambridge, MA 02139
Attention: Mames Mar

Detroit Diesel Allison Div. G.M.C.
P.O. Box 894
Indianapolis, IN 46202
Attention: W.L. McIntire

The Garrett Corporation
AIRResearch Manufacturing Co.
Torrance, CA 90509
Attention: F.E. Faulkner

The Garrett Corporation
AIRResearch Manufacturing Co.
402 S. 36 Street
Phoenix, AZ 85034
Attention: Library

General Electric Co./AEG
1000 Western Avenue
Lynn, MA 01910
Attention: R.E. Nietzel

Pratt & Whitney Aircraft Group/UTC
Commercial Products Division
East Hartford, CT 06108
Attention: W. Gardner (3 copies)
I. Mendelson

Douglas Aircraft Co.
McDonnell Douglas Corp.
3855 Lakewood Boulevard
Long Beach, CA 90846
Attention: R.T. Kawai Code 36-41
M. Klotzsche 36-41

AIRResearch Manufacturing Co.
111 South 34th Street
P.O. Box 5217
Phoenix, AZ 85010
Attention: C.E. Corrigan
(930120/503-4F)

American Airlines
Maint. & Engrg. Center
Tulsa, OK 74151
Attention: W.R. Neeley

Lockheed California Co.
Burbank, CA 91502
Attention: J.F. Stroud, Dept. 75-42
R. Tullis, Dept. 74-21

Grumman Aerospace Corp.
South Oyster Bay Road
Bethpage, NY 11714
Attention: C. Hoeltzer

End of Document